Investigating the Gas-Phase Interactions of Imidazolium Ionic Liquids with the Reactants and Products of a Diels-Alder Reaction

Qiaochu Du

MSc by Research

University of York

Chemistry

December 2016

Abstract

The Diels-Alder reaction between cyclopentadiene and methyl acrylate leads to both *endo*- and *exo*-methyl bicyclo-[2.2.1]-hept-5-ene-2-carboxylate and it has been shown that in the liquid crystal phase of some imidazolium ionic liquids, the *endo*-isomer can be favoured. A study was, therefore, carried out using mass spectrometry methods to investigate possible preferential binding of one isomer or the other to the imidazolium cation in order to understand the selectivity better.

Samples of the *endo* and *exo* isomers of methyl bicyclo-[2.2.1]-hept-5-ene-2-carboxylate, as well as a series of ionic liquids consisting of $[C_nMIM]^+$ (n = 2, 4, 12) cations with the BF_4^- anion, were synthesised. Ionic complexes containing the $[C_nMIM]^{m+}$ (n = 2, 4, 12*; m* = 1-3) with Diels-Alder reaction components (denoted [N]) were then prepared in the gas phase using electrospray ionisation mass spectrometry (ESI-MS). This then allowed for the investigation of the non-covalent interactions between the ionic liquid cations and Diels-Alder reaction components by collision-induced dissociation (CID) within a quadrupole ion trap. For each $[C_nMIM]^{m+}\cdot$[N] cluster, the interactions between the $[BMIM]^+\cdot$[N] clusters appear stronger than the $[EMIM]^+\cdot$[N] clusters, while the $[C_{12}MIM]^+$ cation with a rather large bulk has the weakest coordination with the [N] molecules. The $[C_{12}MIM]^+\cdot$CPD and $[C_{12}MIM]^+\cdot$*exo* isomer could not be observed as stable gas-phase complexes, showing a different result to the study of $[C_{12}MIM][BF_4]$-*exo* behaviour in solution phase.[43]

Finally these experiments were complemented by computational chemistry using DFT and MP2 methods to investigate possible structures, interaction energies and hydrogen bond lengths of the cluster isomers of $[C_nMIM]^+\cdot$[N]. Calculations indicate that the main interaction patterns of the $[C_nMIM]^+\cdot$[N] cluster isomers are formed by non-linear O···H bonds between the carbonyl oxygen of methyl acrylate and the two isomeric products with either the C_2 and methyl hydrogens or the C_2 and methylene hydrogens of the imidazolium cations.

Table of Contents

List of Figures

List of Tables

List of Schemes

Acknowledgements

I would like to thank my supervisors, Professor Dr. Duncan W. Bruce and Dr. Caroline E. H. Dessent, for their patience, guidance and continued advice and support during my research study in University of York.

I'm also indebted to Dr. Sarah for her great patience and help and friendship.

I would also like to thank my fellow experimental technician Jin-Guo Wang, for his continued technical help.

Finally special thanks to my parents, for their understanding and great support on my overseas life and study.

Author's Declaration

I declare that this thesis is a presentation of original work and I am a sole author. This work has not previously been presented for any award at this, or any other, University. All sources are acknowledged as References.

Chapter 1 Introduction

1.1 A Brief History of Ionic Liquids

Salt compounds (*e.g.* NaCl and $MgSO_4$) are always considered to adopt ionic bonding in their solid states. Since the ionic bond is usually stronger than the non-covalent forces between molecules in an ordinary liquid, common salts tend to melt at higher temperatures than other solid molecules.[1] However, in 1888, ethanolammonium nitrate ($[CH_3CH_2OH{\cdot}NH_3]^+[NO_3]^-$) (*Figure 1.1*) was found by Gabriel and Weiner to have a relatively low melting point under 100 °C, which was a by-product in a Friedel-Crafts reaction catalysed by aluminium chloride.[2] The identification and structure of such low melting point salts were vigorously disputed until the development of the nuclear magnetic resonance technique allowed them to be directly characterised.

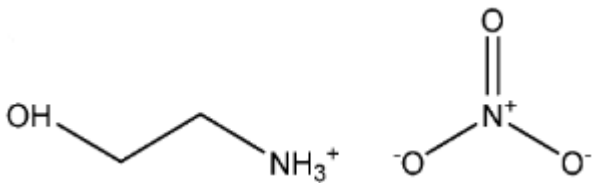

Figure 1.1: Ethanolammonium nitrate

Then in 1914, the first true ionic liquid, ethylammonium nitrate, with a melting point of 12 °C was reported by P. Walden, who was thus considered the "father" of ionic liquids.[3] In the 1970s and 1980s, ionic liquids based on alkyl-substituted imidazolium and pyridinium cations (*Figure 1.2*), with halide or tetrahalogenoaluminate anions, were developed as potential electrolytes in batteries.[4, 5] Currently the description of room-temperature ionic liquids is generally accepted for these compounds, while phrases such as "molten salts" and "fused salts" were still widely used as keywords for these compounds at that time.[6]

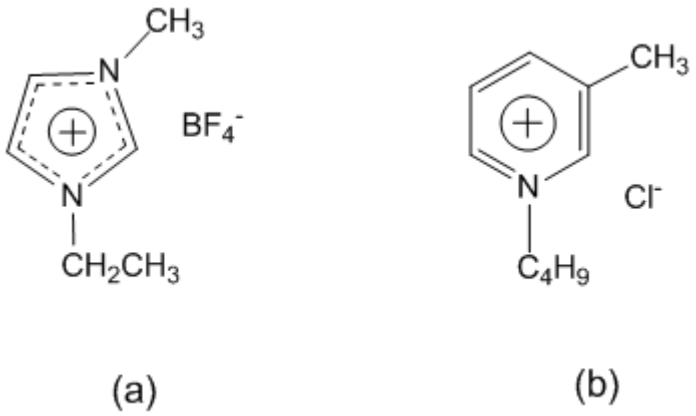

Figure 1.2: Examples of (a) imidazolium and (b) a pyridinium ionic liquid (IL).

1.2 Review of the Current Field of Ionic Liquids

Room-temperature ionic liquids (ILs) are a class of organic salts with unusually low melting temperatures and are constituted entirely by ions. They have attracted considerable attention over the last two decades in the industrial and synthetic chemistry communities for their unique properties, such as low vapour pressure, ability to dissolve organic, inorganic and polymeric materials, and high chemical and thermal stability.[7]

ILs are often composed of large organic cations (*e.g.* 1-butyl-3-methylimidazolium, $[BMIM]^+$) and small inorganic anions (*e.g.* tetrafluoroborate, $[BF_4]^-$), which leads to a low melting point and allows them to act as a solvent for both organic and inorganic chemicals. Properties of non-volatility and low flammability are also obvious advantages compared with traditional organic solvents. Thus, ILs have become a competitive candidate as non-volatile, novel solvents in catalytic, organic reactions and electrochemical, separation processes, and now play a key role in green chemistry.[8]

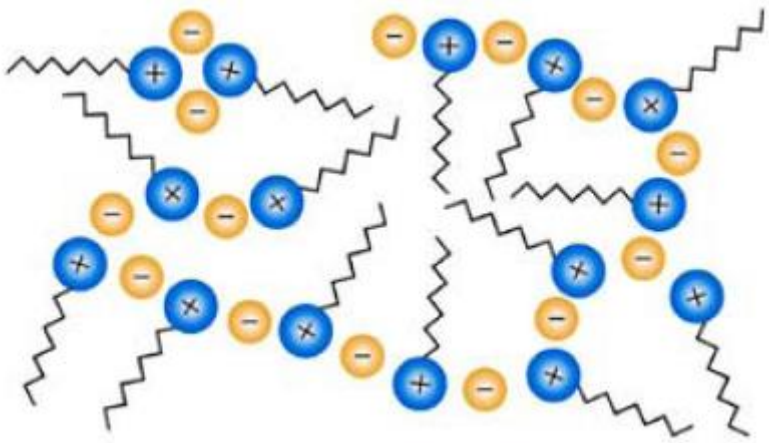

Figure 1.3: Simplified model of an ionic liquid adapted from [9].

Another reason for increased interest in ILs is related to a number of unique properties of their ionic structure, such as conductivity, combined with the liquid state over a wide range of temperatures. This shows the potential for the technological application of ILs as a catalyst for fixing transition metals in biphasic catalytic reactions, as an extraction agent, and as an electrolyte for fuel cell and dye type solar cells.[10] At the same time, the great designability of ILs has started to be recognised.[11] A compound with expected properties can be acquired simply by selecting a proper cation and anion with different substituents, to some extent providing the possibility to synthesise an IL for specific purpose.

Other novel functional applications of ILs were also discovered and reported. For example, in 2002 McCrary and Rogers reported that cellulose can be dissolved in ILs without any auxiliary substances,[12] opening new possibilities in biomass processing and biopolymer solubility of ILs.[13] In addition, ILs can also be used as feeding deterrents,[14] or rubber accelerators,[15] or to preserve soft tissue[16] due to their amazing functional properties. These wide-range practical applications of ILs show that there is great potential and value to study the mechanism of ILs in molecular aspect.

1.3 Reactions in Ionic Liquids

Global environmental issues such as atmospheric emissions and contamination of aqueous effluents are becoming increasingly serious societal problems, putting considerable pressure on the modern synthetic chemical industry to replace some volatile organic compounds (VOCs) that are currently used as used as solvents and catalysts.[17]

Since the first unexpected synthesis in 1888,[2] ionic liquids have been found to possess a variety of characteristic features that fit in well with green chemistry, including almost no vapour pressure, non-flammability, non-combustibility, high thermal stability and relatively low viscosity. Hence, they are expected to play an important role in processing environmentally-friendly reactions.[18, 19]

As well as the normal replacement of toxic/hazardous compounds and organic solvents, there are also more than ten different types of reaction that have been discovered that can be conducted in ionic liquids, with different or better results compared to the traditional reaction methods. For example, the use of ILs containing an imidazolium cation with Cl^-, PF_6^-, BF_4^- and carboxylate anions in Diels-Alder reactions will lead to a higher percentage of the *endo* product;[20, 21] In some Heck reactions, when using cheaper but less reactive substrates, it is necessary to apply more active catalysts to guarantee the sufficient catalytic activity.[22] This can be easily achieved by utilising 1-butyl-3-methylimidazolium bromide ([BMIM]Br) as solvent. The reaction of vinyl ethers with aryl halides using 1-butyl-3-methylimidazolium tetrafluroborate ([BMIM][BF_4]) gives only α-substituents specifically while a mixture of α-substituents and β-substituents would be produced under normal conditions;[23, 24] In the Witting reaction, the separation of the product and the by-product can be much more easily achieved when an IL is used, with a possibility of efficiently reusing the IL.[25]

Other reactions including aldol condensation,[26] Stille reaction,[27] Friedel-Crafts reaction[28, 29] and enzymatic reaction[30, 31] have also been reported by several papers using ILs as catalysts and solvents.

1.4 Ionic Liquids in Diels-Alder Reactions – Hydrogen Bonds

The Diels–Alder reaction was named after Professor Otto Paul Hermann Diels (1876-1954) and his student Hurt Alder (1902-1958), who were also awarded the Nobel Prize in chemistry in 1950 for this landmark discovery.[32 (a)] This cycloaddition reaction is a [4+2] thermal cycloaddition reaction with the sigma-overlap of the pi-orbitals of the two unsaturated systems, producing two new σ bonds and up to four adjacent chiral centres in a single step, and remaining one of the most reliable carbon–carbon bond-forming reactions in synthetic organic chemistry.[32 (b)] The stereochemistry can be presented in many aspects by Diels-Alder reaction such as stereoselectivity, stereospecific, regioselectivity and so on. Also introducing Diels-Alder methodology into synthetic design will greatly simplify the procedure and improve the efficiency of the reaction.

However, the reaction is naturally non-selective, producing a mixture of isomers. Therefore, it is quite attractive to find a way by which one single isomeric product would be generated. Moreover, since the Diels-Alder reaction is spontaneously reversible, some processes aiming to accelerate the reaction will contrarily reduce the equilibrium constant, leading to a *retro* Diels-Alder reaction.[33] Thus, how to increase the rate and control the ratio of the isomer products will be important especially in industrial synthesis. [34, 35]

The Diels–Alder reaction in an ionic liquid was firstly performed by D. A. Jaeger *et al.*, using ethylammonium nitrate in 1989.[36] Later on, many other ILs such as imidazolium ILs were also used to figure out how the nature of the solvent is influencing the reaction, *i.e.* how the IL solvents can increase the ratio of the *endo*/*exo* isomers and the yield at the same time.[37, 38]

According to work from P. A. Hunt *et al.*,[39] some ionic liquids containing cations with acidic hydrogen(s), such as imidazolium-based cations, and anions with lone electron pair typically formed by hydrogen bonding interactions in the condensed phase. This work suggests the possibility that the IL cation could attract the relatively strongly electronegative part of the reactant component in a Diels-Alder reaction. There are also several reports published pointing out that the *endo* selectivity of ILs is based on hydrogen bonds formed between the IL cation and Diels-Alder reactants, but most are theoretical analyses.[40-42] In most cases, the reaction between cyclopentadiene and methyl acrylate in various ionic liquids was studied as a typical Diels-Alder reaction to find out the effect of the ILs. In 2002, A. Aggarwal *et al.* reported how a specific solvent-solute interaction can result in the increase of both the *endo/exo* ratio and the reaction rate.[40] In this work, a comparison of 1-butyl-3-methylimidazolium tetrafluroborate ([BMIM][BF_4]) and 1-butyl-2,3-dimethylimidazolium tetrafluroborate ([BM_2IM][BF_4]) with the 2-position carbon occupied was conducted to investigate the effect of the acidic hydrogen on modifying the Diels-Alder outcome. It turns out that both *endo/exo* ratio and yield were reduced when changing the IL from [BMIM][BF_4] to [BM_2IM][BF_4], further supporting the hydrogen bonding theory.

More recently, a study from D. W. Bruce *et al.* investigating the influence of liquid-crystalline ionic liquids on the Diels-Alder reaction as ordered reaction media, demonstrated that the proportion of the *exo* isomer form the Diels-Alder reaction increases as the reaction medium is changed from an isotropic IL to a liquid-crystalline IL, which has a larger bulk and more ordered structure.[43]

1.5 Ionic Liquids in the Gas Phase

Electrospray ionisation (ESI) and matrix-assisted laser desorption ionisation (MALDI) are two efficient methods to produce gas-phase ions. ESI and MALDI were developed by J. Fenn[44-46] and F. Hillenkamp,[47] respectively, in the 1980s. J. Fenn and K. Tanaka were rewarded the 2002 Nobel Prize in chemistry due to this great achievement,[48, 49] which led to considerable advances in mass spectrometry. Both

techniques are quite useful for the production of gas-phase molecular ions, since they leave very little remaining energy on the analyte, which means that similar molecular decomposition as can happen during heating is less likely to occur. Moreover, these techniques can also allow for weak non-covalent coordination during the process of transferring the analyte into the gas phase, which provides a perfect environment to produce molecular cluster.[50]

Although the explanations of the *endo/exo* isomer-selectivity and increase in reaction rate observed for the Diels-Alder reaction in ILs discussed above are reliable, coming questions remain as the binding constants in these systems measured by GC or NMR are still slightly influenced by both the counter ions and solvents used for these techniques.[51, 52] The gas phase provides an ideal environment for studying the intrinsic binding on IL constituents with the components of the Diels-Alder reaction in the absence of solvent effects and counter ions.[53, 54] The ability to produce both coordinatively unsaturated and ionic H-bonded clusters in the gas phase also allows the binding interactions to be examined as a function of the extent of ligation.

In early 2006, a study carried out by Earle *et al.* found that the ionic liquid of 1-alkyl-3-methylimidazolium bis[(trifluoromethyl)sulfonyl]amides can be vaporised just by placing the IL in vacuum, and furthermore, it can even be separated by distillation.[55] This discovery has raised questions about how the ILs will behave within the gas phase, *e.g.* what structures do they adopt and how is their bonding constituted. Further experiments determined that ILs actually will form ion pairs (cation-anion) within the gas phase,[56-59] and these are similar to those produced under a reduced-pressure distillation. However, later on, some further studies led to a different conclusion that isolated ionic components dominate in a gas-phase sample.[60] All of these studies draw a conclusion that the nature of the ILs detected in the gas phase depends on the conditions of the experiments,[55, 60] which motivate further investigations on gas-phase ionic liquid clusters.[61-63]

1.6 ESI-CID

Electrospray ionisation (ESI)[64-66] in tandem with collision-induced dissociation (CID, also known as CAD)[67] has become an efficient and powerful mass spectrometry technique for both quantitative and qualitative studies of various molecular systems. Usually in mass spectrometry, the structural illustration of unknown clusters is based on the knowledge of given vapour-phase molecules. Thus, it is crucial to study the decomposition behaviour of new complexes stressing the main features and routes.[68]

One notable property of ionic liquids for their use to replace the VOCs is the low vapour pressure, thus it is relatively hard to produce ionic liquid vapour in a normal way by heating. The technique of ESI-CID can provide an alternative route to transferring ILs from solution into the gas phase, due to their high polarity.[69-71] This approach has been conducted since the beginning of the 21st century, proving that certain ionic liquids can be successfully transferred into the vapour under high-vacuum conditions using the ESI technique.[72-75] Initially, ESI was considered as an ionisation method dedicated to protein analysis. Later on, its use was extended not only to other polymers and biopolymers, but also to the analysis of small polar molecules and many inorganic complexes. In addition, there have now been many reports where ionic liquids have been studied *via* mass spectrometry, using ESI as the ionisation method.[76-78]

Collision-induced dissociation mass spectrometry (CID-MS) is a very widely used technique that can be applied to aid the identification of unknown molecular systems in mass spectrometry, *i.e. via* the identification of various molecular fragments that are produced upon CID. It allows one to increase the number of precursor ions that fragment in the reaction region and also the number of fragmentation pathways, which can be used to probe the lowest-energy pathways for the fragmentation of an ion. This can also be used to provide information relating to the structure of the ion. An electric field is used to increase the kinetic energy of the precursor ion and accelerate it into an inert target gas. Over the

course of hundreds of collisions with the target gas, the excess kinetic energy of the ion will be converted into vibrational energy.[79]

Over recent years, such CID investigations have been applied to investigate the nature of the bonding within IL clusters that have been generated by electrospray. One such study was carried out by N. M. Fernandes *et al.*,[80] who aimed to use this approach to elucidate the cation-anion interaction strength in the $[(cation)_2anion]^+$ and/or $[cation(anion)_2]^-$ ions for a wide range of ILs. In addition to this pioneering study, there have been also a number of other studies on ILs using ESI-MS. For example, Z. B. Alfassi *et al.*[81] carried out a study to probe the solubility of ILs in water at ambient temperature by conducting electrospray ionisation mass spectrometry experiments on both the cations and the anions. Other work, carried out by M. A. Henderson and J. S. McIndoe,[59] demonstrated that the addition of small quantities of ILs to solutions of analytes (*e.g.* $[Rh(COD)(PPh_3)_2]^+$) in non-polar solvents (*e.g.* hexane) allowed these solutions to be successfully studied *via* ESI-MS. More recently, there are also studies showing that ESI has been successfully used to produce gas-phase IL clusters that have been investigated using UV photodissociation[82] and IR spectroscopy[83]. All these studies demonstrate that ESI-MS is well suited as an ionisation method for ILs.

1.7 Project aim

While there have been several studies of how *endo*-*exo* ratios of Diels-Alder chemical reactions are affected in IL solvents, including how hydrogen bonds formation between the components of the ILs and the Diels-Alder components, much less is known about how reactivity, and particularly the stereochemistry of a reaction, is influenced by the isomer-IL cluster and how short-range interactions are formed within an IL. Thus it is more crucial to understand the mechanism and to obtain evidence of how the IL•*endo*/*exo* aggregates behave within ILs. In this work, an investigation on whether ESI-MS combined with CID can be applied to better understand the interactions that occur when a Diels-Alder reaction takes place in an IL. To achieve this, we will investigate whether ESI-MS can be used to

produce complexes of the IL components with the Diels-Alder reactants and products. The project will focus on a series of imidazolium-based ionic liquids (both traditional and liquid crystalline) containing the same anion of BF_4^-. Further, if ESI-MS can be used to produce these complexes, they will then be investigated using CID to measure the relative binding energies of the various reactant/product-IL component complexes. In addition, a computational study will also be conducted in order to assist the interpretation of the experimental results. In order that the required mass spectrometry experiments can be conducted, it will first be necessary to synthesise pure samples of the *endo* and *exo* isomers of methyl bicyclo-[2.2.1]-hept-5-ene-2-carboxylate, for the model Diels-Alder reaction to be studied here, as well as the ionic liquids to be investigated.

Chapter 2 Experimental and Theoretical Techniques

2.1 Synthesis

Silica gel (40-75 µm and 20-45 µm for chromatography) was purchased from Sigma-Aldrich and FluoroChem respectively. 1-Dodecyl-3-methylimidazolium chloride was obtained from research mate B. Feng and Amberlyst A-26(OH) ion exchange resin was obtained from Dr. S. Kirchhecker. Other chemicals used for the synthesis of methyl bicyclo-[2.2.1]-hept-5-ene-2-carboxylate and ionic liquids were purchased from Sigma-Aldrich. Solvents for synthesis, separation and purification were HPLC-grade and used as received.

Spectroscopic techniques:

Nuclear Magnetic Resonance. Samples were run on either a JEOL ECX 400 or ECS 400 instrument operating at 400 MHz for ^1H; each was equipped with a sample charger. MestroNova NMR software was used to process the spectra obtained.

2.1.1 Methyl bicyclo-[2.2.1]-hept-5-ene-2-carboxylate

A mixture of two isomers of methyl bicyclo-[2.2.1]-hept-5-ene-2-carboxylate were generated from a Diels-Alder reaction between methyl acrylate and cyclopentadiene (*Scheme 2.1*). Three main different methods were used in order to get a relatively high yield and high percentage of each isomer. [84-86]

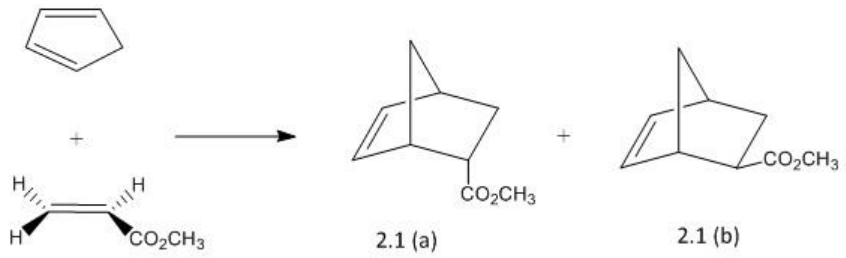

Scheme 2.1: The reaction between methyl acrylate and cyclopentadiene to produce a mixture of the *endo* 2.1(a) and *exo* 2.1(b) isomers of methyl bicyclo-[2.2.1]-hept-5-ene-2-carboxylate.

Method 1: This method was adapted from the research of Huertas *et al.*[84] Acrylic acid (3.61 g, 0.050 mol) with a slight amount of hydroquinone (0.01 g) as polymerisation inhibitor was heated to 210°C (around 190°C in the flask), with dicyclopentadiene (3.31 g, 0.025 mol) being added in over 3 hours. Methanol (20 cm^3) and sulfuric acid (0.50 cm^3, 98% solution in water) were then added after 30 minutes' heating and the mixture was heated under reflux for 1 hour. Then the resulting solution was extracted by ethyl acetate and was partitioned between water (generated from the reaction) and ethyl acetate. The ethyl acetate layer was washed with water, aqueous $NaHCO_3$ and aqueous NaCl in order, then dried by $MgSO_4$, giving a light-yellow liquid product of a mixture of the *endo* (2.51 g, 33% overall yield) and *exo* isomer (2.31 g, 30% overall yield) of methyl bicyclo-[2.2.1]-hept-5-ene-2-carboxylate. Then separation procedures were carried out by chromatography to separate the isomers. First, a 4 x 30 cm gravity column with 40-75 µm silica gel as stationary phase and 1:4 ethyl acetate-hexane as mobile phase was used for separation giving a small amount of mixture rich in the *exo* isomer,

then a repeated chromatography was carried out using a 2 x 20 cm gravity column with the same stationary and mobile phase to try to obtain pure *exo* isomer, but the final product was found still to be a mixture of isomers.

This method is a one-pot solvent-free reaction of *in situ*-generated cyclopentadiene, which was designed in order to combine the cracking of dicyclopentadiene and the Diels-Alder addition into one procedure with relatively equal amount of *endo* and *exo* isomers produced. Even so, the result still failed to meet the expectation because of a certain amount of impurities which could not be removed and can be clearly seen from the NMR spectra as circled (*Figure 3.4, Section 3.1.1.2*).

Method 2: The second method was adapted from Carlos *et al.*[85] According to the slightly different polarity between the *endo* and *exo* isomers, cyclopentadiene and methyl acrylate were reacted respectively in water, in methanol and in hexane and were worked up separately.

Thus, dicyclopentadiene was cracked thermally by heating to 210°C and the monomer was then distilled into a flask held in an ice bath. In the first reaction, freshly cracked cyclopentadiene monomer (6.3 cm^3) and methyl acrylate (5.0 cm^3) were added to water (300 cm^3) and the mixture was stirred at ambient temperature for 72 hours, producing a pure *endo* product straightforwardly with a yield of 11%. Parallel reactions were carried out using identical quantities of reactants in methanol (100 cm^3) or hexane (100 cm^3) as solvents. In each case, at the end of the reaction the solvent was removed using a rotary evaporator after which the remaining cyclopentadiene was removed under higher vacuum. The resulting products were chromatographed using same procedures with *Method 1* on 40-75 μm silica gel with 97% *endo* isomer being obtained from the product generated in methanol.

Then reactions using methanol or hexane as solvents described above were repeated several times to get an adequate amount of product for separation. A

flash column with 20-45 µm silica gel (4 x 35 cm) as stationary phase using same eluent as above was also tried once after the first two separations (first on 4 x 30 cm silica gel and then on 2 x 20 cm silica gel), but this proved less satisfactory for separation and so gravity columns were used thereafter.

Method 3: The third synthetic procedure was adapted from Vidiš *et al.*[86] and was carried out under solvent-free conditions. In this reaction, freshly cracked cyclopentadiene monomer (17.4 cm^3) and methyl acrylate (12.7 cm^3) were added to a round bottom flask and the mixture was stirred at ambient temperature for 72 hours. The mixture of products was then placed under vacuum to remove the remaining cyclopentadiene before the separation process took place. Also a longer column of 4 x 40 cm with with 40-75 µm silica gel as stationary phase and 1:4 ethyl acetate-hexane as mobile phase was used giving a better separation result.

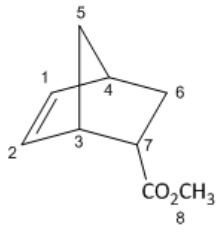

endo

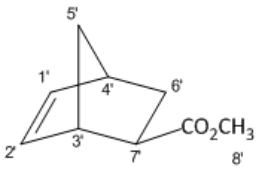

exo

Table 2.1: ^{1}H NMR data for the *endo* isomer.

Chemical shifts [a]	Multiplicity	*J*/Hz	Number of hydrogens
6.18 ppm (H_1)	dd	2.8, 5.6	1 H
5.92 ppm (H_2)	dd	2.8, 5.6	1 H

a) The chemical shifts obtained above are relative to the shift of tetramethylsilane (TMS).

Table 2.2: ^{1}H NMR data for the *exo* isomer.

Chemical shifts [a]	Multiplicity	*J*/Hz	Number of hydrogens
6.14 ppm ($H_{1'}$)	dd	2.8, 5.6	1 H
6.10 ppm ($H_{2'}$)	dd	2.8, 5.6	1 H

a) The chemical shifts obtained above are relative to the shift of tetramethylsilane (TMS).

2.1.2 1-Ethyl-3-methylimidazolium tetrafluoroborate ([EMIM][BF_4])

For the synthesis of [EMIM][BF_4], a conventional method was used adapted from Alcalde *et al.*[87] Bromoethane (20 cm^3) and 1-methylimidazole (5 cm^3) were stirred together at ambient temperature for 24 hours, until very little amount of pale yellow 1-Ethyl-3-methylimidazolium bromide solid appeared, while most of them dissolved in unreacted reactants. After adding Amberlyst A-26 (OH^-) ion exchange resin (30 cm^3) and stirring for another 72 hours, tetrafluoroboric acid (HBF_4) (20 cm^3, 48% solution in water) was added to the mixture to allow for 3 hours stirring. The resulting solution was collected *via* a separating funnel and washed with ethyl acetate, then placed under vacuum to give the product as a yellow liquid (9.87 g, 87%). A small amount (*ca.* 2 cm^3) of the product was taken out into a small tube and added to silver nitrate ($AgNO_3$) (0.001 g) in water (5 cm^3), showing no precipitate. Then ^1H and ^{19}F NMR spectra (*Chapter 3*) were taken to provide a result of the synthesis.

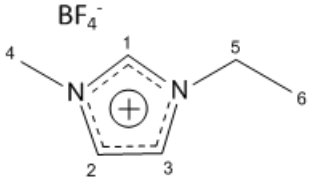

Table 2.3: ^1H NMR data for the [EMIM][BF_4].

Chemical shifts [a]	Multiplicity	*J*/Hz	Number of hydrogens
8.60 ppm (H_1)	s	-	1 H
7.47 ppm (H_2)	s	-	1 H
7.31 ppm (H_3)	s	-	1 H
3.89 ppm (H_4)	s	-	3 H
4.21 ppm (H_5)	q	7.4	2 H
1.47 ppm (H_6)	t	7.4	3 H

a) The chemical shifts obtained above are relative to the shift of tetramethylsilane (TMS).

Table 2.4: ^{19}F NMR data for [EMIM][BF_4].

Chemical shifts [a]	Multiplicity	*J*/Hz	Number of fluorine
-150.36 ppm	m	0.50	4 F (^{10}B coupling)
-150.42 ppm	q	1.60	4 F (^{11}B coupling)

[a] The chemical shifts obtained above are relative to the shift of tetramethylsilane (TMS).

2.1.3 1-Butyl-3-methylimidazolium tetrafluoroborate ([BMIM][BF_4])

The synthesis of [BMIM][BF_4] was first conducted using the same method as for [EMIM][BF_4] employing 1-bromobutane in place of bromoethane. However, this was time-consuming and gave unsatisfactory yields. Then a second method was carried out using microwaves. [88, 89]

A mixture of 1-bromobutane (10 cm^3) and 1-methylimidazole (3 cm^3) was magnetically stirred at 75 °C for 6 minutes in a microwave reaction vial, using a rotational speed of 300 rpm (400 W). After cooling down to room temperature, the yellow lower layer of the liquid was taken and washed with ethyl acetate (3 x 50 cm^3), giving the intermediate 1-methy-3-butylimidazolium bromide ([BMIM]Br). After that, [BMIM]Br (2.19 g, 0.010 mol) and sodium tetrafluoroborate ($NaBF_4$) (1.65 g, 0.015 mol) were mixed in acetone (7 cm^3) and stirred at 40 °C in the same microwave instrument running at speed of 400 rpm for 30 minutes. The product was filtered and washed with acetonitrile (3 x 50 cm^3), then placed under vacuum at 60°C for drying, to yield the tetrafluoroborate salt as a clear pale yellow liquid (2.06 g, 91%).

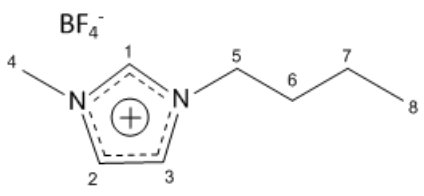

Table 2.5: ^{1}H NMR data for the [BMIM][BF_4].

Chemical shifts [a]	Multiplicity	*J*/Hz	Number of hydrogens
8.73 ppm (H_1)	s	-	1 H
7.46 ppm (H_2)	s	-	1 H
7.41 ppm (H_3)	s	-	1 H
3.93 ppm (H_4)	s	-	3 H
4.19 ppm (H_5)	t	7.1	2 H
1.84 ppm (H_6)	ddd	7.3, 9.2, 12.9	2 H
1.31 ppm (H_7)	tq	-	2 H
0.92 ppm (H_8)	t	7.4	3 H

a) The chemical shifts obtained above are relative to the shift of tetramethylsilane (TMS).

Table 2.6: ^{19}F NMR data for [BMIM][BF_4].

Chemical shifts [a]	Multiplicity	*J*/Hz	Number of fluorine
-150.16 ppm	m	0.50	4 F (^{10}B coupling)
-150.22 ppm	q	1.60	4 F (^{11}B coupling)

a) The chemical shifts obtained above are relative to the shift of tetramethylsilane (TMS).

2.1.4 1-Dodecyl-3-methylimidazolium tetrafluoroborate ([C_{12}MIM][BF_4])

The method for the synthesis of [C_{12}MIM][BF_4] was adapted from Holbrey and Seddon.[90] First, tetrafluoroboric acid (2.63 cm^3, 0.02 mol, 48% solution in water) was added dropwise to a cooled, rapidly stirring solution of a mixture of 1-dodecyl-3-methylimidazolium chloride (5.18 g, 0.02 mol) in cold water (50 cm^3) over 15 min. The lower layer was collected *via* a separating funnel, dissolved in dichloromethane (100 cm^3) and then washed with cold water (3 x 100 cm^3). The organic layer was collected and dried using magnesium sulphate ($MgSO_4$). The liquid was finally placed under vacuum to give a pale beige powder (2.89 g, 89%). The product became semifluid at a temperature of over 35 °C.

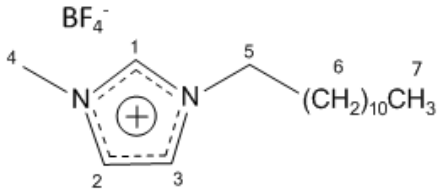

Table 2.7: ^{1}H NMR data for the [C_{12}MIM][BF_4].

Chemical shifts [a]	Multiplicity	*J*/Hz	Number of hydrogens
8.81 ppm (H_1)	s	-	1 H
7.44 ppm (H_2)	s	-	1 H
7.40 ppm (H_3)	s	-	1 H
3.85 ppm (H_4)	s	-	3 H
4.16 ppm (H_5)	t	7.0	2 H
1.25 ppm (H_6)	m	-	10 H
0.67 ppm (H_7)	t	7.4	3H

a) The chemical shifts obtained above are relative to the shift of tetramethylsilane (TMS).

Table 2.8: ^{19}F NMR data for [C_{12}MIM][BF_4].

Chemical shifts [a]	Type of peaks	J value	Number of fluorine
-149.96 ppm	m	0.50 Hz	4 F (^{10}B coupling)
-150.02 ppm	q	1.60 Hz	4 F (^{11}B coupling)

a) The chemical shifts obtained above are relative to the shift of tetramethylsilane (TMS).

2.2 Bruker Esquire 6000 Quadrupole Ion Trap Mass Spectrometer

A Bruker Esquire 6000 Quadrupole Ion Trap mass spectrometry with electrospray ion source was used to perform the mass spectroscopy experiments.[91]

The mass spectrometer is an instrument containing three parts: the electrospray ionisation (ESI) source, the ion optics and the quadrupole ion trap mass analyser. It is also designed as a tandem mass spectrometer which allows for collision induced dissociation (CID) in the quadrupole ion trap. The details are described in the following sections.

Mass spectra with a mass-to-charge ratio (*m/z*) of 35-3000 a.u. can be taken by this instrument, with a typical resolution of *m/z* 0.35 a.u. (full width half maximum). In this work tandem mass spectrometry of MS, MS^2 (*i.e.* MS/MS) and MS^3 (*i.e.* triplicate measurements of MS) were used in CID process while the machine allows for up to MS^{11}.

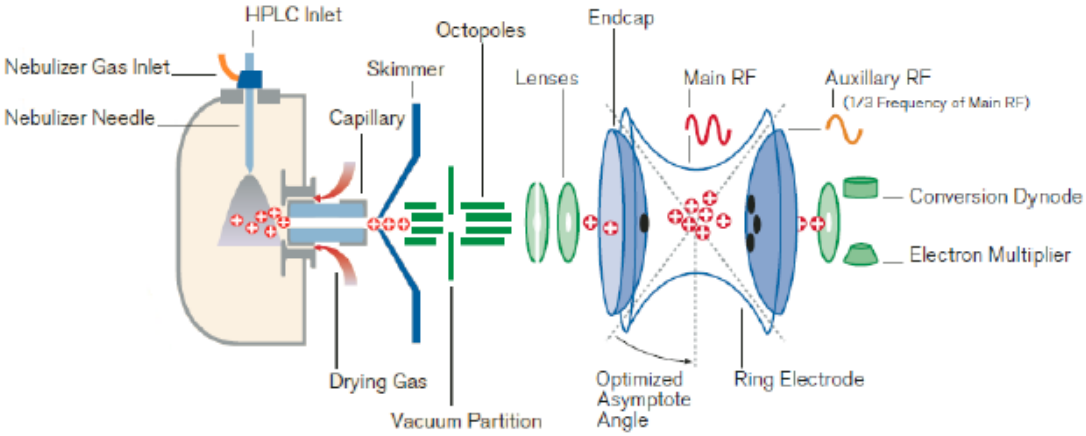

Figure 2.1: Schematic of the Bruker Esquire 6000 mass spectrometer, adapted from [91].

2.2.1 Electrospray Ionisation

The first step in the mass spectrometric analysis of compounds is the production of gas-phase ions of the compound, in this case by electrospray ionisation. The Agilent ESI source is set up with an orthogonal sprayer design and is slightly different compared with the normal design. The orthogonal design has a higher sensitivity, robustness and reproducibility to the spectrometer for various injection conditions.[92] The sample solution is put into a syringe injected through a fused-silica capillary at a constant rate (typically 300 µL h^{-1}) by syringe driver. ESI then is produced under atmosphere pressure by applying a strong electric field to a liquid passing through the capillary. This electric field can be obtained by applying a potential difference of 3-6 kV between the capillary tube and the counter-electrode.[93, 94]

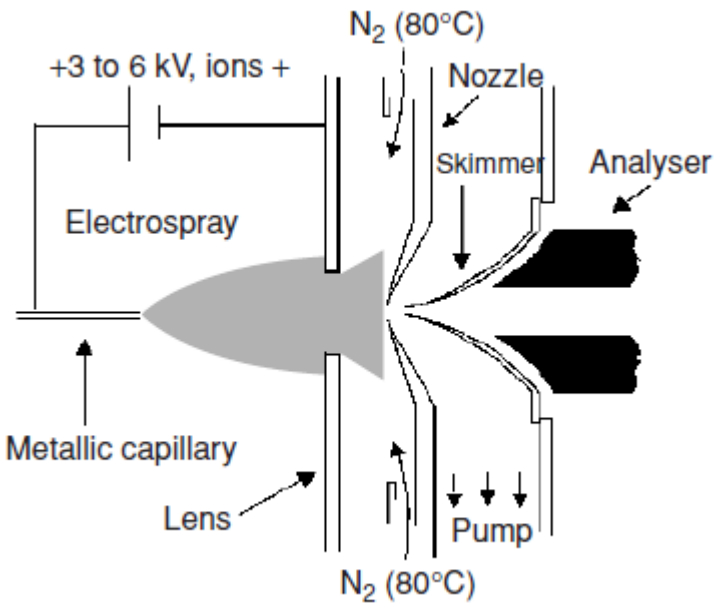

Figure 2.2: Electrospray source using a skimmer for ion focalisation and a curtain of heated nitrogen gas for desolvation adapted from [95]

When increasing the voltage, the drop at the tip of the capillary would firstly appear spherical, then elongate under the pressure caused by accumulated charges, and form a shape of "Taylor cone" when the surface tension is broken, thus producing the spray.[96, 97]

Figure 2.3: The shape of drops at the capillary tip while producing spray adapted from [96].

There are basically two models to explain how the charged droplets finally convert into completely gas-phase ions. The first one is the ion evaporation model. In this model, the Coulombic repulsions become adequately strong while the droplets reach to a certain small size, and an ion will be ejected from the surface of the droplet into the gas phase.[98] In another model, the charge residue model, the cycle of Coulomb fission and solvent evaporation will be continuous until only one ion

remains in a drop; at the same time, the solvent will be vaporised and thus produce a bare ion.[99, 100] Both theories have been proven to occur under certain conditions.[101] After transferring into gas phase, the ions will be directed through a heated capillary (normally 100-300 °C) along with a drying gas to remove any remaining solvent from the ions. Finally, the ions will pass through a skimmer and into the ion optic region of the mass spectrometer.[102]

2.2.2 Ion Optics

It is necessary for the ions to move from atmospheric pressure to the low-pressure ion trap region in order to be detected, which can be achieved using a series of ion optics for transportation between those different regions. The ions will enter the first octapole, then being directed into the second one through a vacuum section. After that the ions will pass through a couple of electrostatic lenses, focusing the ions into the quadrupole ion trap.

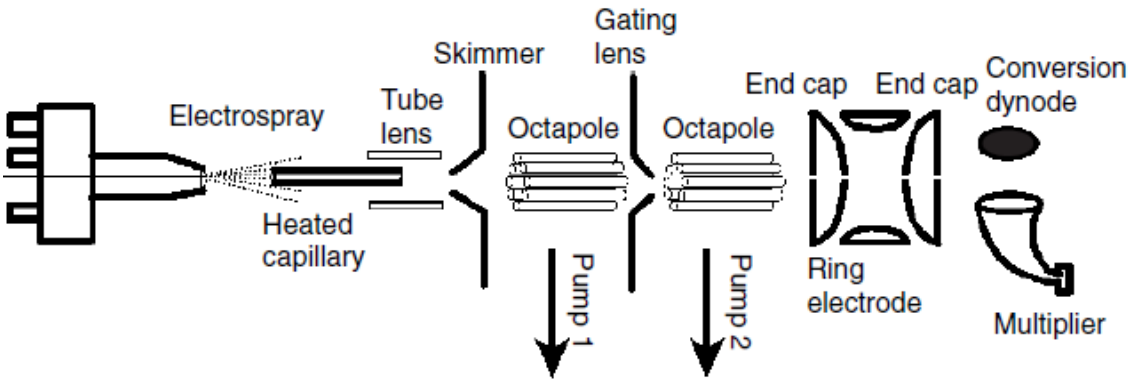

Figure 2.4: Ions produced by the ESI source are focused through a skimmer and octapole lenses to the ion trap adapted from [103]

2.2.3 Quadrupole Ion Trap

The quadrupole ion trap (QIT) consists of three electrodes: two hyperbolic end-cap electrodes and one ring electrode, which provide the main force for the ions to be trapped within the space,[104, 105] making them move along the Bowditch curve (sinusoidal locus in the vertical direction), as described by the Mathieu equation.[106, 107] The ions with same charge will repel each other, which results in a gradual expansion of the trajectories and finally making the ions eject out of control from the trap. This situation can be avoided by colliding with helium, which is the buffer gas in this experiment, at a relatively low pressure.

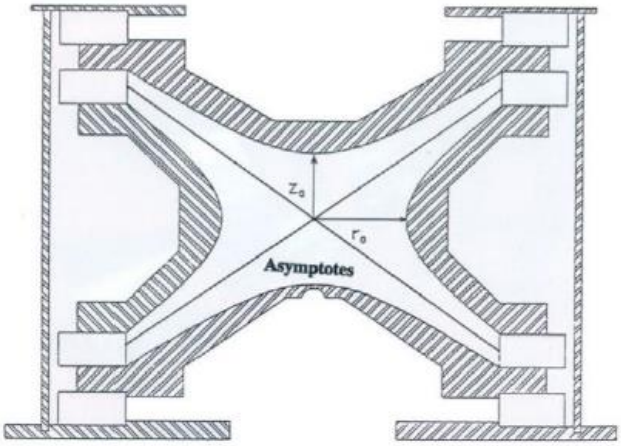

Figure 2.5: Schematic representation of the quadrupole ion trap, adapted from [104].

In the Bruker Esquire 6000 mass spectrometer, ions firstly enter the QIT through a hole in one of the end cap electrodes, being held in the trap for a short period of time and then being scanned out by resonance excitation into a detector. This will generate a plot of ion intensity against RF voltage, producing the mass spectrum. The mass spectra presented in this thesis are produced by averaging three individual mass spectra produced in the manner described here.

2.2.4 Collision Induced Dissociation

Tandem mass spectrometry requires the fragmentation of precursor ions selected by the first analyser to allow the second analyser to analyse the product ions. There are three types of ions produced by the source; the first two are the ions with a lifetime greater than 10^{-6} s and less than 10^{-7} s. Neither can produce fragments after leaving the source and before reaching the detector. The last type, also called metastable ions, have an intermediate lifetime which allows them to be selected by the first analyser while containing sufficient excess energy for fragmentation before reaching the second analyser. But the possibility of the third type is quite low (1%). Hence there is a necessity to use collision-activated decomposition (CAD), also known as collision-induced dissociation (CID), which gives a collisional activation for precursor ions to increase their internal energy. The CID procedure can be described in two steps. The first step is the collision of the ion and the target (typically helium molecules), bringing the ion into a thermally vibrational state, which usually happened only in 10^{-14} to 10^{-16} s. The next step is the decomposition of the activated ion.[79]

Several methods can be used to activate the ions through collisions for the Bruker Esquire 6000 mass spectrometer. The most typical method contains collision between the low-energy accelerated ions and the gas molecules, and this is used in this experiment.

Since the fragmentation pathways depend on the amount of energy deposited, it is important for the energy transferred to the ions to be controlled, and this can be easily achieved by adjusting the end cap voltage.[108] Comparing the energies at which ions fragment will give an insight into the relative barrier heights for the fragmentation mechanisms of different ions.[109] In this thesis, this is achieved by plotting the relative intensities of the precursor and fragment ions against fragmentation energy to produce a CID curve and taking the energy at which the relative intensity of the precursor ion reaches 50% ($E_{1/2}$).

The energy transferred to the ions upon excitation is not perfectly uniform, and larger ions receive slightly less energy and so will fragment at higher voltages. This means that the fragmentation energies should not be directly compared for ions with significantly different mass-to-charge ratios. The collision energies in this thesis are therefore quoted as '% CID energy', where 100% is the maximum end cap voltage of the spectrometer.[110]

2.3 Computational Methods

Calculations were conducted using Gaussian 09.[111] The geometry optimisations were carried out using the hybrid exchange correlation functional included using Grimme's-D3 dispersion correction[114] (B3LYP-D3)[113] to account for the dispersion interactions, with the 6-311+G(d,p) basis. The fundamental vibrational frequency calculations were carried out at the same level of the theory to ensure the true minima. Then the energies for each cluster and isolated monomer were obtained by carrying out single-point calculations at MP2[112] level with the aug-cc-pVTZ basis set. Basis set superposition error (BSSE) has been determined using the counterpoise method[115, 116] to get corrected energies for the aggregates.

Quantum mechanical calculations are based on solving the time-independent, non-relativistic Schrödinger equation [2.1]

$$\hat{\mathrm{H}}\psi = E\psi \qquad [\mathbf{2.1}]$$

where $\hat{H}$ is the Hamiltonian operator, E is the energy and ψ is the wave function of the system.

Solving the Schrödinger equation is the basic principle by which *ab initio* structure optimisations are conducted. By doing this, the energy of a specific molecular arrangement can be determined, obtaining a potential energy surface (PES). Local minima on the PES can also be acquired by calculating the first derivative of the

energy. The Schrödinger equation can be greatly simplified by the Born Oppenheimer approximation, which consider the electrons as moving in the field of fixed nuclei, due to the much slower movement of nuclei than the electrons, leading to a reduction of Hamiltonian.[117]

The primary motivation of using these DFT methods is to figure out the governing interaction to determine the property and reactivity of ionic liquids with a single ion pair, as DFT methods normally generate an accurate and detailed description of the system, and thus can be useful when there are fewer ion pairs in the system. In this project, the DFT/B3LYP method can be quite efficient and accurate for the optimisation and energy calculations on monomers (*i.e.* methyl acrylate, cyclopentadiene, the *endo* and *exo* isomer). Because this level of method is less computationally demanding, which means it requires less computational space and time, and is considerably practical for geometry calculations. This can be supported by several works that having discussed the effectiveness of other different methods.[127 (a), 127(d)]

However, ionic liquids contain highly polarisable species, negative ions and involve closed-shell interactions (hydrogen-bonding, π-π stacking interactions and alkyl chain associations). Considering the existence of the variety of these short-range interactions and also long-range Coulombic forces in ionic liquids, it is necessary to include proper dispersions, especially for the clusters of ionic liquid with other molecules. As DFT methods do not recover dispersion (or correlation) perfectly,[127 (a)-(c)] it has been suggested that the use of less costly methods including B3LYP method is not sufficient to predict accurate ion pair binding energies for ionic liquids comparing to MP2 methods as the benchmark method.[118] Thus the MP2 method was also used for the calculations.[39]

Second-order Møller-Plesset perturbation theory is a conceptually and technically simple post-Hartree-Fock (HF), *ab initio* correlation method and attempts to solve the wavefunction by including the effects of dispersion. It also gives system

energies that are more approximated to the real energies than DFT methods, which is quite useful to see the real tendency of a system. Thus MP2, rather than DFT methods, is more desirable when performing energy calculations. It can be derived by expanding the solution of the electronic Schrödinger equation as a Taylor series in the fluctuation potential (*vide infra*). This can be done either in the framework of configuration interaction theory or using the single-reference coupled-cluster ansatz for the wavefunction. It improves on the HF method by adding electron correlation effects, and is good in calculating large systems containing interactions such as hydrogen-bonding, π-π interactions and alkyl chain association.

Chapter 3 Results and Discussion

3.1 Synthesis

Detailed synthetic experimental methods were described in *Chapter 2.*

3.1.1 Methyl bicyclo-[2.2.1]-hept-5-ene-2-carboxylate

This project aims to investigate the coordination behaviour of a set of imidazolium ionic liquids with a tetrafluoroborate anion in the Diels-Alder reaction of methyl acrylate and cyclopentadiene, which always gives a mixed product with a majority of the *endo* isomer of methyl bicyclo-[2.2.1]-hept-5-ene-2-carboxylate. In order to carry out a series of mass spectrometry experiments on the mixture of ionic liquids with the two isomers separately, it is necessary to get pure *endo* and *exo* isomer. There will be a solvent effect of ionic liquids ($[C_nMIM][BF_4]$, n = 2, 4, 12 in this case) on the reaction of methyl acrylate and cyclopentadiene due to their relatively high polarisation, which will further increase the ratio of *endo* : *exo*, thus it can be more challenging to get pure *exo* isomer. All reactions to produce methyl bicyclo-[2.2.1]-hept-5-ene-2-carboxylate gave a product of light yellow liquid with a smell of terpenes.

3.1.1.1 Three Routes for Obtaining Pure Isomers

The whole procedure to obtain pure isomers can be divided into two parts: the synthesis part and the separation part. Three main methods were used here for the synthesis part.

Method 1: A solvent-free Diels-Alder reaction of *in situ* generated cyclopentadiene was first carried out. This method was used by Huertas *et al.*[84] for synthesis to give a product that can be successfully separated into pure *endo* and *exo* isomers. Also this method produces a mixture with a relatively equivalent amount of each isomer (*Figure 3.4*) in reasonable yields, which was considered as an advantage that both isomers could be obtained pure within one chromatographic separation. The purpose of adding dicyclopentadiene slowly and carefully over three hours is to reduce the possibility to form side products of acrylic acid and dicyclopentadiene in the solution, which actually could not be fully avoided. Since acrylic acid can be vaporised at such a high temperature and can condense at the tip of the needle (where dicyclopentadiene is injected and where there is no depolymerisation agent), it can then either self-polymerise or react with dicyclopentadiene to give dicyclopentenyl acrylate (DCPA), leading to impurities. The self-polymerisation of acrylic acid may cause a block at the needle tip and prevent dicyclopentadiene from coming out. This will also lead to an inadequate amount of methyl acrylate and leave more cyclopentadiene unreacted, which makes it more difficult to separate. Thus, considering that this method produced quite a lot of impurities and its relatively complicated operability, it was not pursued further.

Method 2: This method was designed to conduct the Diels-Alder reaction of methyl acrylate and cyclopentadiene in different solvents with different polarity to give products with either high a percentage of the *endo* isomer or as much *exo* isomer as possible, which tend to be easier to conduct comparing to *Method 1* and was also expected to be easier for separations to obtain pure isomers. Water was tried first as the most accessible polar solvent to get dominant *endo* product. This was

also found used to produce 93% *endo* product[67] even though cyclopentadiene is hardly dissolved in the reaction. Tiny droplets were found and aggregated on the wall of the flask as the reaction proceeded, which might be undissolved cyclopentadiene as previously predicted. Though actions were taken periodically to remix the reactant with the solvent, the overall yield was rather low. This reaction did produce pure *endo* isomer (*Figure 3.5*) with no separation needed, however the amount of product was still inadequate for further mass spectrometry experiments. Methanol was then used as a substitute for water considering the high solubility of the reactants therein, giving a product of 84.1% *endo* isomer with an acceptable yield of 76%. As a 97% *endo* product (*Figure 3.6*) together with a series of products containing 90%-95% of *endo* isomer were finally obtained from repeated separations by this method, it can be considered as an approachable and efficient method with impurities barely generated. A parallel reaction in hexane as non-polar solvent was also carried out to get a product with relatively high ratio of *exo* isomer. Though the overall yield appeared similar to the reaction in methanol, the yield of the *exo* isomer did not meet the expectation, as the 83.3% *exo* isomer obtained from the first gravity column (*Figure 3.8*) was too small for another repeat chromatography.

Method 3: This method follows a similar procedure to *Method 2* but under solvent-free conditions, which gives a higher proportion of the *exo* isomer and higher overall yields, thus would be the best way to get pure *exo* isomer. However, it also produces a lot of dicyclopentadiene impurities (*Figure 3.9*) which has an influence on separation, as cyclopentadiene can easily re-dimerise at ambient temperature without solvent. This problem can be solved by placing the resulting solution in the freezer considering the high melting point of dicyclopentadiene. Though dicyclopentadiene can be dissolved in the product, this measure would still remove most of this according to the experiments. Finally after several repeated chromatography columns, a sample of 100% pure *exo* isomer was obtained (*Figure 3.10*).

Separation: Separations were done by column chromatography using protocols adapted from Huertas *et al.*[84] In order to test the separation efficiency of the mobile phase a series of thin layer chromatography experiments were carried out with different ethyl acetate-to-hexane ratios, and finally a solvent of 1:4 ethyl acetate-hexane was employed as mobile phase. Both gravity columns with 40-75 µm silica gel and flash columns with 20-45 µm silica gel were tried. Flash columns gave a product containing more mixed isomers than gravity columns, thus further repeated chromatography were done using gravity columns.

During the collection process, the *exo* isomer was eluted first, closely followed by the *endo* isomer. Because the *exo* isomer exhibited tailing and sometimes continued to elute after elution of the *endo* isomer, usually a repeated chromatography was needed to obtain pure *endo* isomer. Even so getting pure *endo* isomer can still be achieved within one column when using methanol as the solvent for the Diels-Alder reaction (*Method 2*) or under solvent-free condition (*Method 3*), as long as an adequate amount of the mixed product from the reaction was obtained and the eluting product was divided into as many fractions as possible. While the separation for the product from *Method 1* gave neither pure *endo* nor pure *exo* isomer with all eluting fractions containing impurities which can hardly be removed even after a repeated chromatography, pure *endo* isomer was successfully obtained from the product by *Method 2* using methanol as reacting solvent.

Because all mixtures of products from *Method 2* and *3* are *endo* dominant, and the *exo* isomer will smear in the column with even a slight amount of cyclopentadiene in the mixture, it is quite challenging to get pure *exo* isomer and full attention should be paid to the collection operation at the beginning of the elution. For the separation of products from *Method 2* in hexane, as described in *Chapter 2*, an *exo*-dominant product was obtained from the first gravity column and then chromatographed on a second column, while the ratio of the *exo* isomer did not increase compared to the product from the former column. And this did not

improve even after repeating several times, indicating that the column might not be long enough to separate the *exo* isomer from a small quantity of the *endo* isomer and other impurities. Considering this, it can be assumed that the longer the column, the better the separation will be. However, the room left for the solvent should also be taken into consideration, thus longer columns with 4 x 40 cm silica gel were used for the separation in *Method 3*, with a product of 100% *exo* isomer eventually obtained.

3.1.1.2 ^{1}H NMR Results for the Isomers

A ^{1}H NMR spectrum of the *endo* isomer from Huertas *et al.*[84] was used as a reference to define the results from the separation (*Figure 3.1*). As there is little reference found for the spectrum of the *exo* isomer, a spectrum for the mixture of bicyclo-[2.2.1]-hept-5-ene-2-carboxylic acid isomers from Huertas *et al.*[84] was also used (*Figure 3.2*). Considering that there is still a difference between the two isomers, it is necessary to find a way to further extract the spectra from the reference. Thus ^{1}H NMR predictions were made using the B3LYP-D3 method with a 6-311+G(d,p) basis set. The NMR spectra results by this method were closer to the reference spectrum[84] than other methods. As shown in *Figure 3.3*, two vinylic hydrogens (H_1 and H_2) of the *endo* isomer are observed at 5.85 ppm and 6.25 ppm, while in the spectrum of *exo* isomer, they appear at 5.98 ppm and 6.10 ppm. Also, the methyl hydrogens (H_8) are slightly shifted to high field from the *endo* isomer to *exo*, which is another main difference between the two isomers. It should be noted that the ^{1}H NMR predictions do not include multiplicities and so is not adequately accurate. Still it is a convenient and useful way to obtain an approximate spectrum for the *exo* isomer, as it shows a major difference of the vinylic hydrogens between the two isomers and indicates a difference between the methyl hydrogens that has not been displayed in the reference spectra, which will be further consistent with the ^{1}H NMR spectra.

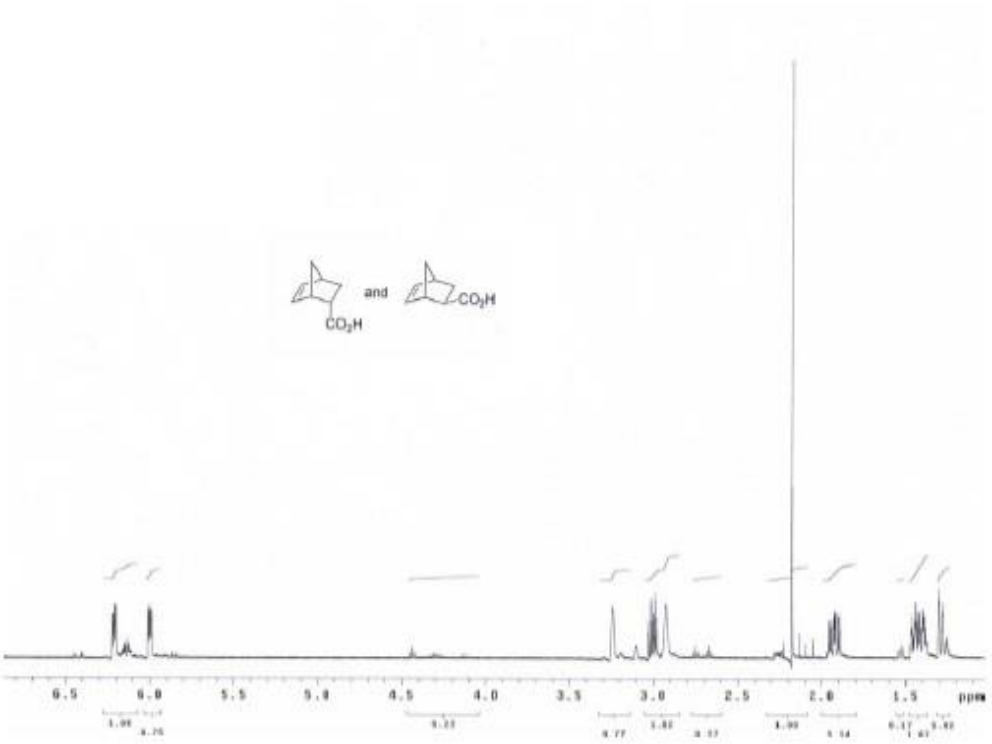

Figure 3.1: ^{1}H NMR spectrum of the mixture of the *endo* and *exo* isomers of bicyclo-[2.2.1]-hept-5-ene-2-carboxylic acid from Huertas *et al.*[84]

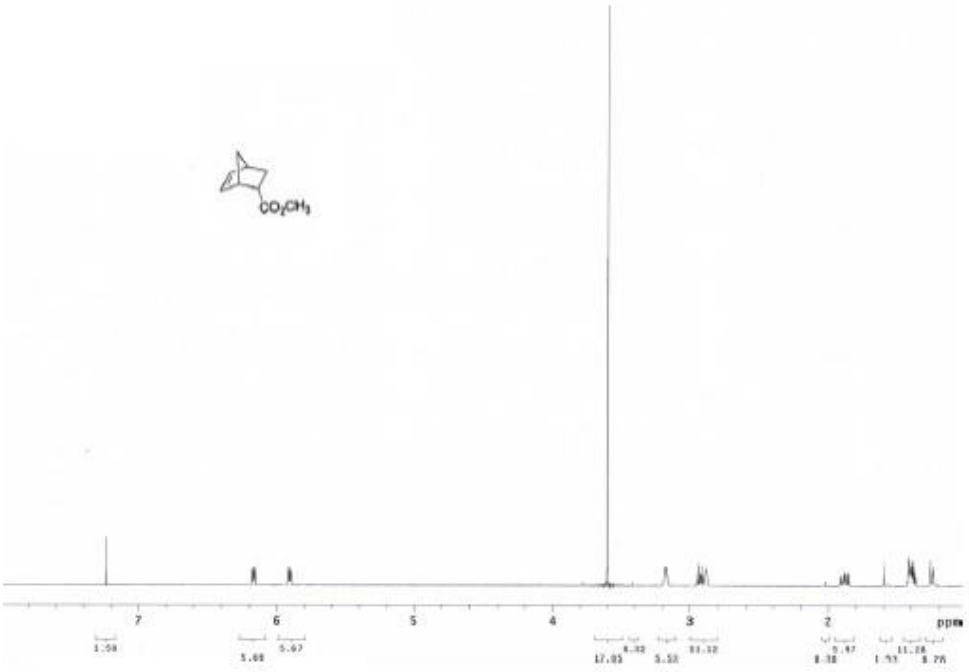

Figure 3.2: ^{1}H NMR spectrum of the pure *endo* isomer of methyl bicyclo-[2.2.1]-hept-5-ene-2-carboxylate in chloroform-d_3 from Huertas *et al.*[84]

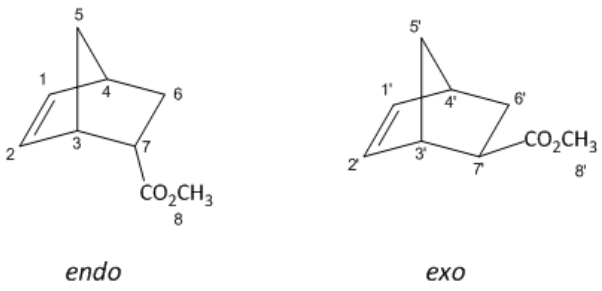

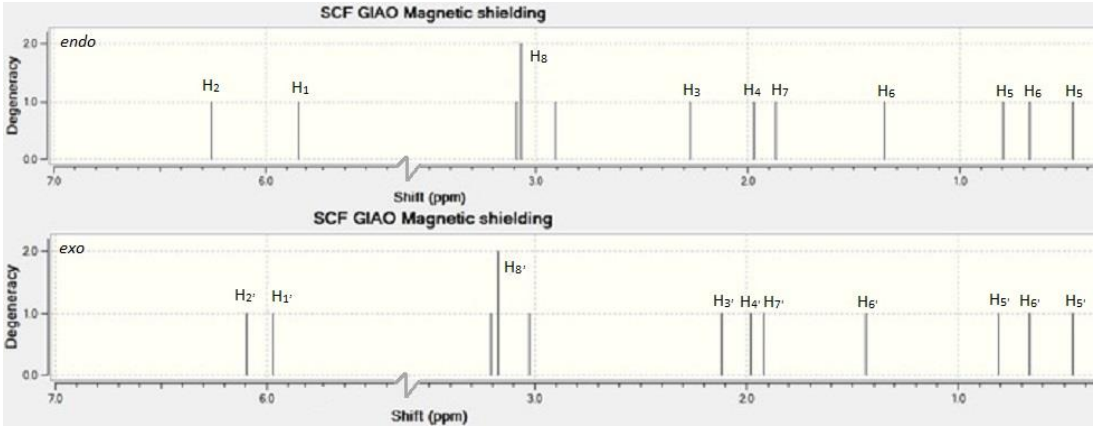

Figure 3.3: Predicted ^{1}H NMR spectra of the *endo* and *exo* isomers of methyl bicyclo-[2.2.1]-hept-5-ene-2-carboxylate.

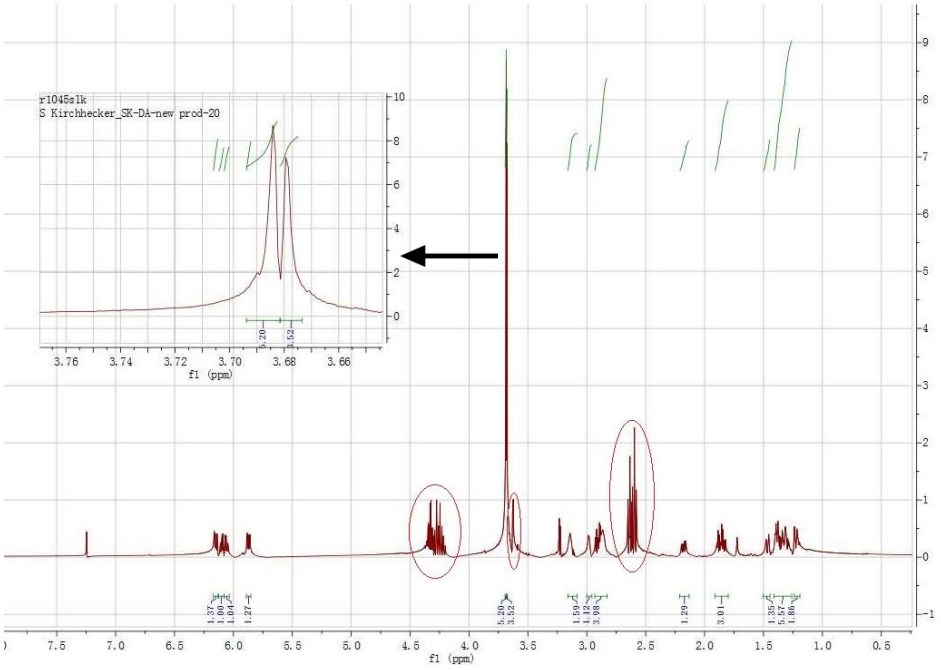

Figure 3.4: ^{1}H NMR spectrum of the product from *Method 1* which produced equivalent amount of each isomer, with peaks for unidentified impurities circled and peaks for H_8 and H_8' enlarged.

It can be observed (*Figure 3.5*) that the pure *endo* product from *Method 2* in water is clean, while the reaction in hexane gives a mixture with 29% of the *exo* isomer along with an unidentified singlet at 1.5 ppm. The product from the reactions in methanol and hexane appears adequately clean after separation according to *Figure 3.6 and 3.7*. The integration values of four quartets between 5.90 ppm and 6.20 ppm in *Figures 3.6* show the ratio of 29:1:1:29 (from right to left), indicating an *endo*-to-*exo* ratio 29:1 for the product in methanol after separation while the integration values of four quartets within the same range in *Figure 3.7* show the ratio of 23:10:10:23 (from right to left), indicating an *endo*-to-*exo* ratio 23:10 for the product in hexane after separation. Only two very small fractions with 74.1% and 83.3% of *exo* isomer were obtained from the reaction in hexane, which is not enough for the mass spectroscopy experiments.

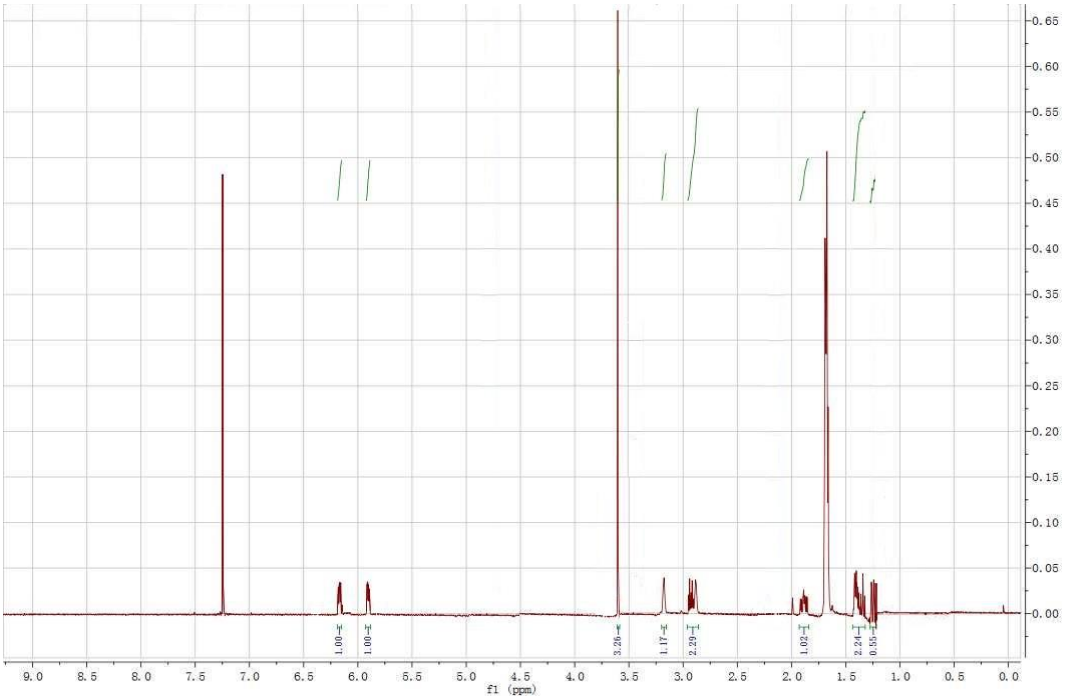

Figure 3.5: ^{1}H NMR spectrum of the product from the Diels-Alder reaction in water.

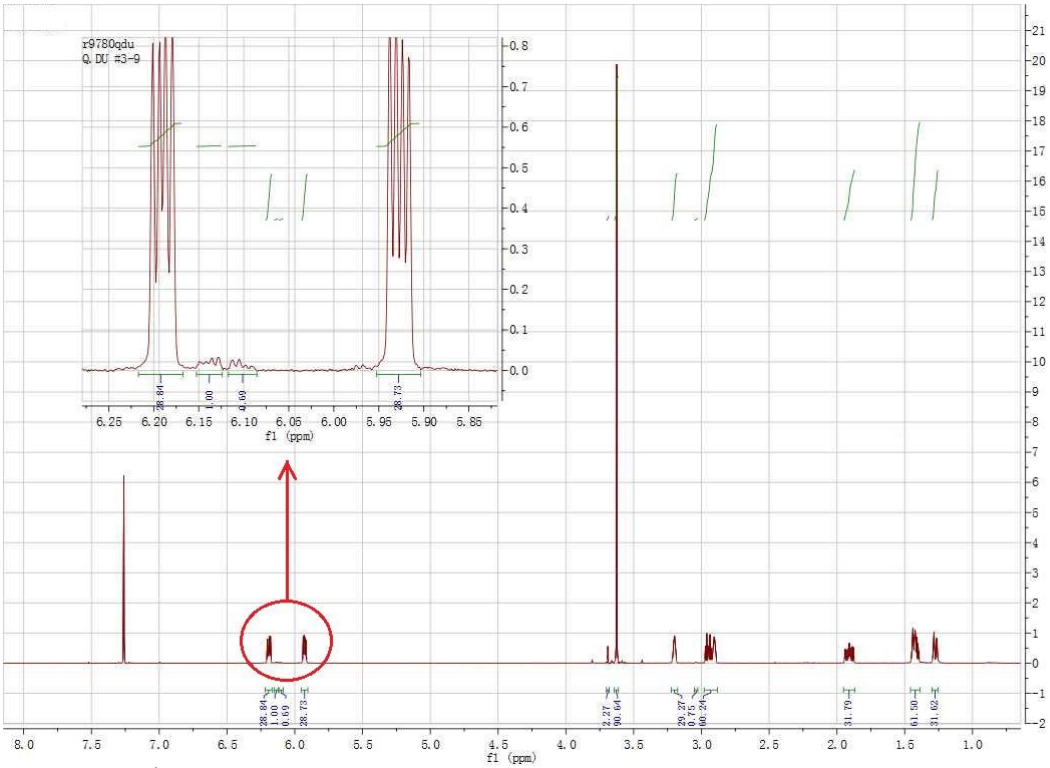

Figure 3.6: ^{1}H NMR spectrum of 97% *endo* product after separation from the Diels-Alder reaction in methanol with the peaks for vinylic hydrogens enlarged.

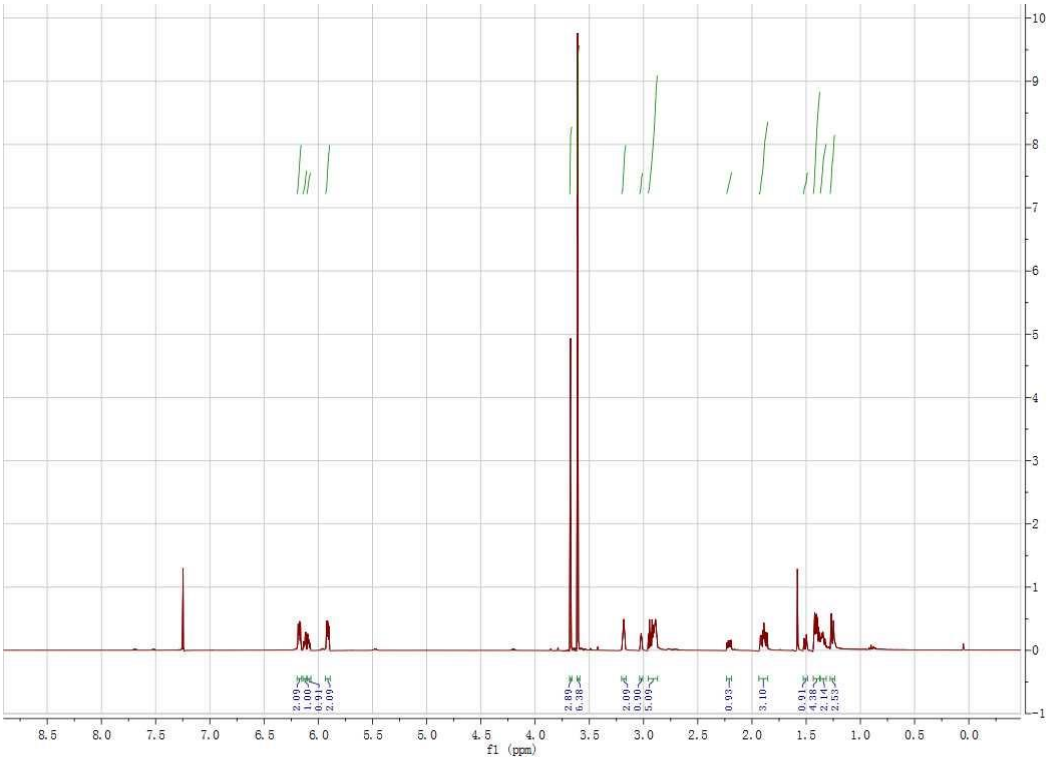

Figure 3.7: ^{1}H NMR spectrum of the product from the Diels-Alder reaction in hexane.

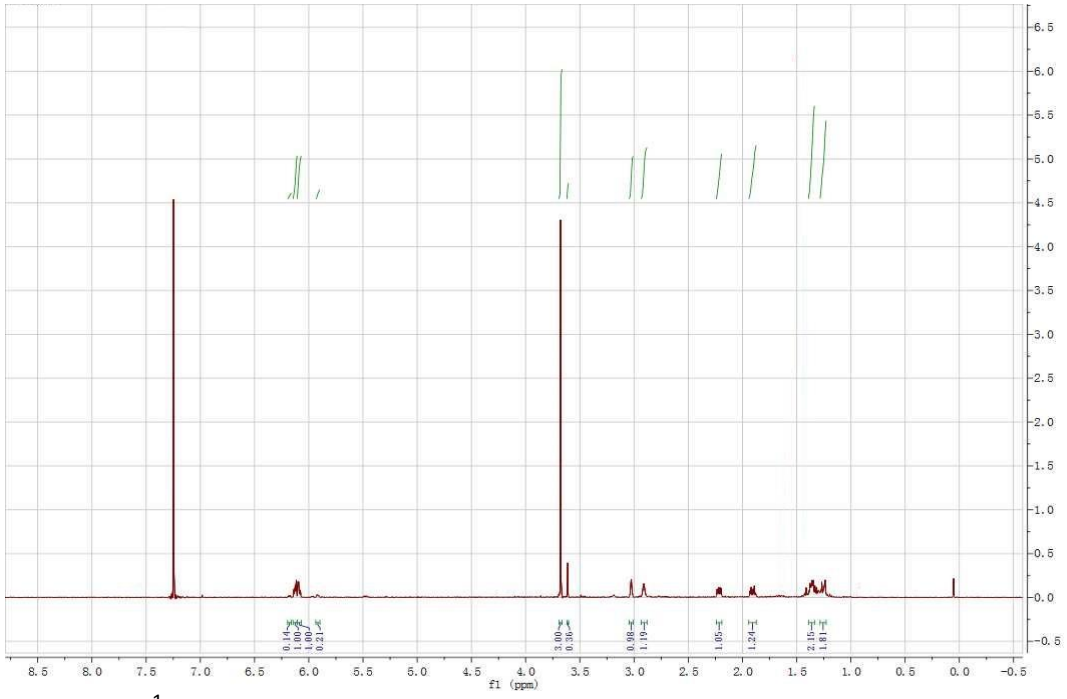

Figure 3.8: ^{1}H NMR spectrum of the 83.3% *exo* product after separation from the Diels-Alder reaction in hexane.

The reaction using *Method 3* gives 63.8% *endo* product with 14.9% of dicyclopentadiene impurities (*Figure 3.9*). All peaks for dicyclopentadiene were assigned and labelled above, with the signal representing one of the vinylic hydrogens (H_2) overlapping with the peak for a vinylic hydrogen of the *endo* isomer. The ^{1}H NMR spectrum of pure *exo* isomer is displayed in *Figure 3.10* showing a clean product.

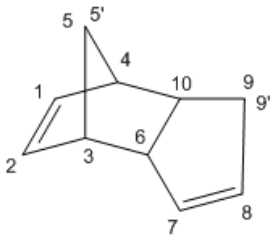

DCPD

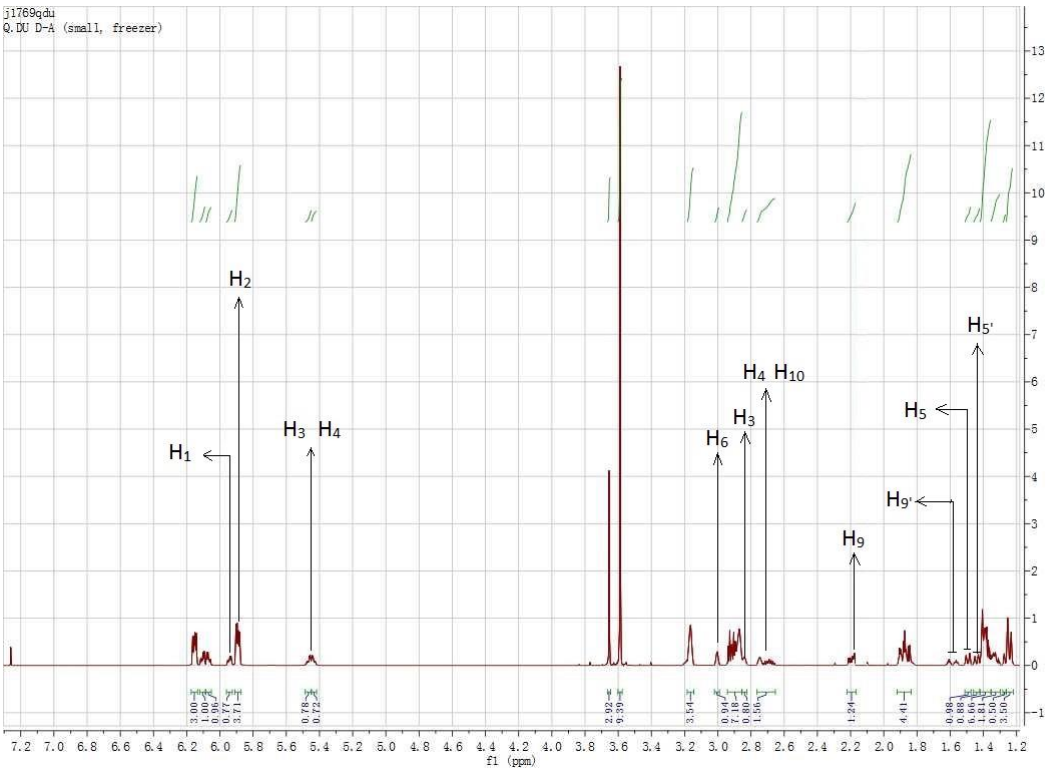

Figure 3.9: ^{1}H NMR spectrum of the product from the solvent-free Diels-Alder reaction, with all peaks for dicyclopentadiene impurities assigned and labelled above.

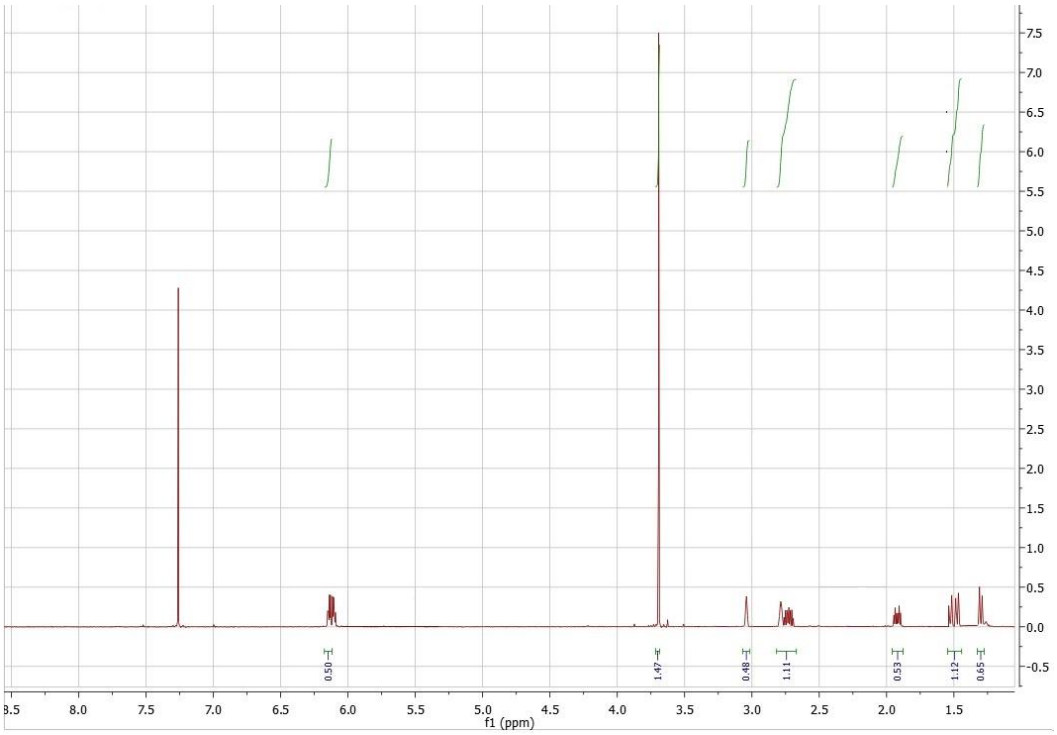

Figure 3.10: ^{1}H NMR spectrum of the pure *exo* product after separation from the solvent-free Diels-Alder reaction.

Table 3.1: Results of Diels-Alder reaction of methyl acrylate and cyclopentadiene under different conditions.

Method/Solvent	Conditions	Yield (%)	Ratio (%*endo)*	Separation results
Method 1	4 hrs/210 °C	63	54.5	-
Method 2 (in water)	72 hrs/25 °C	11	100	100% *endo*
Method 2 (in methanol)	72 hrs/25 °C	76	84.1	97% *endo*
Method 2 (in hexane)	72 hrs/25 °C	73	65.7	83.3% *exo*
Method 3	72 hrs/25 °C	87	63.8	100% *exo*

3.1.2 1-Ethyl-3-methylimidazolium tetrafluoroborate ([EMIM][BF_4])

A conventional method was used to synthesise [EMIM][BF_4]. Thus, bromoethane and 1-methylimidazole were stirred together overnight, after which an anion exchange procedure using hydroxide resin was conducted followed by adding tetrafluoroboric acid (HBF_4) and then stirring for 72 hours at room temperature. Once finished, the solution was washed and extracted with ethyl acetate and put under vacuum to remove the solvent and the last bit of 1-methylimidazole. The product was obtained as a yellow liquid.

The ^{1}H NMR spectrum of the product is shown in *Figure 3.11*, with all peaks assigned and labelled with relevant hydrogens. The peak in the lower field region at 8.6 ppm represents the most acidic hydrogen of the cation (H_1). Two hydrogens on the imidazolium ring (H_2, H_3) can be observed at 7.47 ppm and 7.31 ppm next to H_1. The ratio of these three hydrogens is 1:1:1 given by the integration values. The

peak that appears at 4.79 ppm is due to D_2O. The quartet at 4.21 ppm and the triplet at 1.47 ppm represent ethyl hydrogens (H_5, H_6), and the last peak at 3.89 ppm represents the methyl hydrogen H_4. The ^{19}F NMR spectrum (*Figure 3.12*) shows two chemical shifts, which correspond to $[^{10}BF_4]^-$ and $[^{11}BF_4]^-$ at -150.36 and -150.42 ppm, respectively. The two shifts arise because of the extreme sensitivity of ^{19}F to changes in its environment; the B-F couplings are, however, not resolved.

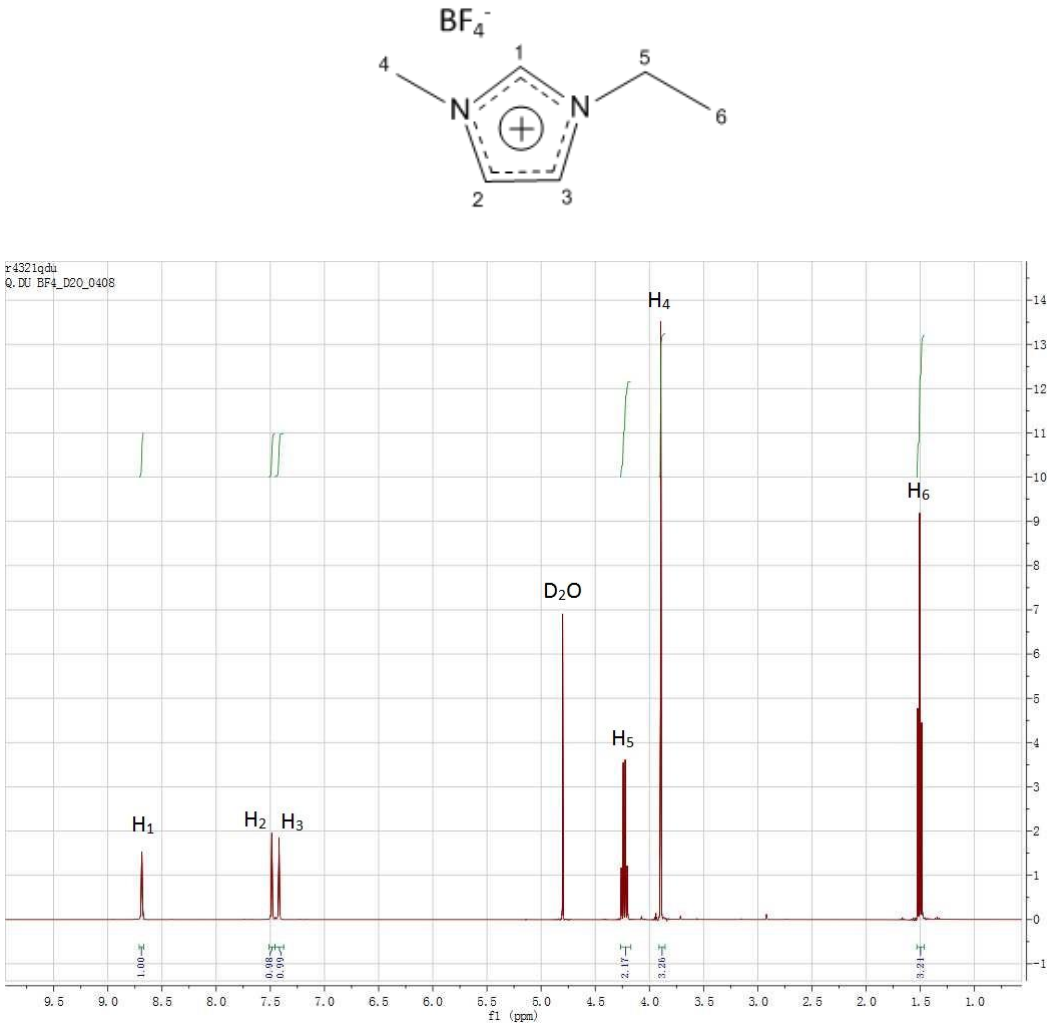

Figure 3.11: ^1H NMR spectrum of the product of [EMIM][BF_4] with each peak assigned and labelled above.

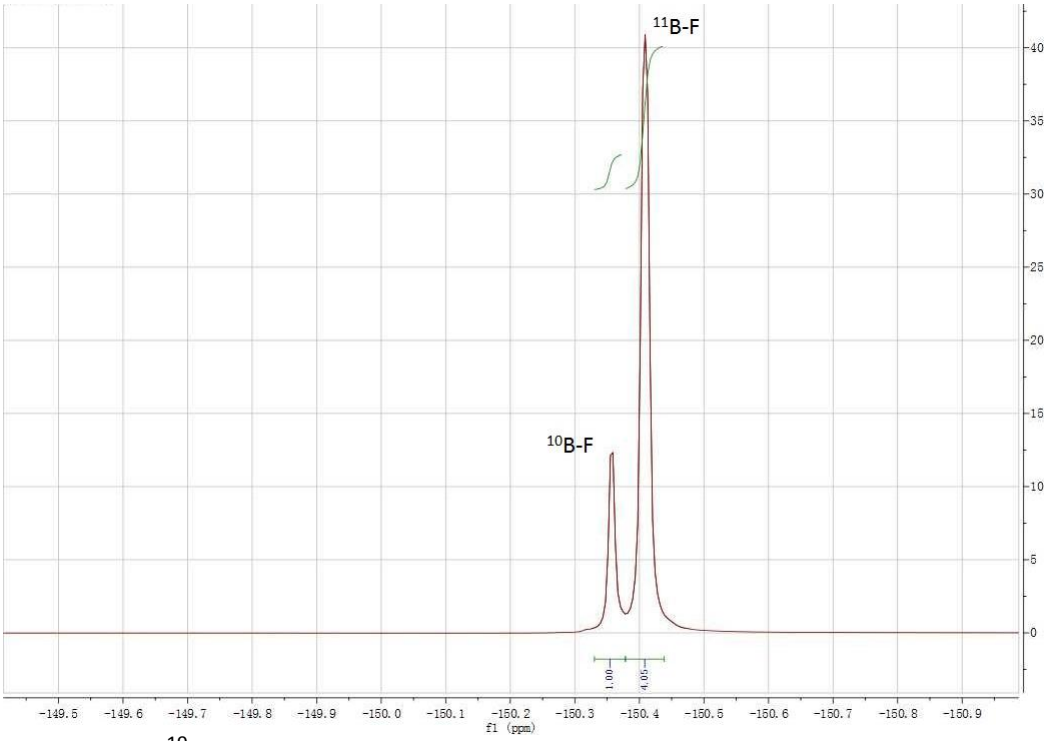

Figure 3.12: ^{19}F NMR spectrum of the product of [EMIM][BF_4] with each coupling peak assigned and labelled above.

3.1.3 1-Butyl-3-methylimidazolium tetrafluoroborate ([BMIM][BF_4])

A similar method to that for [EMIM][BF_4] was initially used for the synthesis of [BMIM][BF_4], namely reaction of 1-bromobutane with 1-methylimidazole, but this was found time-consuming and to give a relatively low yield. Hence a microwave-assisted method was carried out in which the reaction was complete in one hour, giving a clear semifluid with a good yield.[88]

According to the ^1H NMR spectrum of the product (*Figure 3.13*) with all hydrogens assigned to relevant peaks, the most acidic hydrogen of the cation (H_1) can be observed in the lower field region at 8.73 ppm, together with the other two hydrogens on the imidazolium-ring (H_2, H_3) at 7.46 ppm and 7.41 ppm with the ratio 1:1:1 given by the integration values. The butyl group appears as four main peaks, a triplet at 4.19 ppm (H_5), a doublet of doublet of doublets at 1.84 ppm (H_6), a triplet of quartets at 1.31 ppm (H_7) and a triplet at 0.92 ppm (H_8), and the

integration values provide the ratio 2:2:2:3. While the peak appearing at 4.79 ppm is the solvent peak of D_2O and the last peak at 3.93 ppm represents the methyl hydrogen H_4. The ^{19}F NMR spectrum also appears the same as with [EMIM][BF_4] (*Figure 3.12*).

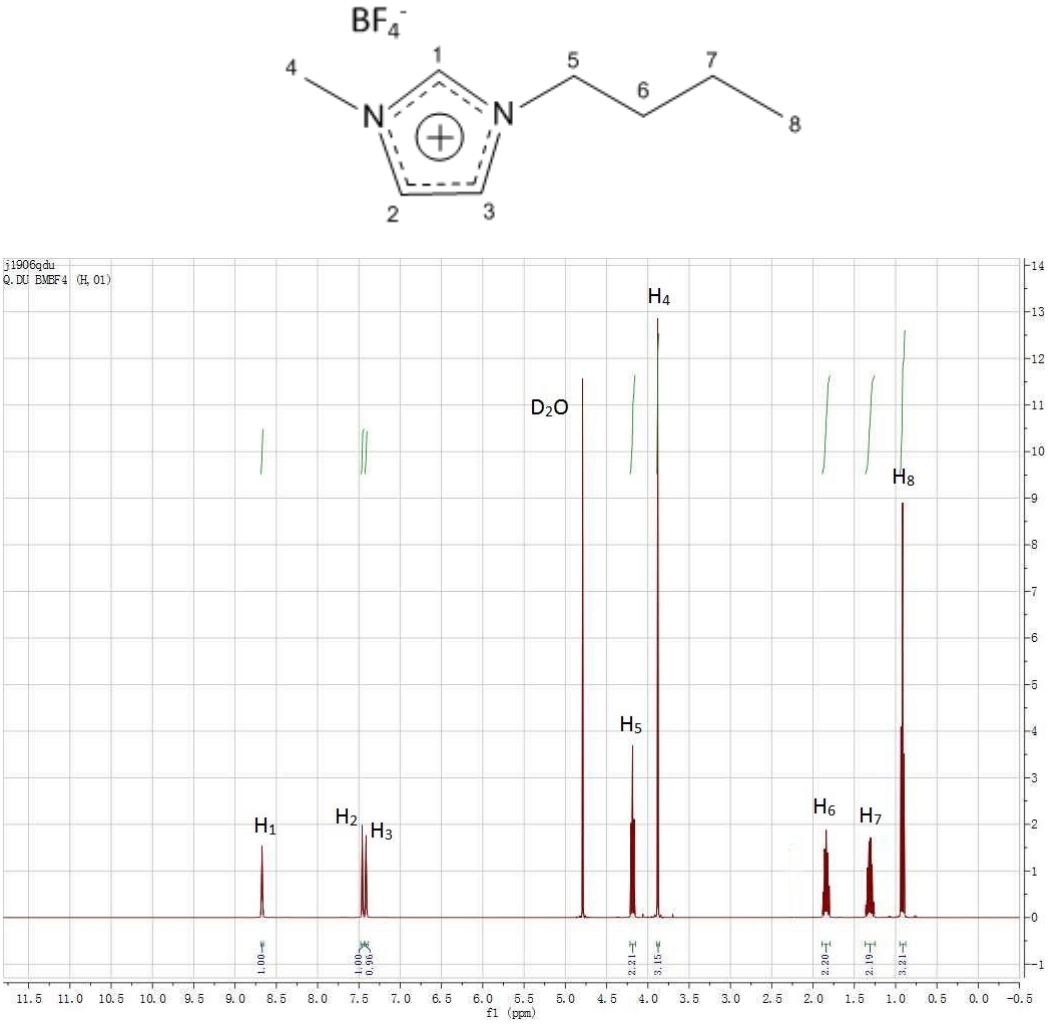

Figure 3.13: ^1H NMR spectrum of the product of [BMIM][BF_4] with each peak assigned and labelled above.

3.1.4 1-Dodecyl-3-methylimidazolium tetrafluoroborate ($[C_{12}MIM][BF_4]$)

First, tetrafluoroboric acid (2.63 cm^3, 0.02 mol, 48% solution in water) was added dropwise to a cooled, rapidly stirring solution of a mixture of 1-dodecyl-3-methylimidazolium chloride (5.18 g, 0.02 mol) in cold water (50 cm^3) over 15 min. The lower layer was collected *via* a separating funnel, dissolved in dichloromethane (100 cm^3) and then washed with cold water (3 x 100 cm^3). The organic layer was collected and dried using magnesium sulphate ($MgSO_4$).

For the synthesis of $[C_{12}MIM][BF_4]$, tetrafluoroboric acid (HBF_4) was slowly added to a rapidly stirring cold water solution of mixture of 1-dodecyl-3-methylimidazolium chloride ($[C_{12}MIM]Cl$) in 15 min, followed by extraction with dichloromethane and washing with cold water. The dichloromethane layer was collected and dried with $MgSO_4$ and then put under vacuum to remove the solvent. The product was obtained as a pale beige powder.

The ^1H NMR spectrum of the product is shown below (*Figure 3.14*). The peaks representing three hydrogens on the imidazolium ring (H_1, H_2 and H_3) appear at a similar position (8.81, 7.44 and 7.40 ppm)as labelled in the spectrum with the same order and ratio obtained by the integration values comparing to $[EMIM][BF_4]$ and $[BMIM][BF_4]$. The peak of the solvent D_2O appears at 4.79 ppm. The multiplet peaks of hydrogens on the ten methylene groups (H_6) connected with the terminal methyl group overlap at 1.25 ppm. Two methyl groups can be observed at 3.85 ppm (H_4) and 0.67 ppm (H_3), respectively. The last hydrogens (H_5) on the methylene can be found at 4.16 ppm. The ^{19}F NMR spectrum again appears the same as for $[EMIM][BF_4]$ (*Figure 3.12*).

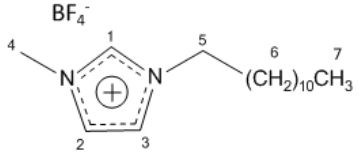

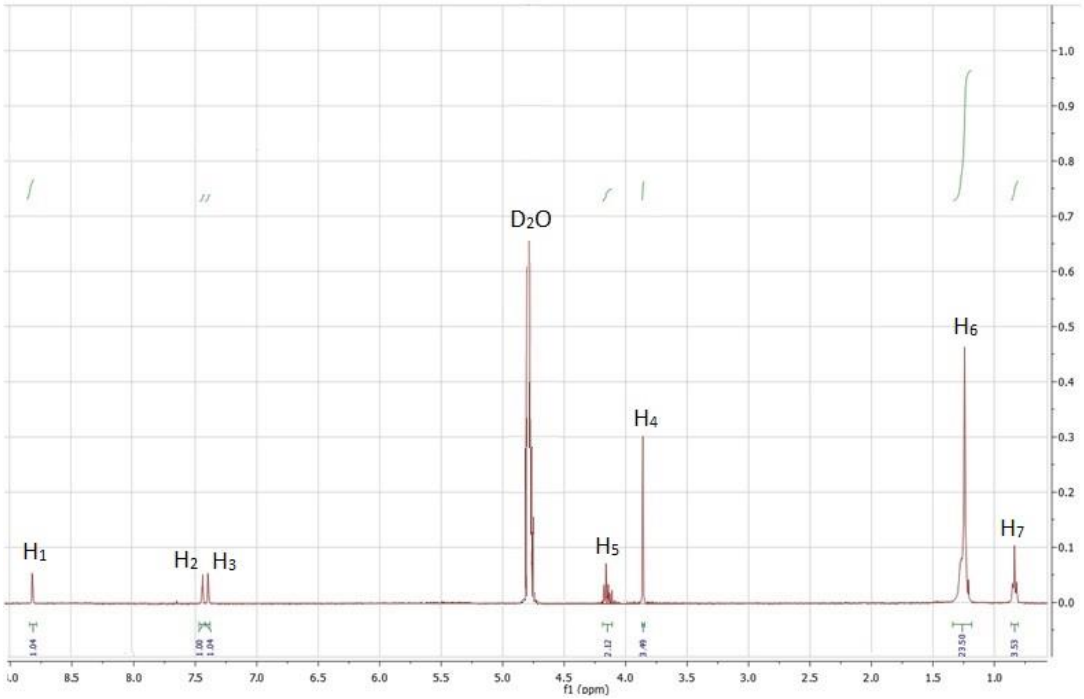

Figure 3.14: ^{1}H NMR spectrum of the product of $[C_{12}MIM][BF_4]$ with each peak assigned and labelled above.

3.2 Mass Spectrometry results

Experiments using mass spectrometry were carried out to investigate directly the complexation behaviour of imidazolium ionic liquids ($[C_nMIM][BF_4]$, n = 2, 4, 12) with different species involved in the Diels-Alder reaction between methyl acrylate and cyclopentadiene. All the results presented here were obtained in positive ion mode from on the mass spectrometer, started from 100 m/z for $[EMIM][BF_4]$ and $[BMIM][BF_4]$ and 200 m/z for $[C_{12}MIM][BF_4]$. Experiments in negative mode to investigate the interaction between the BF_4^- anion and the reactants and products from the same Diels-Alder reaction were also conducted, but no relevant peaks (*e.g.* BF_4^-▪reactant and BF_4^-▪isomer) were found in the primary mass spectrometry. However, because of lack of time, unfortunately the spectrum data in negative mode were not analysed for further proof of other impurities such as Br^- at 79/80, which will be discussed in future work. This can happen if the interactions between BF_4^- and the reactants and products are very weak. Thus, further fragmentation and CID works for the BF_4^- clusters were not included.

3.2.1 Methyl bicyclo-[2.2.1]-hept-5-ene-2-carboxylate Isomers

The positive ion mode electrospray ionisation mass spectra (ESI-MS) of methanol solutions of the 97% *endo* isomer and the 100% *exo* isomer of methyl bicyclo-[2.2.1]-hept-5-ene-2-carboxylate are exhibited in *Figure 3.15*. The peaks for the two pronated isomers are clearly visible as dominant peaks, while tiny peaks represent the Diels-Alder reactants *i.e.* methyl acrylate and cyclopentadiene with protons can also be observed, which may be caused by the slight decomposition of the isomers during the process of generating ions in gas phase.

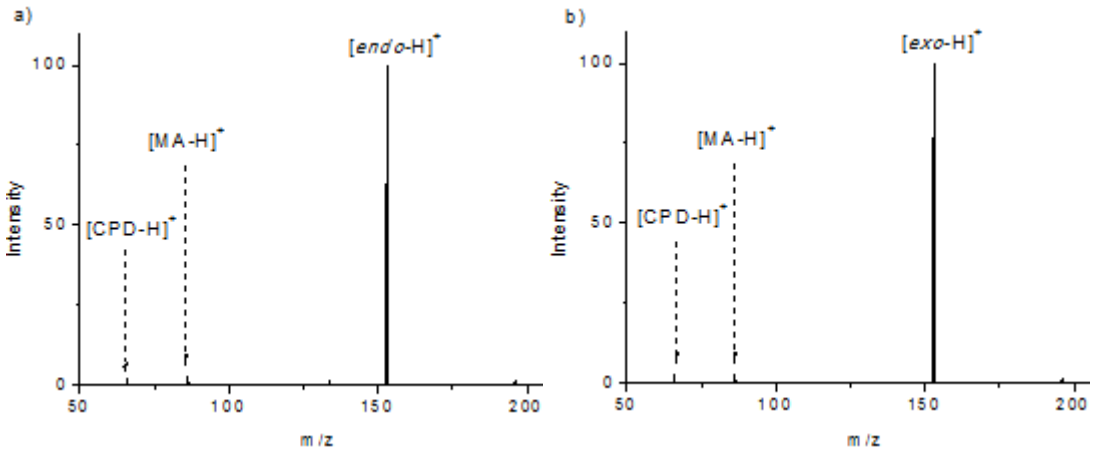

Figure 3.15: Positive ion mode ESI-MS spectra for a) the *endo* isomer of methyl bicyclo-[2.2.1]-hept-5-ene-2-carboxylate and b) the *exo* isomer of methyl bicyclo-[2.2.1]-hept-5-ene-2-carboxylate.

Fragmentation mass spectra were obtained by isolating the parent ions and fragmenting them by collision-induced dissociation with helium molecules within the quadrupole ion trap. *Figure 3.16* shows the fragmentation mass spectra of the *endo* and *exo* isomers of methyl bicyclo-[2.2.1]-hept-5-ene-2-carboxylate. It can be clearly observed that both isomers produced fragment ions of methyl acrylate and cyclopentadiene, which are the reactants of the Diels-Alder reaction in this study,

indicating that there is a *retro* Diels-Alder reaction when performing CID on the products.

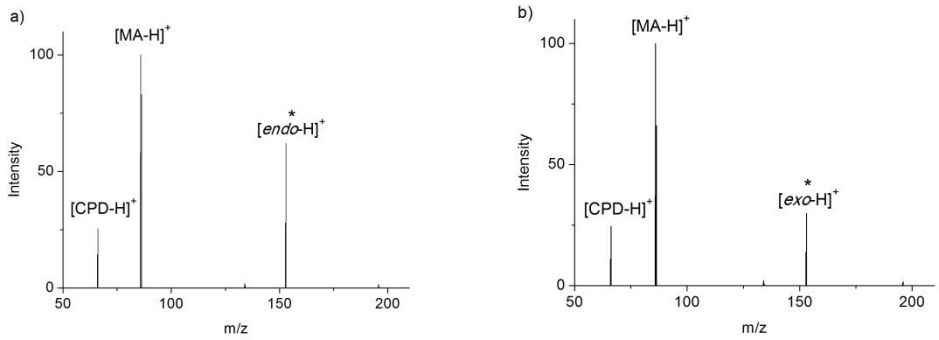

Figure 3.16: Fragmentation mass spectra for a) the *endo* isomer at 6.8% collision energy and b) the *exo* isomer at 6.4% collision energy. Precursor ions are marked with *.

3.2.2 $[EMIM]^+$ Clusters

Figure 3.17 displays the positive ion mode ESI-MS of methanol solutions of 1-ethyl-3-methylimidazolium tetrafluoroborate ([EMIM][BF_4]) with the Diels-Alder reactants and products, methyl acrylate (MA), cyclopentadiene (CPD), *endo* and *exo* isomers of methyl bicyclo-[2.2.1]-hept-5-ene-2-carboxylate. Peaks resulting from adducts of Diels-Alder reactants and products with $[EMIM]^+$, $[EMIM]^+$▪[N] (N = MA, CPD, *endo* or *exo*) can be clearly observed in the mass spectra, though all of the spectra are dominated by the ionic liquid cluster peaks of $[EMIM]_3^{3+}$▪$[BF_4]^-$, $[EMIM]_2^{2+}$▪$[BF_4]^-$ as well as the $[EMIM]^+$ cation resulting from the [EMIM][BF_4] ionic liquid, which appeared the same for solutions with different ratios of the [EMIM][BF_4] ionic liquid and the Diels-Alder reactants and products. By comparing the ESI-MS of the two isomers with [EMIM][BF_4] (*Figure 3.17c* and *d*), it is easy to see that the *endo* isomer can form clusters with either one or two $[EMIM]^+$ cation(s), while the *exo* isomer can only form a cluster with one cation. This suggests that the interaction of the cation with the *endo* isomer may be stronger than with the *exo* isomer. The four adducts are expected to form hydrogen bonds to the C_2 hydrogen on the $[EMIM]^+$ cation within these clusters.

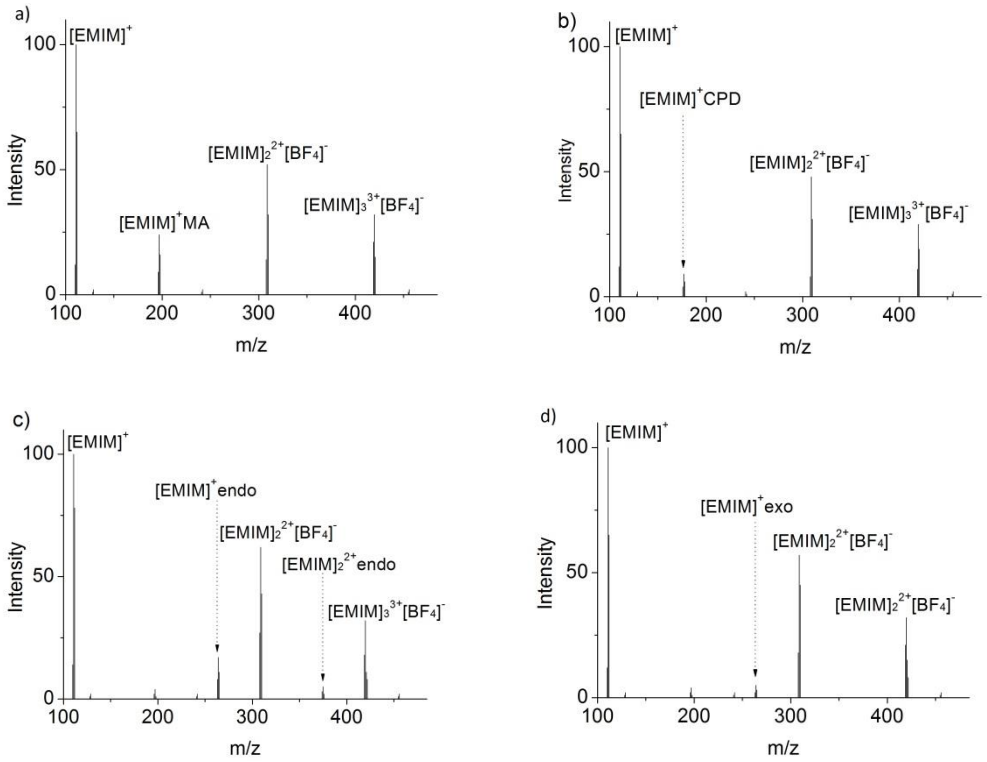

Figure 3.17: Positive ion mode ESI-MS spectra for the solutions of the [EMIM][BF_4] ionic liquid with a) MA, b) CPD, c) the *endo* isomer of methyl bicyclo-[2.2.1]-hept-5-ene-2-carboxylate and d) the *exo* isomer of methyl bicyclo-[2.2.1]-hept-5-ene-2-carboxylate.

Figure 3.18 shows the fragmentation mass spectra of the clusters observed from the positive ion mode ESI-MS above (*i.e.* the $[EMIM]^+$ cation with methyl acrylate, cyclopentadiene, the *endo* or *exo* isomer of methyl bicyclo-[2.2.1]-hept-5-ene-2-carboxylate and double $[EMIM]_2^{2+}$ with the *endo* isomer). Some small fragment peaks appeared during the isolation of the cluster, which means that these species are metastable.[119] For those clusters containing one $[EMIM]^+$ cation (*Figure 3.18 a-d*), there is only one fragmentation channel that can be found which can be described as the dissociation of the neutral part from the cluster, giving the bare $[EMIM]^+$ cation as the only ionic fragment, *[3.1]*.

$$[\mathrm{EMIM}]^+ \cdot [\mathrm{N}] \rightarrow [\mathrm{EMIM}]^+ + [\mathrm{N}] \qquad [\mathbf{3.1}]$$

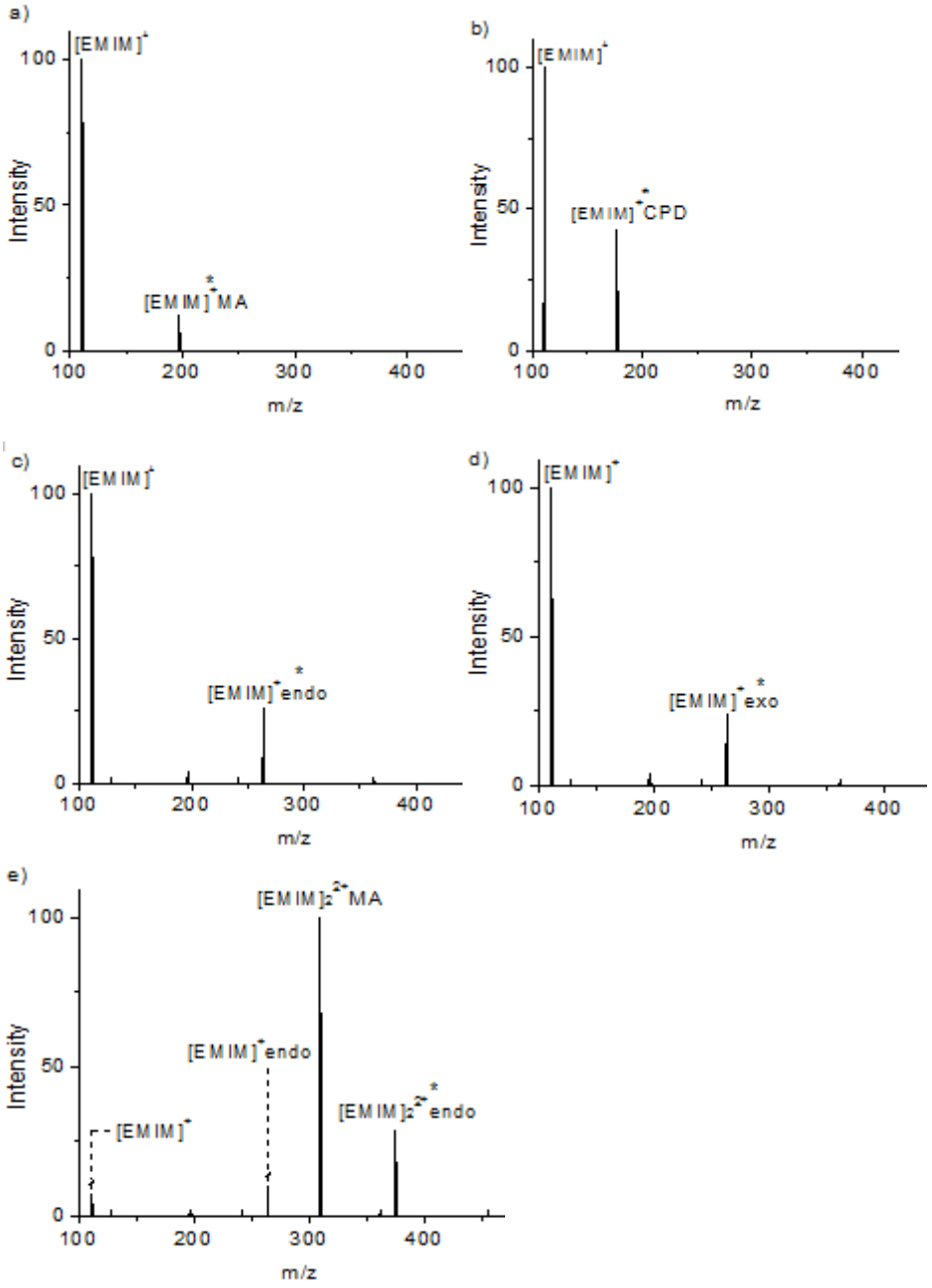

Figure 3.18: Fragmentation mass spectra for the clusters of $[EMIM]_n^{n+}$▪[N] (*n* = 1, 2), where a) N = MA at 9.0% collision energy, b) N = CPD at 6.0% collision energy, c) N = *endo* isomer at 10.8% collision energy, d) N = *exo* isomer at 4.0% collision energy and e) N = *endo* isomer at 8.0% collision energy. Precursor ions are marked with *.

The $[EMIM]_2^{2+}$▪*endo* cluster containing two $[EMIM]^+$ cations (*Figure 3.18 e*) fragments into the $[EMIM]_2^{2+}$▪MA fragment ion, which undergoes a *retro* Diels-Alder reaction and returns to the reactants, losing the cyclopentadiene molecule *[3.2a]*. Then at higher collision energies, two other peaks corresponding to the

$[EMIM]^+$ and the $[EMIM]^+$▪*endo* product ions are observed. The $[EMIM]^+$▪*endo* ion must be produced from the precursor ion *[3.2b]* while the fragmentation to give $[EMIM]^+$ cation could occur through two possible pathways: either straightforwardly from the precursor ion *[3.2c]*, or from the $[EMIM]^+$▪*endo* ion through a secondary fragmentation process *[3.2d]*.

$$[\mathrm{EMIM}]_2{}^{2+} \cdot endo \rightarrow [\mathrm{EMIM}]_2{}^{2+} \cdot \mathrm{MA} \qquad [\mathbf{3.2a}]$$

$$[\mathrm{EMIM}]_2{}^{2+} \cdot endo \rightarrow [\mathrm{EMIM}]^+ \cdot endo \qquad [\mathbf{3.2b}]$$

$$[\mathrm{EMIM}]_2{}^{2+} \cdot endo \rightarrow [\mathrm{EMIM}]^+ \qquad [\mathbf{3.2c}]$$

$$[\mathrm{EMIM}]^+ \cdot endo \rightarrow [\mathrm{EMIM}]^+ \qquad [\mathbf{3.2d}]$$

Table 3.2: Fragment ions observed upon CID of the $[EMIM]_n{}^{n+}$▪[N] clusters, where N = MA, CPD, *endo*, *exo*, *n* = 1, 2

m/z	**Precursor Ion**	**Product Ions** [a, b]
197.3	$[EMIM]^+$▪MA	$[EMIM]^+$
177.3	$[EMIM]^+$▪CPD	$[EMIM]^+$
263.4	$[EMIM]^+$▪*endo*	$[EMIM]^+$
374.5	$[EMIM]_2{}^{2+}$▪*endo*	$[EMIM]_2{}^{2+}$▪MA, $[EMIM]^+$▪*endo*, $[EMIM]^+$
263.4	$[EMIM]^+$▪*exo*	$[EMIM]^+$

[a)] Product ions are reported with the most intensive ions listed first.

[b)] The fragmentation behaviours under different source conditions (*e.g.* source temperature) were observed the same as above but with comparatively lower intensities.

From a theoretical aspect, both oxygens on the carboxylate group can accommodate up to four bare hydrogens to form hydrogen bonds by the double lone electron pairs on each oxygen, but normally it is unlikely for the non-carbonyl oxygen to form hydrogen bonds. This is because the π electrons from the C=O double bond together with the electrons from each lone electron pair on another

oxygen are delocalised to form a delocalised π bond, which will weaken the nucleophilicity of the oxygen connected with alkyl group while the carbonyl oxygen has a stronger electronegativity. Though in most cases there is actually one hydrogen bond formed by the carbonyl oxygen due to steric hindrance, it is still possible for methyl acrylate and the two product isomers (*i.e. endo* and *exo* methyl bicyclo-[2.2.1]-hept-5-ene-2-carboxylate) to form two relatively weak hydrogen bonds with two $[EMIM]^+$ cations, while only the $[EMIM]_2^{2+}$▪*endo* precursor ion was observed in the experiments conducted here. The reason for the $[EMIM]_2^{2+}$▪*exo* cluster being unobserved can be attribute to the fact that the *exo* isomer is disfavoured by $[EMIM][BF_4]$ (*i.e. endo* selectivity of ILs), and one possible explanation for methyl acrylate is that there might be intermolecular hydrogen bonding interactions between methyl acrylate molecules, which stabilise or destabilise the different cluster to different extents.

There are two possible structures for the $[EMIM]_2^{2+}$▪*endo* cluster: either the carbonyl oxygen in the *endo* isomer forms two hydrogen bonds with the C_2 hydrogens of the $[EMIM]^+$ cations (*Figure 3.19a*) by two lone electron pairs, or the carboxylate group coordinates with two imidazolium rings by the interaction between distributed positive and negative charges (*Figure 3.19b*). While the imidazolium ring of the $[EMIM]^+$ cation is indeed formally aromatic as there are six delocalised π electrons and thus has an evenly distributed positive charge, and the delocalised π bond across the two oxygens in the carboxylate group has nucleophilicity, it is potential to form structure ***b*** by the mutual attraction between the positive and negative charges. It should be noted that these structures of clusters with more than one imidazolium cations were postulated based on the electron distribution and hydrogen bonding mechanism described above, and further *ab initio* calculations on these clusters are expected to be conducted to support this.

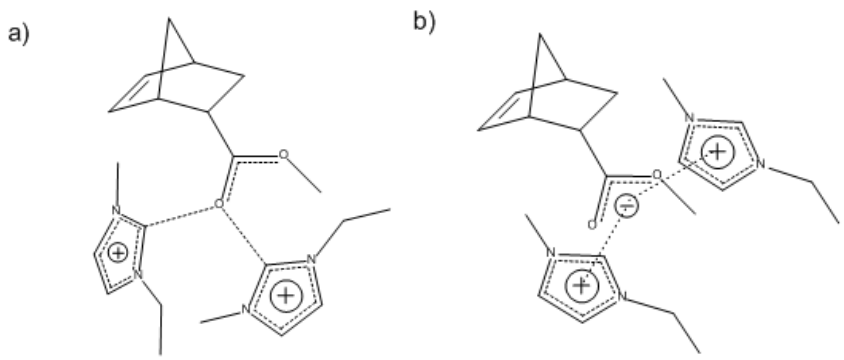

Figure 3.19: Postulated structures for the $[EMIM]_2^{2+}$▪*endo* cluster, of which a) the carbonyl oxygen coordinating with C_2 hydrogens of $[EMIM]^+$ cations by hydrogen binding interaction and b) the $[EMIM]^+$ cations coordinating with the *endo* isomer by interaction between delocalised positive and negative charges.

3.2.3 $[BMIM]^+$ Clusters

Figure 3.20 illustrates the positive ion mode ESI mass spectra obtained from a series of similar mixtures of 1-butyl-3-methylimidazolium tetrafluoroborate ($[BMIM][BF_4]$) with Diels-Alder reactants and products, methyl acrylate (MA), cyclopentadiene (CPD), *endo* and *exo* isomers of methyl bicyclo-[2.2.1]-hept-5-ene-2-carboxylate. Peaks corresponding to Diels-Alder reactant and product adduct clusters with the $[BMIM]^+$ cation are clearly visible in the mass spectra. The mass spectra were all dominated by peaks for the $[BMIM]^+$ cation and the $[BMIM]_n^{n+}$▪$[BF_4]^-$ (n = 1, 2) clusters. This observation remains the same when changing the ratio of the $[BMIM][BF_4]$ ionic liquid and Diels-Alder reactants and isomers. The mixture of the $[BMIM][BF_4]$ ionic liquids and the *endo* isomer appears to produce a set of $[BMIM]_n^{n+}$▪*endo* clusters, while the other molecules investigated only generated $[BMIM]^+$▪[N] clusters (*i.e.* N = MA, CPD or *exo* isomer)

$[BMIM]^+$ is larger than $[EMIM]^+$ with greater steric bulk on the side chain. This means that it can be more likely for multiple $[BMIM]^+$ cations to gather together and coordinate with one *endo* isomer compared to the $[EMIM]^+$ system. Furthermore, the longer alkyl side chain in $[BMIM]^+$ may make it more stable in the

gas phase due to its lower electron density and could provide adequate ions in the trap, which explains the higher formation of the $[BMIM]_n^{n+}$▪*endo* clusters.

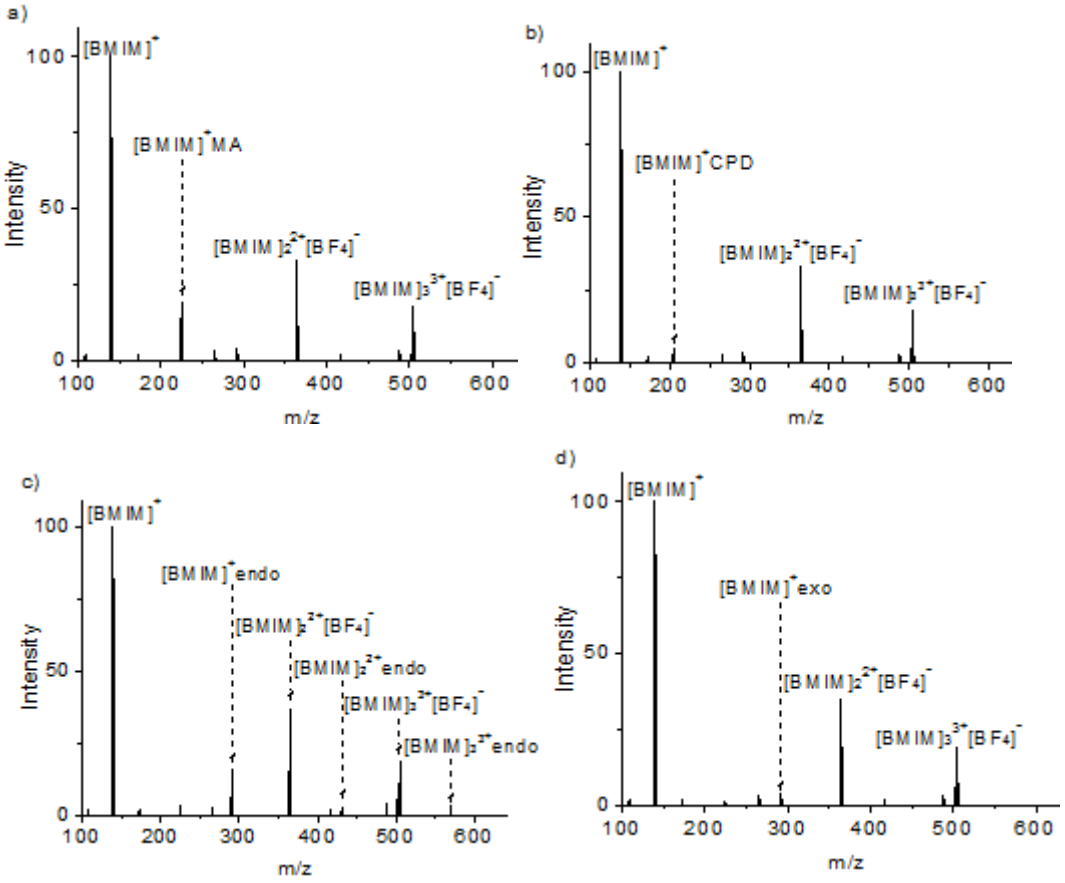

Figure 3.20: Positive ion mode ESI-MS spectra for the solutions of [BMIM][BF_4] ionic liquid with a) MA, b) CPD, c) the *endo* isomer of methyl bicyclo-[2.2.1]-hept-5-ene-2-carboxylate and d) the *exo* isomer of methyl bicyclo-[2.2.1]-hept-5-ene-2-carboxylate.

Figure 3.21 displays the positive mode fragmentation spectra of the 1:1 $[BMIM]^+$▪[N] parent clusters, which fragmented in a similar way to the $[EMIM]^+$▪[N] clusters. Only one fragmentation channel was observed, involves the loss of a single neutral [N] particle, leaving a bare $[BMIM]^+$ cation.

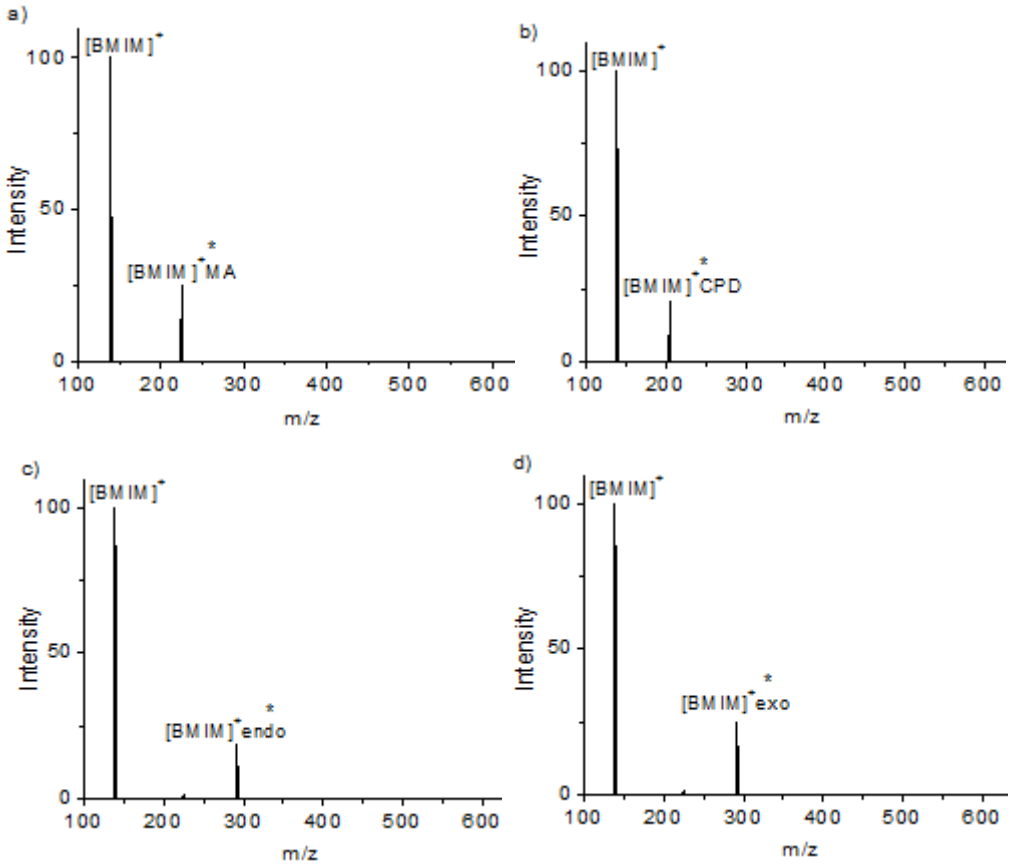

Figure 3.21: Fragmentation mass spectra for the $[BMIM]_n^{n+}$▪[N] (*n* = 1, 2) cluster ions, where a) N = MA at 7.3% collision energy, b) N = CPD at 6.8% collision energy, c) N = *endo* isomer at 15.6% collision energy, d) N = *exo* isomer at 6.0% collision energy. Precursor ions are marked with *.

The fragmentation mass spectra of the $[BMIM]_n^{n+}$▪*endo* (n = 2, 3) clusters are shown in *Figure 3.22.* In the primary fragmentation pathway of the $[BMIM]_2^{2+}$▪*endo* cluster *[3.3a]* it did not produce the $[BMIM]_2^{2+}$▪MA cluster, which appears to be different from the $[EMIM]_2^{2+}$▪*endo* cluster, indicating that the complexation of methyl acrylate and cyclopentadiene in the [BMIM][BF_4] to produce *endo* isomer might be stronger than in the [EMIM][BF_4] ionic liquid. Another possible reason for not seeing the $[BMIM]_2^{2+}$▪MA cluster is that, the cations with long alkyl chain associated to each other to put the isomer in the middle, and to some extent prevent the isomer from decomposition. Then when given higher energies, $[BMIM]^+$ cation was able to be observed. This fragmentation pathway could happen through the two different mechanisms suggested for the $[EMIM]_2^{2+}$▪*endo* cluster

above: all the $[BMIM]^+$ cations dissociate from the precursor ion either at the same time *[3.3b]* or sequentially *[3.3c]*.

$$[BMIM]_2{}^{2+} \cdot endo \rightarrow [BMIM]^+ \cdot endo \qquad [\mathbf{3.3a}]$$

$$[BMIM]_2{}^{2+} \cdot endo \rightarrow [BMIM]^+ \qquad [\mathbf{3.3b}]$$

$$[BMIM]_2{}^{2+} \cdot endo \rightarrow [BMIM]^+ \cdot endo \rightarrow [BMIM]^+ \qquad [\mathbf{3.3c}]$$

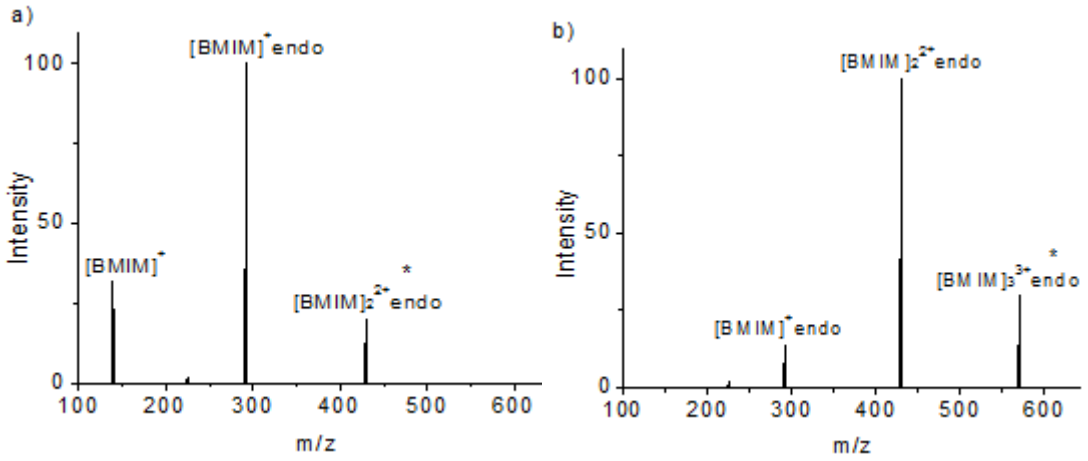

Figure 3.22: Fragmentation mass spectra for the clusters of a) $[BMIM]_2{}^{2+}$▪*endo*, at 8.5% collision energy, b) $[BMIM]_3{}^{3+}$▪*endo* at 6.8% collision energy. Precursor ions are marked with *.

The $[BMIM]_3{}^{3+}$▪*endo* cluster produces the $[BMIM]_2{}^{2+}$▪*endo* fragment readily at a relatively low collision energy (onset 2.8% collision energy) and then produces a small amount of the $[BMIM]^+$▪*endo* fragment ion when the energy is increased (from 4.8% collision energy), which indicates that the way one of the three $[BMIM]^+$ cations coordinates with the *endo* isomer might be different from the way in which the other two coordinate. One significant difference between the fragmentation of the $[BMIM]_3{}^{3+}$▪*endo* cluster and all the other clusters is it did not produce the bare $[BMIM]^+$ cation upon collisional excitation.

One possible conformation of the $[BMIM]_3^{3+}$▪*endo* cluster is illustrated in *Figure 3.23.* Two $[BMIM]^+$ cations form hydrogen bonds with the carbonyl oxygen of the *endo* isomer by two pairs of lone electrons on the oxygen, with the third one forming a weaker interaction with the negatively charged delocalised π bond *via* the evenly distributed positive charge on the imidazolium ring. Again this structure of the $[BMIM]_3^{3+}$▪*endo* cluster was postulated based on the electron distribution and hydrogen bonding mechanism described above, and would be consistent with the fragmentation behaviour described above. Further *ab initio* calculations for this cluster are also needed to be conducted in future work.

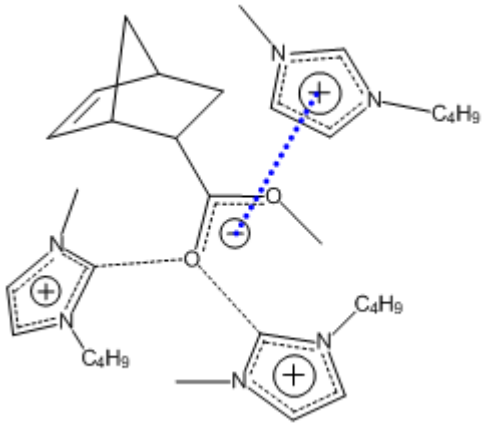

Figure 3.23: Potential conformation for the $[BMIM]_3^{3+}$▪*endo* cluster, with the C_2 hydrogens of two $[BMIM]^+$ cations attached to the carbonyl oxygen by hydrogen bonds (present with regular dashed lines) and the positively charged imidazolium ring of one $[BMIM]^+$ attracted by delocalised negative charge on the carboxylate group (present with bold dashed line).

Table 3.3: Fragment ions observed upon CID of the $[BMIM]_n^{n+}$▪[N] clusters. N = MA, CPD, *endo*, *exo*, *n* = 1-2

m/z	Precursor Ion	Product Ions [a, b]
225.3	$[BMIM]^+$▪MA	$[BMIM]^+$
205.3	$[BMIM]^+$▪CPD	$[BMIM]^+$
291.4	$[BMIM]^+$▪*endo*	$[BMIM]^+$
430.6	$[BMIM]_2^{2+}$▪*endo*	$[BMIM]^+$▪*endo*, $[BMIM]^+$
569.9	$[BMIM]_3^{3+}$▪*endo*	$[BMIM]_2^{2+}$▪*endo*, $[BMIM]^+$▪*endo*
291.4	$[BMIM]^+$▪*exo*	$[BMIM]^+$

[a)] Product ions are reported with the most intensive ions listed first.

[b)] The fragmentation behaviours under different source conditions (*e.g.* source temperature) were observed the same as above but with comparatively lower intensities.

3.2.4 $[C_{12}MIM]^+$ Clusters

Figure 3.24 displays the positive mode ESI mass spectra of analogous mixtures of the 1-dodecyl-3-methylimidazolium tetrafluoroborate ($[C_{12}MIM][BF_4]$) ionic liquid with the same group of Diels-Alder reactants and products, methyl acrylate (MA), cyclopentadiene (CPD), the *endo* and *exo* isomers of methyl bicyclo-[2.2.1]-hept-5-ene-2-carboxylate. From the ESI-MS, it can be clearly seen that only peaks resulting from the clusters of methyl acrylate and the *endo* isomer with one $[C_{12}MIM]^+$ ion are obtained, with all of the ESI-MS being dominated by the $[C_{12}MIM]_3^{3+}$▪$[BF_4]^-$ and $[C_{12}MIM]_2^{2+}$▪$[BF4]^-$ clusters along with the $[C_{12}MIM]^+$ cation from the $[C_{12}MIM][BF_4]$ ionic liquid, the observation of which was the same for solutions with different ratio of the $[C_{12}MIM][BF_4]$ ionic liquid and the Diels-Alder reactant and products. Unlike the $[EMIM]^+$ and $[BMIM]^+$ clusters, the $[C_{12}MIM]^+$ cation has a considerably longer alkyl chain, which to some extent can be considered to block the contact between the methyl acrylate, cyclopentadiene or the *endo* and *exo* isomers with the imidazolium cation. Thus, the chance to form $[C_{12}MIM]^+$ clusters is reduced. According to the mass spectra, cyclopentadiene and the *exo* isomer did not complex with the $[C_{12}MIM]^+$ cation, and the intensities of $[C_{12}\ MIM]^+$▪*endo* and $[C_{12}$

MIM]$^+$▪MA clusters are also relatively low compared to the previously studied ionic liquids.

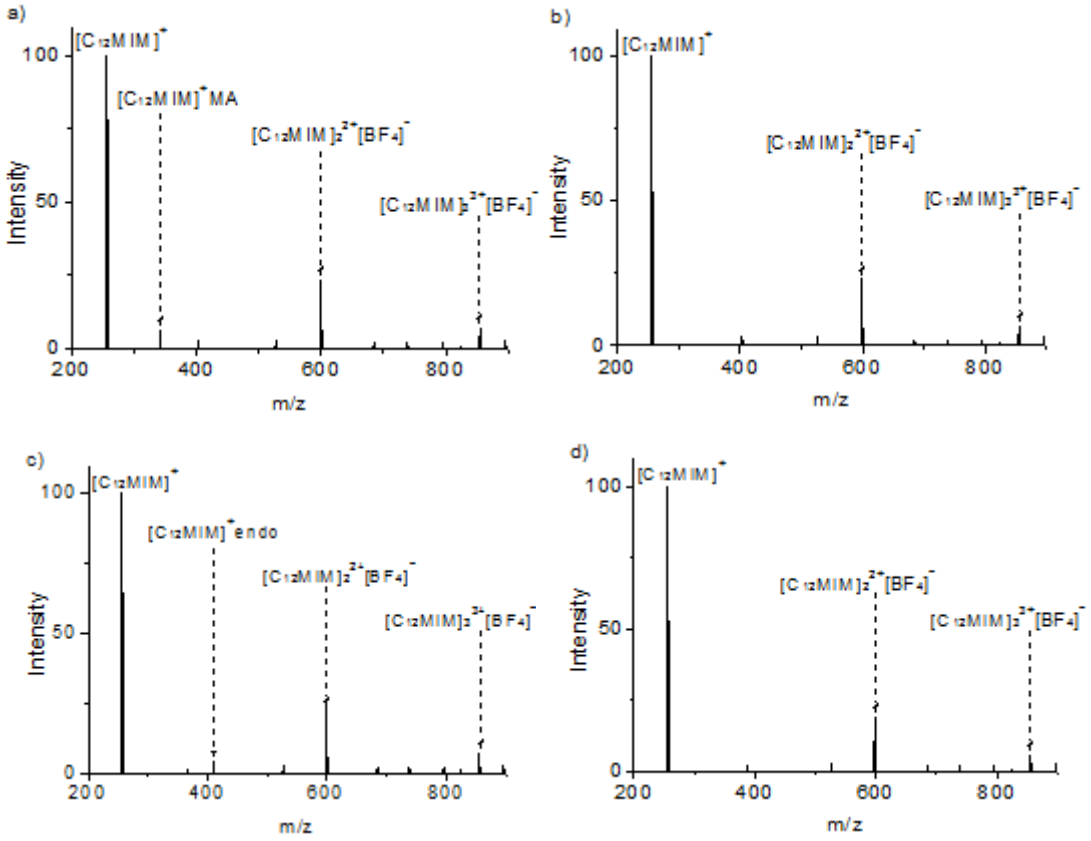

Figure 3.24: Positive ion mode ESI-MS spectra for the solutions of the $[C_{12}MIM][BF_4]$ ionic liquid with a) MA, b) CPD, c) the *endo* isomer of methyl bicyclo-[2.2.1]-hept-5-ene-2-carboxylate and d) the *exo* isomer of methyl bicyclo-[2.2.1]-hept-5-ene-2-carboxylate.

The fragmentation behaviours of the observed clusters are quite similar to the 1:1 ratio clusters studied above, in which the uncharged methyl acrylate or the *endo* isomer dissociate from the cluster and produce bare $[C_{12}MIM]^+$ cations as the only cationic product ion.

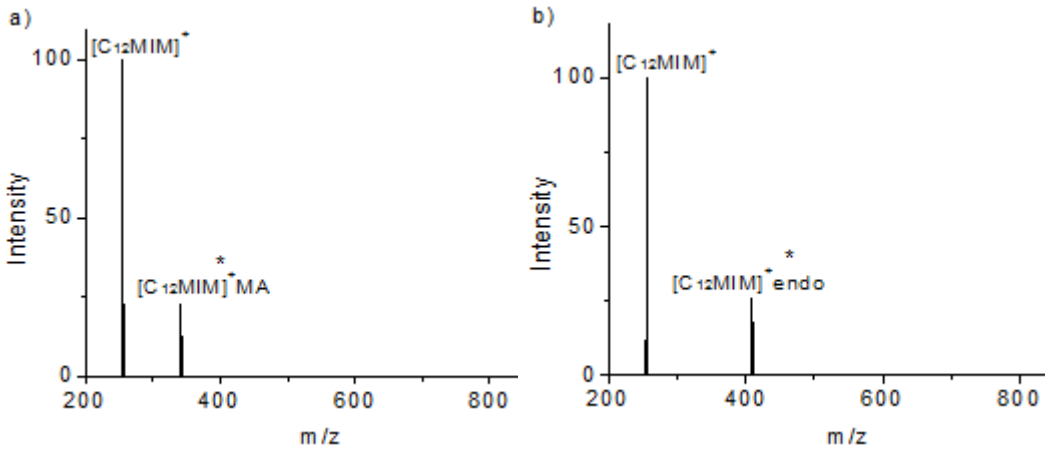

Figure 3.25: Fragmentation mass spectra for the clusters of a) $[C_{12}MIM]^+$▪MA, at 3.6% collision energy and b) $[C_{12}MIM]^+$▪*endo* at 4.9% collision energy. Precursor ions are marked with *.

Table 3.4: Fragment ions observed upon CID of the $[C_{12}MIM]^+$▪[N] clusters. N = MA and *endo*.

m/z	Precursor Ion	Product Ions [a, b]
337.5	$[C_{12}MIM]^+$▪MA	$[C_{12}MIM]^+$
403.6	$[C_{12}MIM]^+$▪*endo*	$[C_{12}MIM]^+$

[a)] Product ions are reported with the most intensive ions listed first.

[b)] The fragmentation behaviours under different source conditions (*e.g.* source temperature) were observed the same as above but with comparatively lower intensities.

3.2.5 Comparisons of Fragmentation Energies

Normally, chemical reactions occur during collisions, with bonds being broken and reformed. Not all collisions result in reactions, yet the collision energy must exceed the activation energy, also known as the height of the energy barrier, with the right orientation of the reactants to make the reaction happen. The higher the energy barrier is, the more energy will be needed for a reaction to occur, meaning the more stable the reactants are. Thus, in order to compare the relative barrier heights for fragmentation of the clusters, it is necessary to compare the fragmentation energies of the clusters from the various studies. This can be achieved by plotting the relative intensities of the signals in the fragmentation MS

relating to the parent and fragment ions against collision energy which are quoted as "% CID energy" (*i.e.* the percentage of the maximum resonance excitation voltage) in this study, where 100% represents the maximum end cap voltage (2.50 V) of the mass spectrometer. Typical experimental errors obtained from at least three repeat runs on the same day for each cluster were ±2%. Error bars are presented on the curves of parent ions in *Figures a* in each system (*i.e.* the isomers, $[EMIM]_n^{n+}$, $[BMIM]_n^{n+}$ and $[C_{12}MIM]^+$ systems). The collision energy at which the relative intensity of the precursor ion reaches 50% is hereafter referred to as $E_{1/2}$. The clusters containing the *endo* isomer could be easily isolated with adequate parent ions to create good quality CID curves, but the other clusters, especially for the $[C_{12}MIM]^+$ system and those containing cyclopentadiene particles, need much more repeated work on mass selection and CID stages to make sure the ion intensity is high enough to allow for the CID curves being plotted.

In addition to this, it was found that the ionic liquids become stickier in the mass spectrometer with longer alkyl chain, which may be caused by the steric interactions between the very long chains, leading to the association of the cations. This means there might be residual $[BMIM]^+$ cations and even more $[C_{12}MIM]^+$ cations in the mass spectrometer after the sample running out (*e.g.* within the desolvation capillary) which will remain in the machine for a relatively long time. Therefore, further experiments were carried out in the order of $[EMIM]^+$ clusters, $[BMIM]^+$ clusters and then $[C_{12}MIM]^+$ clusters, with the machine inlet washed several times between works on the $[BMIM]^+$ and $[C_{12}MIM]^+$ clusters. To obtain reliable comparisons of the CID fragmentation curves, it is necessary to obtain data for different systems close in time *i.e.* on the same day.[120, 121] Typically, for comparing the fragmentation energies a maximum difference of mass-to-charge ratio of up to 100 a.u. is required.[110] For the systems studied here all of the clusters are within the m/z 100 a.u. limit of each other, meaning that they can be compared directly.

CID curves for the *endo* and *exo* isomers of methyl bicyclo-[2.2.1]-hept-5-ene-2-carboxylate are displayed in *Figure 3.26*, from which it can be seen that the two fragments *i.e.* methyl acrylate and cyclopentadiene were generated simultaneously from the *endo* isomer at 4.4% collision energy and from the *exo* isomer at 3.6% collision energy, with the fragmentation energy of the *exo* isomer being slightly lower ($E_{1/2}$ = 5.6%) than the *endo* isomer ($E_{1/2}$ = 6.4%), indicating that the barrier height for fragmentation on the potential energy surface of the *exo* isomer is lower than the *endo* isomer. This means it is harder for methyl acrylate and cyclopentadiene to form the *exo* conformation than the *endo* isomer, which is consistent with the fact that the Diels-Alder reaction naturally gives a product dominated by the *endo* isomer.

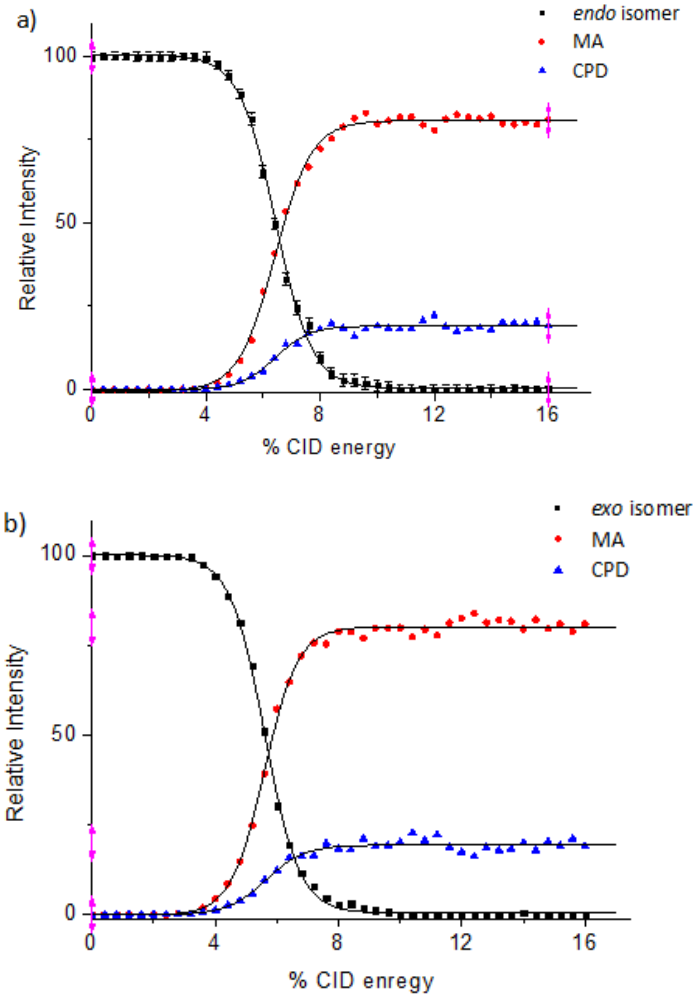

Figure 3.26: % CID curves for a) the *endo* isomer of methyl bicyclo-[2.2.1]-hept-5-ene-2-carboxylate and b) the *exo* isomer of methyl bicyclo-[2.2.1]-hept-5-ene-2-carboxylate.

CID fragmentation curves for the $[EMIM]^+$▪reactants clusters are shown in *Figure 3.27 a-b*. Both precursor clusters of the two complexes appeared stable across the low-energy CID excitation range, indicating that these clusters do not undergo metastable decay prior to resonance excitation.[122] The stabilities of each cluster can be compared by comparing the fragmentation energies. While both methyl acrylate and cyclopentadiene can be coordinated with the $[EMIM]^+$ cation， the $E_{1/2}$ value for $[EMIM]^+$▪MA (8.0%) was found to be much higher than for $[EMIM]^+$ ▪CPD (5.6%). This can be attributed to the different coordinating manner of the two reactants with the imidazolium ring. Methyl acrylate has a carbonyl oxygen group with a strong electronegativity which can form hydrogen bonds with the acidic C_2 hydrogen on the imidazolium ring, while cyclopentadiene can only form a weaker connection with the imidazolium ring by π-π stacking in accordance with their similar ring structures.[123] In addition, the low fragmentation energy of $[EMIM]^+$▪CPD indicates that although cyclopentadiene has a reactive methylene group, it has not reacted with the double carbon bond on $[EMIM]^+$ in the cluster to create stable single bonds.

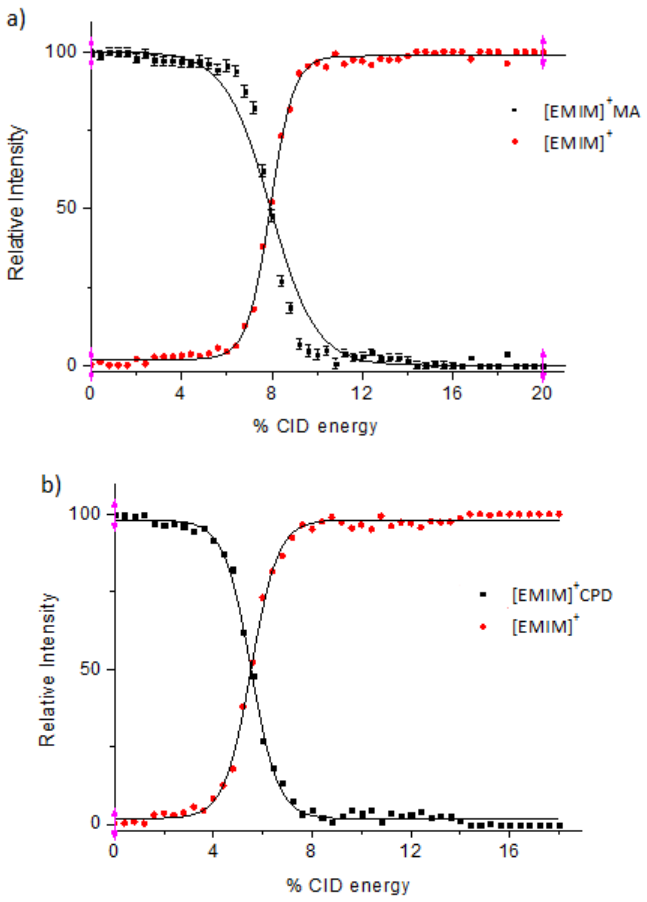

Figure 3.27 (a-b): % CID curves for the $[EMIM]^+$▪reactant clusters, for a) $[EMIM]^+$▪MA and b) $[EMIM]^+$▪CPD. Typical experimental errors were ±2% with error bars presented on the precursor curve of the $[EMIM]^+$▪MA cluster.

Figure 3.27 (c-e) displays the CID fragmentation curves for the $[EMIM]^+$▪*endo*, $[EMIM]^+$▪*exo* and $[EMIM]_2^{2+}$▪*endo* clusters. Comparison can first be made between the $[EMIM]^+$ clusters (*Figure 3.27 c-d*) to investigate the stabilities of $[EMIM]^+$ with different isomers. It can be easily observed that there is significant difference between the dissociation energies of the $[EMIM]^+$▪*endo* cluster ($E_{1/2}$ = 10.1%) and the $[EMIM]^+$▪*exo* cluster ($E_{1/2}$ = 3.6%), showing that the interaction between $[EMIM]^+$ and the *endo* isomer can be considerably strong, while the *exo* isomer is relatively disfavoured by the $[EMIM]^+$ cation. For the $[EMIM]_2^{2+}$▪*endo* cluster (*Figure 3.27 e*), the onset curves clearly illustrate that the loss of a single cyclopentadiene unit first appears at lower collision energies, followed by the loss of one $[EMIM]^+$ cation to give a $[EMIM]^+$▪*endo* fragment and the appearance of the single $[EMIM]^+$ cation in succession at relatively higher fragmentation energies. The

dissociation energy of the $[EMIM]_2^{2+}$▪*endo* cluster (7.9%) is comparatively lower than the $[EMIM]^+$▪*endo* cluster (10.1%), which means that the coordination formed by the *endo* isomer with two $[EMIM]^+$ cations is weaker than with just one.

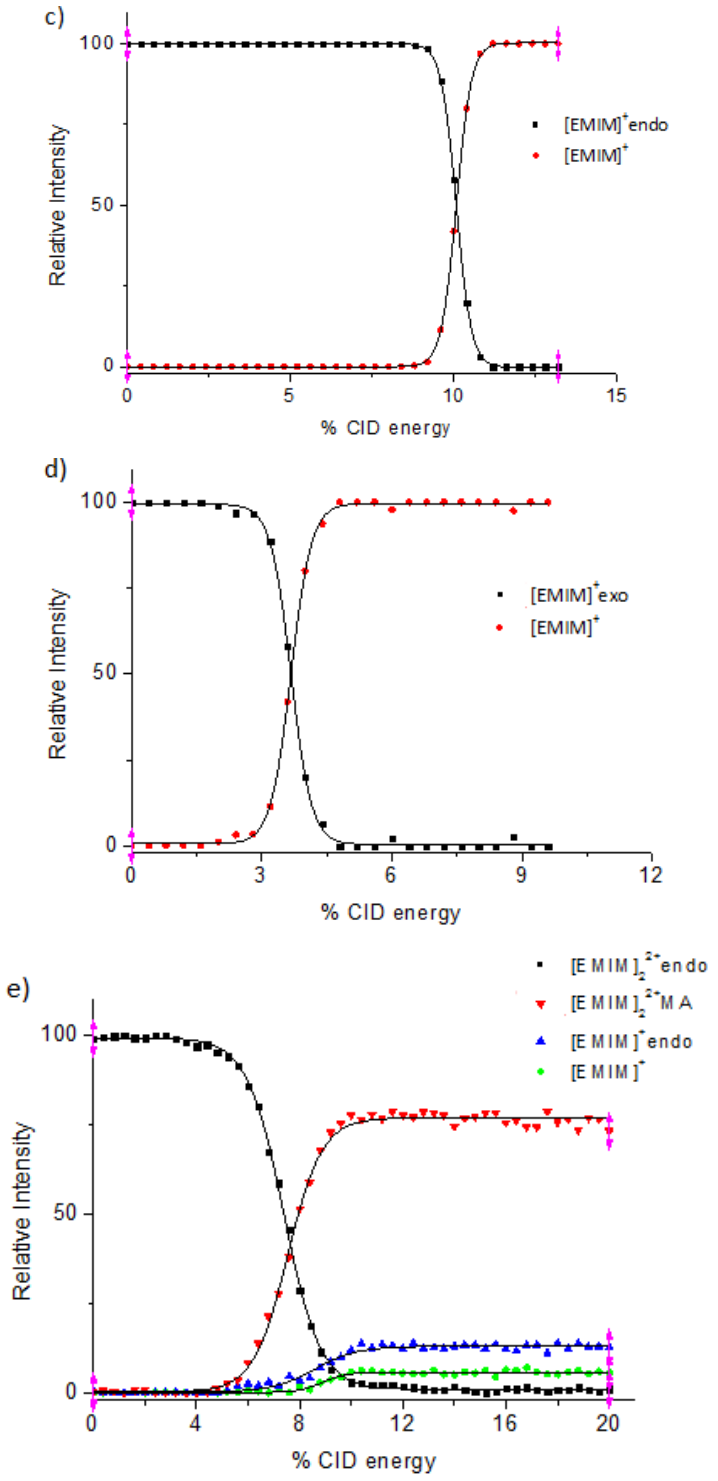

Figure 3.27 (c-e): % CID curves for the c) $[EMIM]^+$▪*endo*, d) $[EMIM]^+$▪*exo* and e) $[EMIM]_2^{2+}$▪*endo* clusters.

CID fragmentation curves for the $[BMIM]^+$▪reactant clusters are displayed in *Figure 3.28 (a-b)*. Similar to what was observed with the $[EMIM]^+$▪reactant clusters, the $E_{1/2}$ value of the $[BMIM]^+$▪MA cluster (8.5%) appears higher than the $[BMIM]^+$▪CPD cluster (6.0%), which can be explained by the same reason as described for the $[EMIM]^+$▪reactant analogues above.

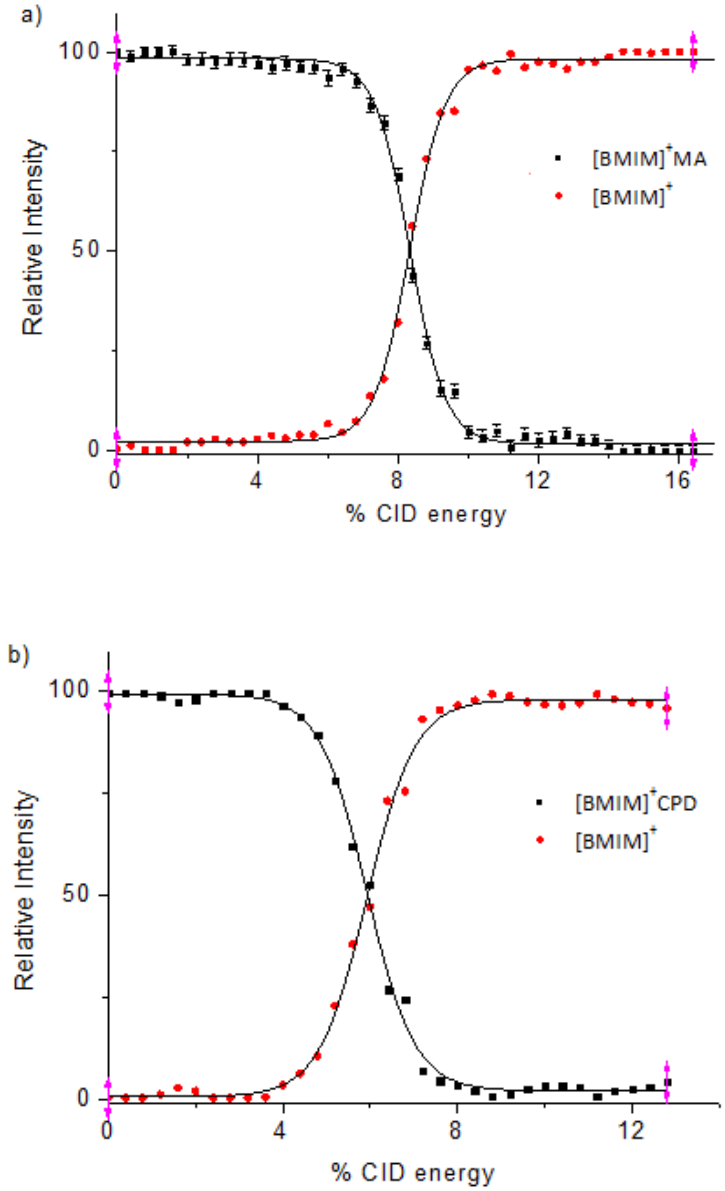

Figure 3.28 (a-b): % CID curves for the $[BMIM]^+$▪reactant clusters, where a) $[BMIM]^+$▪MA, b) $[BMIM]^+$▪CPD. Typical experimental errors were ±2% with error bars presented on the precursor curve of the $[BMIM]^+$▪MA cluster.

For the clusters of $[BMIM]^+$ cations with the isomers of methyl bicyclo-[2.2.1]-hept-5-ene-2-carboxylate (*Figure 3.28 c-f*), the fragmentation energy of the $[BMIM]^+$▪*exo* cluster appears the lowest of all the clusters, which is ins accordance with the $[EMIM]^+$ clusters. For the clusters containing more than one $[BMIM]^+$ cation, no MA clusters were observed, which means that unlike the fragmentation manner of the $[EMIM]_2^{2+}$▪*endo* cluster, cyclopentadiene does not dissociate from the clusters of the *endo* isomer with two or three $[BMIM]^+$ cations, indicating that a certain increase of the number of $[BMIM]^+$ cations will not lead to a *retro* Diels-Alder reaction. This suggests that the aggregation of the $[BMIM]^+$ cations might form a block to prevent the isomer from decomposition. The $[BMIM]_3^{3+}$▪*endo* cluster fragments mostly into $[BMIM]_2^{2+}$▪*endo* cluster at lower collision energies and then produces a small amount of the $[BMIM]^+$▪*endo* fragment at higher collision energies.

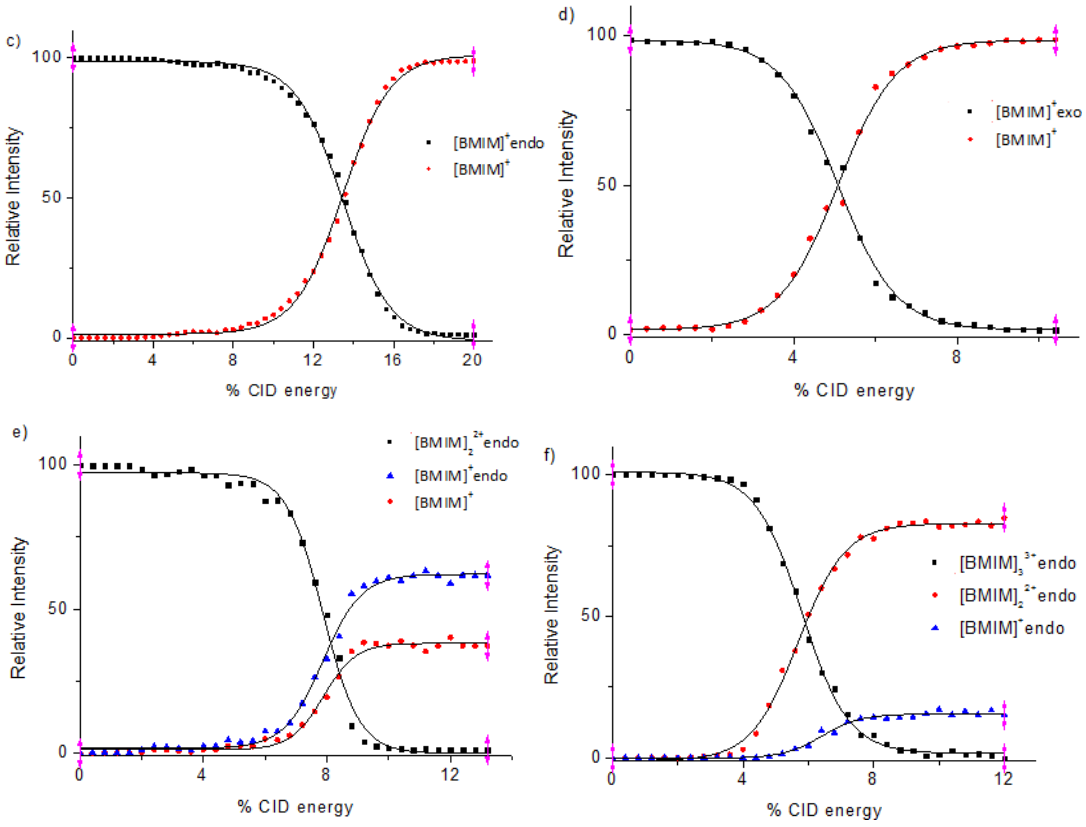

Figure 3.28 (c-f): % CID curves for the $[BMIM]_n^{n+}$▪product clusters, for c) $[BMIM]^+$▪*endo*, d) $[BMIM]^+$▪*exo*, e) $[BMIM]_2^{2+}$▪*endo*, and f) $[BMIM]_3^{3+}$▪*endo*.

CID curves for the $[C_{12}MIM]^+$ clusters are illustrated in *Figure 3.29*. Unlike the other two ionic liquids in this study, the clusters of $[C_{12}MIM]^+$ with the *exo* isomer and with cyclopentadiene were unable to be observed, thus only the CID curves of $[C_{12}MIM]^+$ with methyl acrylate and the *endo* isomer are plotted here, from which it can be observed that the fragmentation energies of these two clusters are very similar, for $[C_{12}MIM]^+$▪MA at 3.3% CID energy and $[C_{12}MIM]^+$▪*endo* at 3.4% CID energy. Since the $[C_{12}MIM]^+$ cation has a much longer alkyl chain than $[EMIM]^+$ and $[BMIM]^+$, and the interactions between the imidazolium cations with cyclopentadiene or the *exo* isomer can be considerably weak as described for the $[EMIM]^+$ and $[BMIM]^+$ cations before, this long alkyl chain might be the major steric block for cyclopentadiene and the *exo* isomer to form coordination with the imidazolium ring.

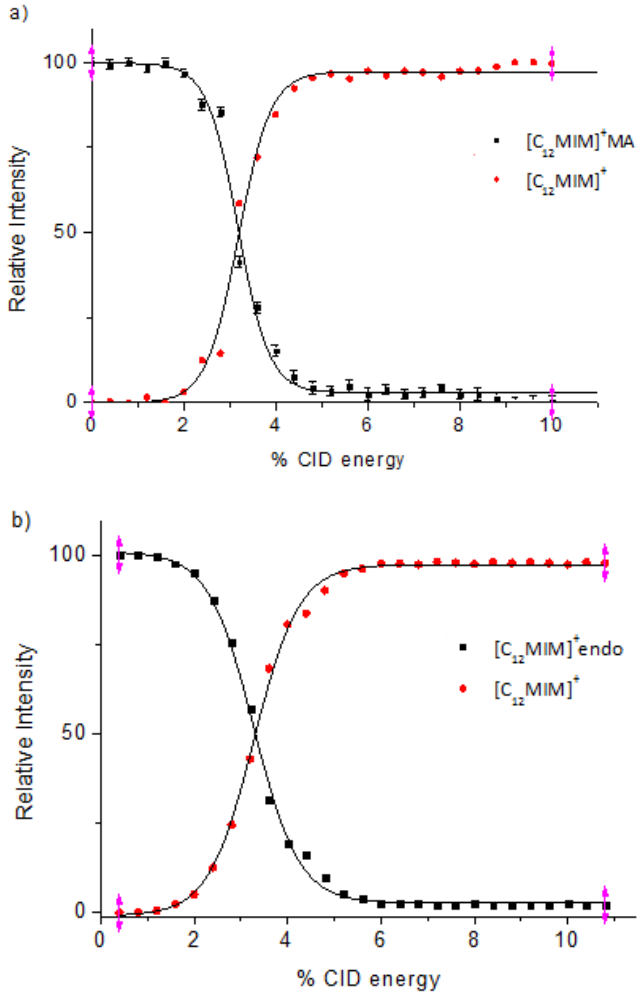

Figure 3.29: % CID curves for a) $[C_{12}MIM]^+$▪ MA clusters and b) $[C_{12}MIM]^+$▪*endo* cluster.

3.2.6 Conclusion of Mass Spectrometry Results

Comparisons of the binding energies can be achieved by comparing the fragmentation energies of different clusters of imidazolium cations (*i.e.* $[EMIM]_n^{n+}$, $[BMIM]_n^{n+}$ and $[C_{12}MIM]^+$) with Diels-Alder components. Because the difference of m/z value between the $[C_{12}MIM]^+$ clusters and clusters of the other two ionic liquids is greater than 100 a.u.,[110] the fragmentation energies of the $[C_{12}MIM]^+$ clusters could not be compared straightforwardly with the $[EMIM]^+$ and $[BMIM]^+$ clusters. Hence the comparisons of fragmentation energies were only made between the $[EMIM]^+$ and $[BMIM]^+$ clusters (*Figure 3.30*).

Figure 3.30 a displays the overlaid % fragmentation decay curves for the $[EMIM]^+$▪MA and $[BMIM]^+$▪MA clusters, with the $[BMIM]^+$ cluster showing a higher fragmentation energy (8.5% CID energy) than the $[EMIM]^+$ cluster (8.0% CID energy). The same trends are also observed in *Figure 3.30 b-e* for the clusters with cyclopentadiene, the *endo* and *exo* isomers, with the $[BMIM]_n^{n+}$ clusters always requiring higher % collision energies to fragment, indicating that the fragmentation barrier height is comparatively higher for these clusters.

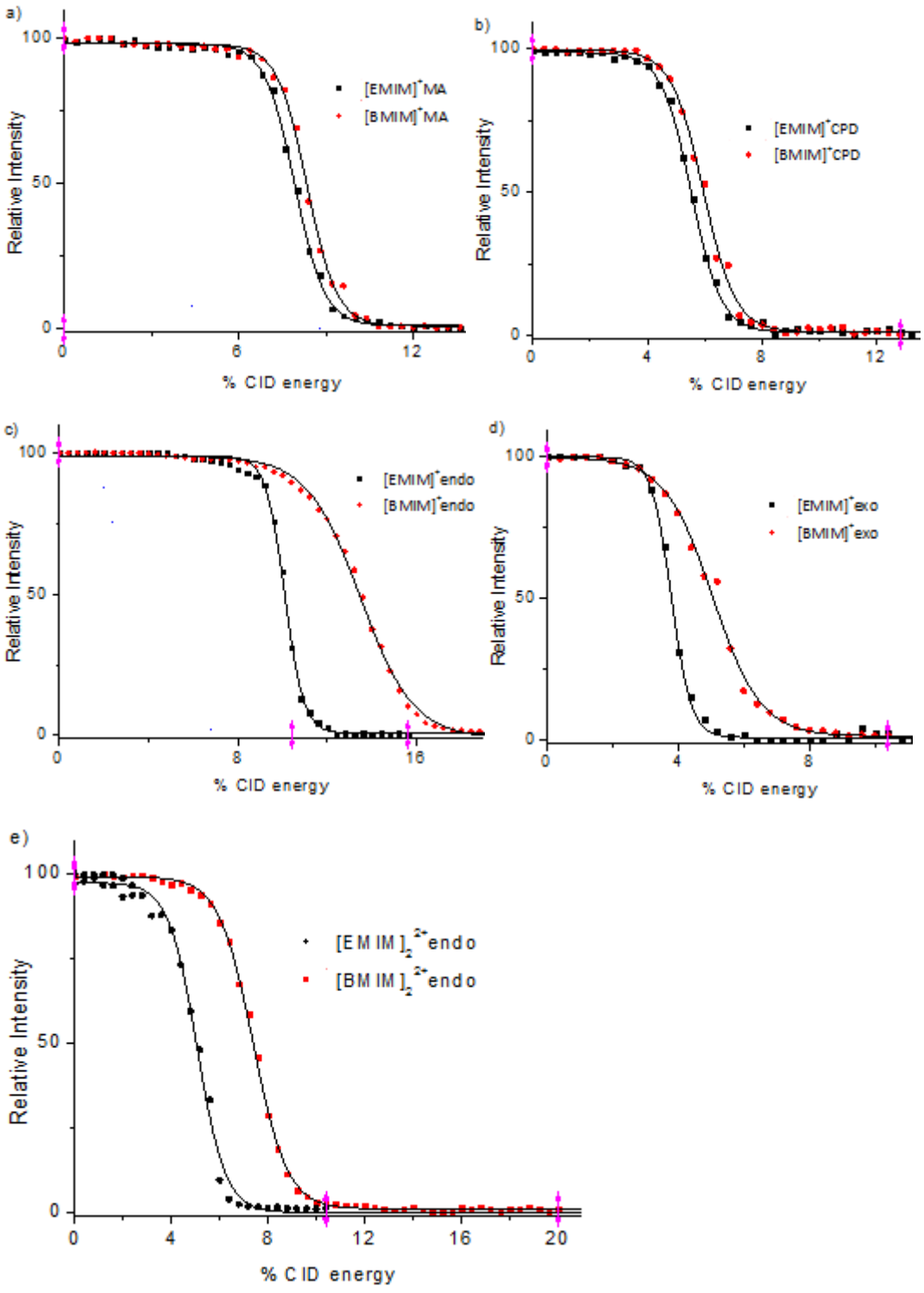

Figure 3.30: % Fragmentation decay curves for $[C_mMIM]_n^{n+}$▪[N] (*m* = 1, 2) clusters, where a) *n* = 1, N = MA, b) *n* = 1, N = CPD, c) *n* = 1, N = *endo*, d) *n* = 1, N = *exo* and e) *n* = 2, N = *endo*.

According to the results described with the clusters of the $[EMIM]^+$ and $[BMIM]^+$ cations, the $[C_mMIM]^+$▪*exo* cluster is less stable than the $[C_mMIM]^+$▪*endo* cluster (*m* = 1, 2), and have smaller fragmentation energies, which can be considered as binding energies between the imidazolium cations and the isomers. From this, it can be hypothesised that, during the process of the Diels-Alder reaction between methyl acrylate and cyclopentadiene in the $[EMIM][BF_4]$ or $[BMIM][BF_4]$ ionic liquids, it is more likely to produce *endo* isomers, as the *endo* isomer is more favoured by the $[C_mMIM]^+$ cations in the ILs. In addition, the binding energy of the $[BMIM]^+$▪*endo* cluster is higher than the $[EMIM]^+$▪*endo* cluster, thus the *endo* isomer appears more favoured by the $[BMIM][BF_4]$ ionic liquid than $[EMIM][BF_4]$, which indicates a higher *endo* selectivity of the $[BMIM][BF_4]$ ionic liquid.

For the clusters containing more than one imidazolium cation, it will lower the electron intensity when the *endo* isomer forms two hydrogen bonds with two $[EMIM]^+$ cations but the extent can be quite small, while adding another $[EMIM]^+$ cation to the $[EMIM]^+$▪*endo* cluster will be more sterically difficult. The most intense fragmentation channel of the $[EMIM]_2^{2+}$▪*endo* cluster is to produce the $[EMIM]_2^{2+}$▪MA ion, undergoing a *retro* Diels-Alder reaction, which indicates that an increase in the number of the $[EMIM]^+$ cations may weaken the interaction between $[EMIM]^+$ and the isomers, to some extent lowering its selectivity of *endo* isomer.

The steric effect of the $[EMIM]_2^{2+}$▪*endo* cluster is smaller than that for the $[BMIM]_2^{2+}$▪*endo* cluster, thus from a theoretical aspect the interaction between the *endo* isomer with $[EMIM]_2^{2+}$ should be stronger than $[BMIM]_2^{2+}$, while the dissociation energies of these two clusters indicate that this is not the case. One of the reasons leading to this might be that the aggregation of the $[BMIM]^+$ cations is more stable than $[EMIM]^+$ due to the interaction between the longer alkyl chains, which blocked the way for the *endo* isomer to dissociate from the cluster. This can also explain the observation of the $[BMIM]_3^{3+}$▪*endo* cluster while there is no $[EMIM]_3^{3+}$▪*endo* cluster produced by fragmentation process.

$[EMIM]_n^{n+}$ and $[BMIM]_n^{n+}$ (n = 1, 2) systems with the Diels-Alder reactants and isomers. The $[BMIM]_n^{n+}$ clusters display higher fragmentation energies than the $[EMIM]_n^{n+}$ clusters with $E_{1/2}$ values listed in *Table 3.4* which can be easily compared.

Table 3.5: $E_{1/2}$ fragmentation energies for the $[C_mMIM]_n^{n+}$▪[N] clusters. N = MA, CPD, *endo*, *exo*; m = 2, 4, 12; n = 1, 2.

Clusters	$E_{1/2}$	**Clusters**	$E_{1/2}$	**Clusters**	$E_{1/2}$
$[EMIM]^+$▪MA	8.0%	$[BMIM]^+$▪MA	8.5%	$[C_{12}MIM]^+$▪MA	3.3%
$[EMIM]^+$▪CPD	5.6%	$[BMIM]^+$▪CPD	6.0%	$[C_{12}MIM]^+$▪*endo*	3.4%
$[EMIM]^+$▪*endo*	10.1%	$[BMIM]^+$▪*endo*	13.2%		
$[EMIM]^+$▪*exo*	3.6%	$[BMIM]^+$▪*exo*	5.0%		
$[EMIM]_2^{2+}$▪*endo*	5.2%	$[BMIM]_2^{2+}$▪*endo*	7.8%		
		$[BMIM]_3^{3+}$▪*endo*	5.7%		

In general, the results from the mass spectrometry experiments show that the $[BMIM][BF_4]$ ionic liquid has a stronger *endo* selectivity than the $[EMIM][BF_4]$ and $[C_{12}MIM][BF_4]$ ionic liquid in the Diels-Alder reaction between methyl acrylate and cyclopentadiene, while the components of the D-A reaction perform more stable coordination with $[BMIM]^+$ than other imidazolium cations studied here. While the Diels-Alder reactions actually always occur in solution phase, there might be limitations using ESI-MS-CID to study the coordination behaviour between Diels-Alder components and ionic liquids as the products have a possibility to perform *retro* Diels-Alder reactions in gas phase. Even so ESI-MS-CID is still a useful technique to give a good perspective of how the Diels-Alder reactivity in this study is modified when being carried out in ionic liquids, especially for investigating the fragmentation patterns and binding energies.

3.3 Computational results

Computational chemistry has been used extensively in recent years to complement experimental studies in the ionic liquids area with a great deal of success.[72, 118, 124] To focus on one area, studies have been conducted that combine both experimental and computational work to understand the influence of an ionic liquid solvent on the outcome of a reaction that is performed in it.[80, 122] To obtain further insights into the interaction between the imidazolium cations and methyl acrylate and isomers of methyl bicyclo-[2.2.1]-hept-5-ene-2-carboxylate which are the participants in the Diels-Alder reaction studied here, quantum chemical calculations were carried out. These calculations are also important as they aid the interpretation of the mass spectrometry results.

There have been extensive DFT computational studies on a variety of different Diels-Alder reactions over the past decade.[126] For example, B. Jursic *et al.*[125] have carried out a study using a set of DFT methods to calculate the transition states and energy barriers of the Diels-Alder reaction of ethylene with buta-1,3-diene and cyclopentadiene. While calculations conducted using (post-HF) methods (*e.g.* MCTDH, MP2, G2, etc) have also proved reliable,[41] they are limited by their computational cost even calculating the properties of small system. DFT methods offer a good compromise between efficiency and accuracy for modelling medium-sized molecular systems, as well as providing a useful tool for understanding the reactivity of molecules in their ground states.[127] Hence, a series of density functional theory (DFT) calculations were first performed at the B3LYP level to obtain geometric structures and ground-state energies for the methyl acrylate, and *endo* and *exo* monomers.

As previously mentioned in *Chapter 2 (Section 2.3)*, the main limitation of standard DFT methods is that they lack of accuracy in describing dispersive interactions which is known to be quite important for accurate calculations of ionic liquid systems. Though this issue can be partly circumvented by using functionals that include dispersion corrections (*e.g.* DFT-D functional,[114] this approach still does not

give energies as reliable as the MP2 method. Thus a set of second-order Møller-Plesset perturbation theory (MP2) calculations[112] were also conducted for the $[C_nMIM]^+$ (n = 2, 4, 12) cations, and all the clusters of $[C_nMIM]^+$▪[N] (N = methyl acrylate, *endo* or *exo* isomers). MP2 is typically used as a benchmark method for calculating the relative energies and geometric structures,[118] and has been used successfully to investigate hydrogen bonding interactions and energies in ionic liquid systems by P. A. Hunt *et al*.[39]

The results were obtained by optimisation based on trial and error (*Section 2.3*) and frequency calculations using the B3LYP-D3/6-311+G(d,p) level of the theory, followed by single-point energies calculations by the MP2 method with the aug-cc-pVTZ basis set.

3.3.1 $[EMIM]^+$ Clusters

The optimised structures of $[EMIM]^+$ with methyl acrylate, and the *endo* and *exo* isomers of methyl bicyclo-[2.2.1]-hept-5-ene-2-carboxylate are displayed in *Figures 3.31-3.33* and are labelled as **a**, **b**, and **c**, respectively, in order of increasing relative energy. Each cluster isomer is obtained with the neutral molecules (MA, the *endo* and *exo* products) frozen and the imidazolium cation fully flexible to probe different interactions. Inspection of the structures reveals that the O···H hydrogen bonds are not linear from the carbonyl oxygen to C_2 hydrogen as for the two lowest-energy cluster isomers (***a*** and ***b***). The carbonyl oxygen sits slightly displaced forming a weaker secondary hydrogen bond with either the methyl group (II) or the first methylene group on the alkyl chain (III), while the C_2 hydrogen on the imidazolium ring still appears to be the main target to form a more typical hydrogen bond (bond length < 2 Å), as expected due to its relatively high acidity. Additionally, there is another possibility to form hydrogen bonding interactions with the two single hydrogens on the imidazolium ring (*Structure **c***), in which case the carbonyl oxygen sits in the middle of these two hydrogens and forms bonds with relatively equivalent lengths (*Table 3.9*).

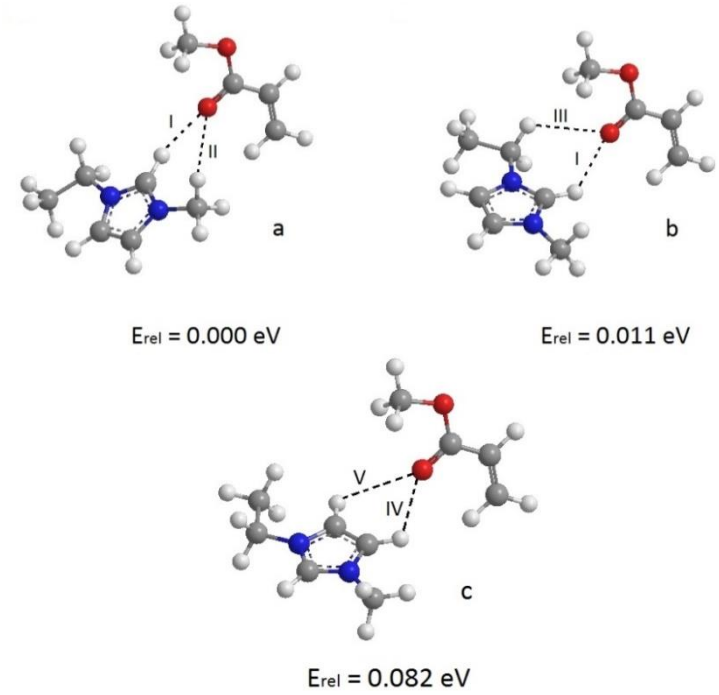

Figure 3.31: Geometric structures (B3LYP/6-311+G(d,p)) of the $[EMIM]^+$▪MA cluster with relative energy (MP2/aug-cc-pVTZ) displayed under each cluster isomer. H-bonds between the carbonyl oxygen and different hydrogens are labelled as I-V and are indicated as dashed lines.

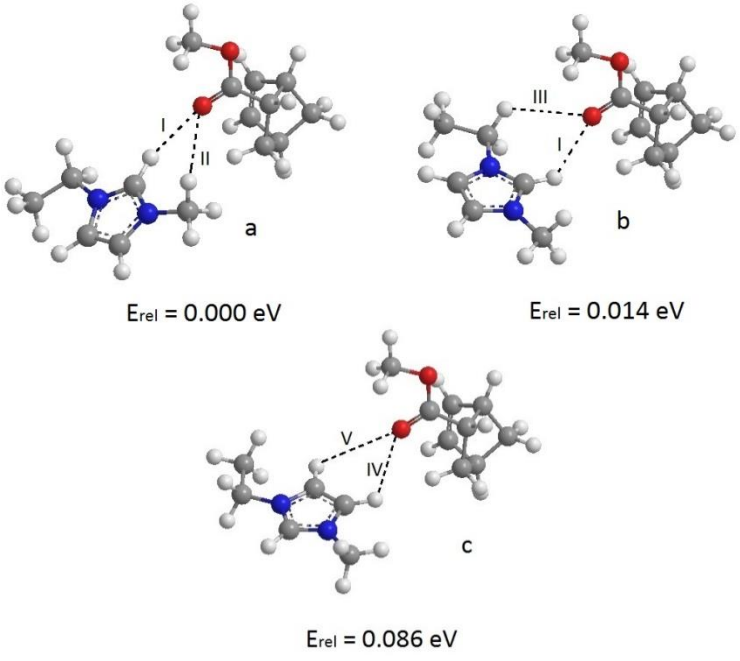

Figure 3.32: Geometric structures (B3LYP/6-311+G(d,p)) of the $[EMIM]^+$▪*endo* with relative energy (MP2/aug-cc-pVTZ) displayed under each cluster isomer. H-bonds between the carbonyl oxygen and different hydrogens are labelled as I-V and are indicated as dashed lines.

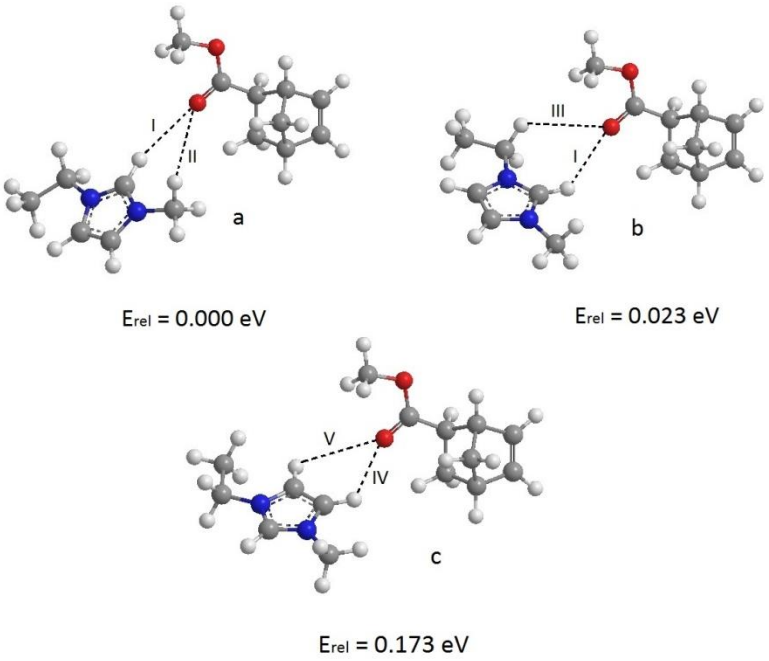

E_{rel} = 0.000 eV

E_{rel} = 0.023 eV

E_{rel} = 0.173 eV

Figure 3.33: Geometric structures (B3LYP/6-311+G(d,p)) of the $[EMIM]^+$▪*exo* cluster with relative energy (MP2/aug-cc-pVTZ) displayed under each cluster isomer. H-bonds between the carbonyl oxygen and different hydrogens are labelled as I-V and are indicated as dashed lines.

The relative energies of three cluster isomers of each of the $[EMIM]^+$ clusters displayed in *Figure 3.31-3.33* were listed in *Table 3.6*, the inspection of which reveals that the first two structures (***a*** and ***b***) lie relatively close in energy while the **c** structures lie much higher in energy, for all three of the $[EMIM]^+$ clusters.

The Boltzmann distribution (also known as the Gibbs distribution) gives the probability distribution for occupation of different states as a function of that state's energy, and the temperature of the system.[128] This should provide a reasonable estimate of the gas-phase population of the cluster isomers studied. Thus the relative abundances for each of the cluster isomers can be calculated using the Boltzmann distribution equation:

$$p_i = \frac{N_i}{N} = \frac{e^{-E_i/k_B T}}{\sum_{j=1}^{M} e^{-E_i/k_B T}} \qquad [\mathbf{3.4}]$$

where the p_i is the probability of structure *i*, E_i is the energy of structure *i*, k_B is the Boltzmann constant, *M* is the number of all structures in the system, and T is the temperature (assumed to be the source temperature in the ESI-MS, *i.e.* 373K). The results are listed in *Table 3.6*, illustrating that a mixture of isomers **a** and **b** could be expected to be produced in our experiment, with the isomer **c** structure being only a minor constituent.

Table 3.6: Relative energies and abundances of cluster isomers of the $[EMIM]^+$▪[N] complexes. [a]

[N]	Relative Energy, E_{rel} / eV			Relative Abundance [a]		
	a	**b**	**c**	**a**	**b**	**c**
MA	0.000	0.011	0.082	59.4%	37.6%	3.0%
endo	0.000	0.014	0.086	61.2%	36.4%	2.4%
exo	0.000	0.023	0.173	64.3%	31.8%	3.9%

[a)] Calculated from the Boltzmann distribution at *T* = 373K.

3.3.2 $[BMIM]^+$ Clusters

Figures 3.34-3.36 illustrate the optimised structures of $[BMIM]^+$ with methyl acrylate and the *endo* and *exo* isomers of methyl bicyclo-[2.2.1]-hept-5-ene-2-carboxylate which are labelled as **a**, **b**, and **c**, with their computed energies increasing in the same order. Each isomer is obtained with the neutral molecules (MA, the *endo* and *exo* products) frozen and the imidazolium cation fully flexible to probe different interactions within the complexes. The hydrogen-bonding patterns appear similar to $[EMIM]^+$ clusters (*Section 3.3.1*) with the carbonyl oxygen forming non-linear hydrogen bonds respectively with C_2-methyl hydrogens (I, II), C_2-methylene hydrogens (I, III) and the two hydrogens on the imidazole ring (IV, V), with these last two bonds in the **c** isomers exhibiting equivalent lengths (*Table 3.10*).

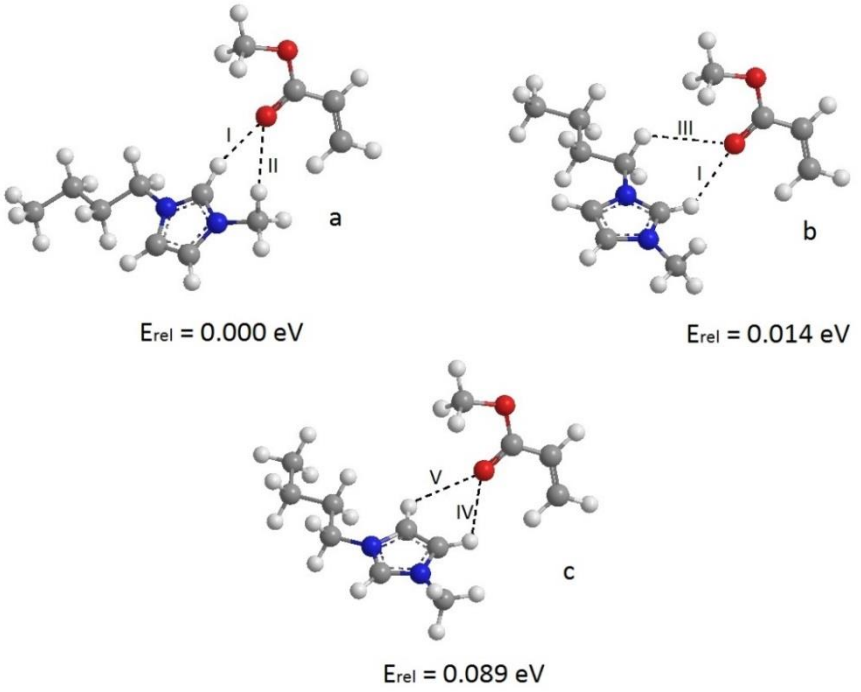

Figure 3.34: Geometric structures (B3LYP/6-311+G(d,p)) of the $[BMIM]^{+}$▪MA cluster with relative energy (MP2/aug-cc-pVTZ) displayed under each cluster isomer. H-bonds between the carbonyl oxygen and different hydrogens are labelled as I-V and are indicated as dashed lines.

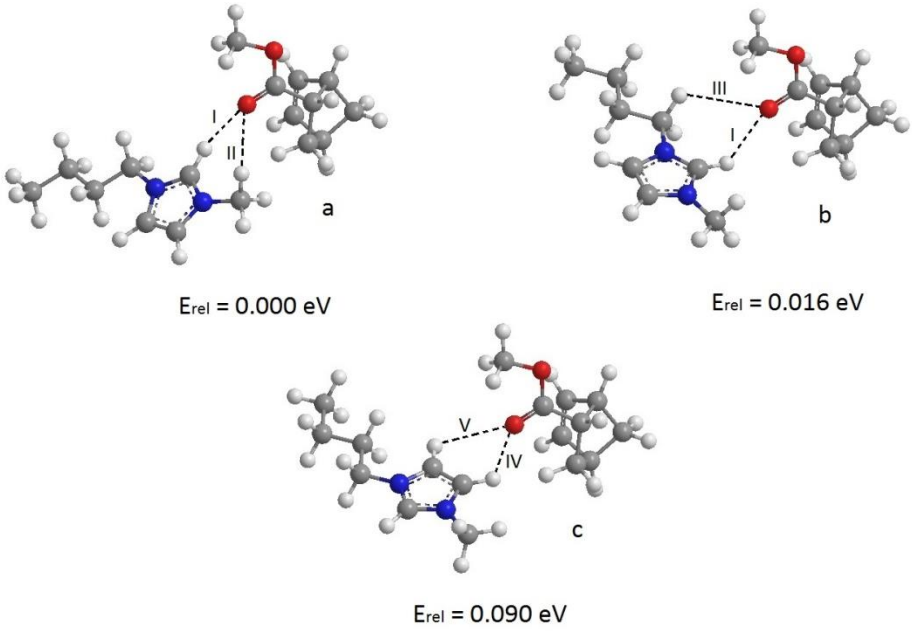

Figure 3.35: Geometric structures (B3LYP/6-311+G(d,p)) of the $[BMIM]^{+}$▪*endo* cluster with relative energy (MP2/aug-cc-pVTZ) displayed under each cluster isomer. H-bonds between the carbonyl oxygen and different hydrogens are labelled as I-V and are indicated as dashed lines.

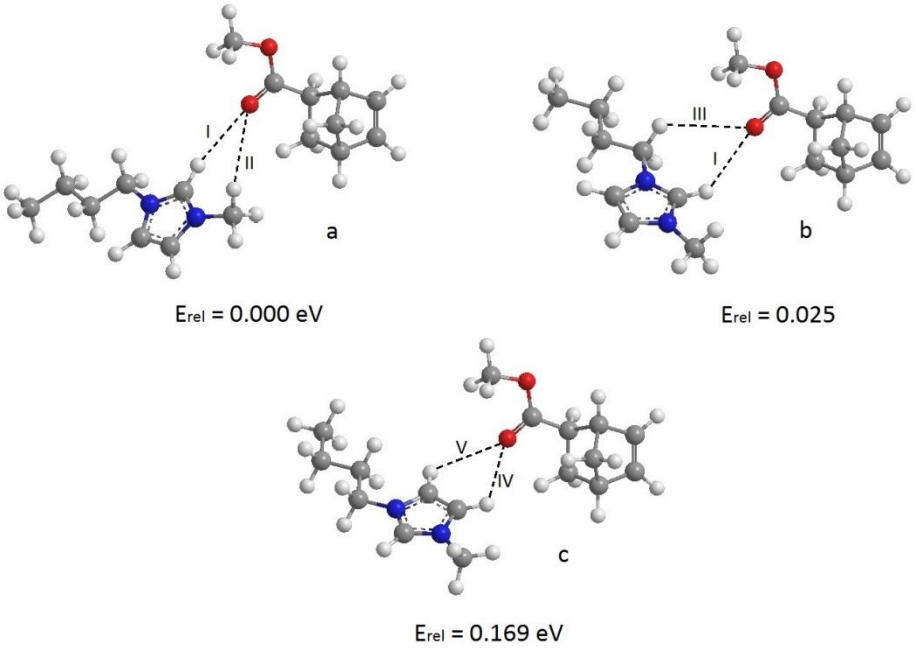

Figure 3.36: Geometric structures (B3LYP/6-311+G(d,p)) of the $[BMIM]^+$▪*exo* cluster with relative energy (MP2/aug-cc-pVTZ) displayed under each cluster isomer. H-bonds between the carbonyl oxygen and different hydrogens are labelled as I-V and are indicated as dashed lines.

It can be observed from the relative energies listed in *Table 3.7* that the difference of relative energies between structures **a** and **b** has increased a little bit in comparison to the $[EMIM]^+$ clusters (*Section 3.3.1*), indicating that the cluster interactions might be weakened by the increase of the alkyl chain length. This is likely due to increasing repulsive interaction between alkyl side chain of $[BMIM]^+$ and the adjacent methyl group of the cation. The relative abundances for three structures of all clusters were again obtained by the Boltzmann distribution equation *[3.4]* as with $[EMIM]^+$ clusters. The results of the Boltzmann distribution are listed in *Table 3.7*. These calculations indicate that isomers **a** and **b** will be produced in an approximate ratio of 2:1 in our experiment, while only a very small amount of isomers **c** present.

Table 3.7: Relative energies and abundances of structures of the clusters $[BMIM]^+$▪[N].

[N]	Relative Energy, E_{rel} / eV			Relative Abundance [a]		
	a	**b**	**c**	**a**	**b**	**c**
MA	0.000	0.014	0.089	63.9%	33.7%	2.9%
endo	0.000	0.016	0.090	65.1%	32.4%	2.2%
exo	0.000	0.025	0.169	64.8%	31.1%	4.1%

[a)] Calculated from the Boltzmann distribution at T = 373K.

3.3.3 $[C_{12}MIM]^+$ Clusters

Optimised structures of cluster isomers of $[C_{12}MIM]^+$ with methyl acrylate and the *endo* and *exo* isomers of methyl bicyclo-[2.2.1]-hept-5-ene-2-carboxylate are shown in *Figures 3.37-3.39*, and are labelled as **a**, **b**, and **c** for the lowest, second lowest and highest energy structures respectively. Relative abundance results of the $[C_{12}MIM]^+$ clusters were obtained and displayed in *Table 3.8*. Compared to the $[EMIM]^+$ and $[BMIM]^+$ results, the $[C_{12}MIM]^+$ clusters shows a decrease of **b** isomers compared to **a** isomers, and a slightly growing relative abundance of **c** isomers. It appears that the cluster geometries possible for the $[C_{12}MIM]^+$ clusters are able to increase the repulsive steric interactions compared to $[BMIM]^+$.

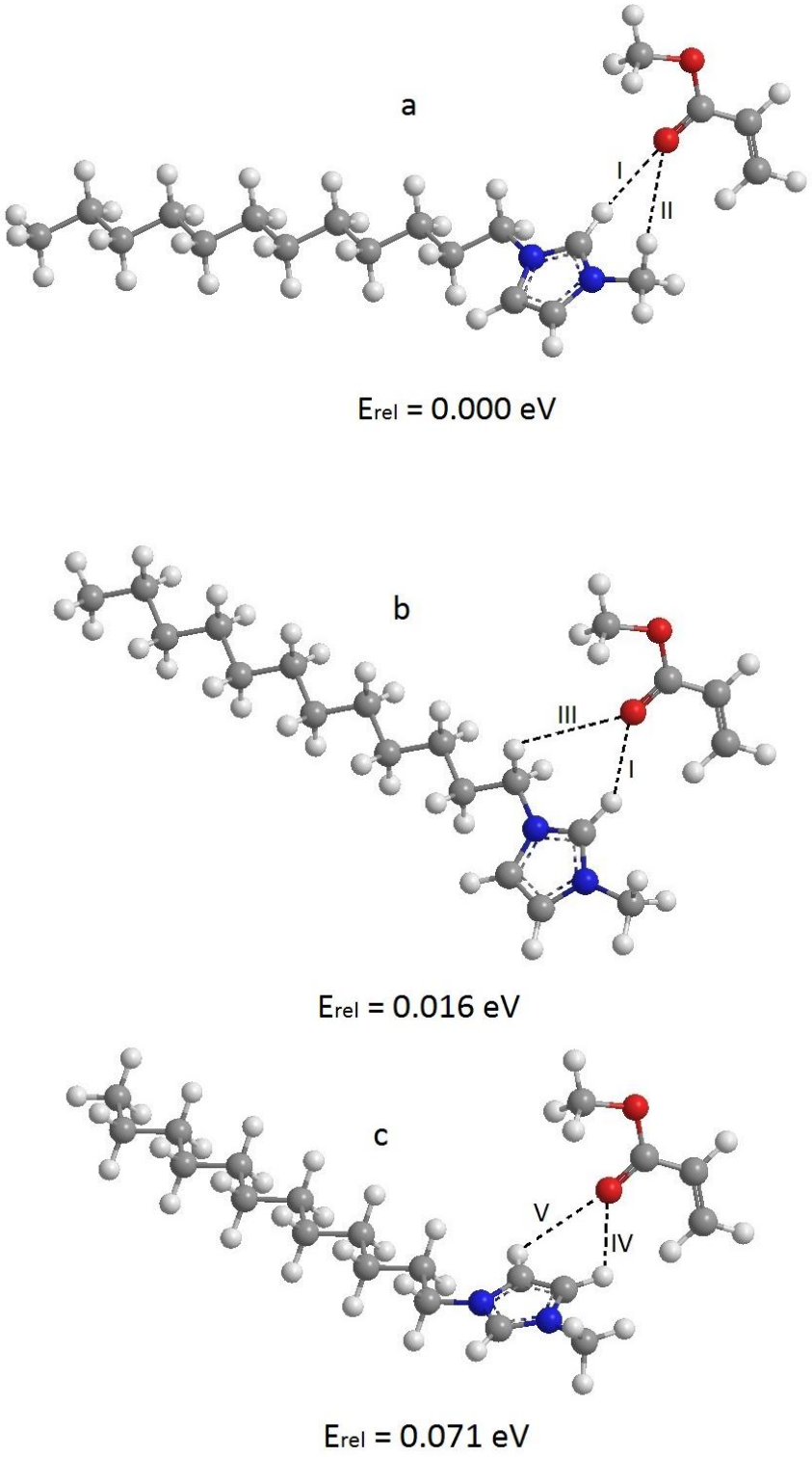

Figure 3.37: Geometric structures (B3LYP/6-311+G(d,p)) of the $[C_{12}MIM]^{+}$▪MA cluster with relative energy (MP2/aug-cc-pVTZ) displayed under each cluster isomer. H-bonds between the carbonyl oxygen and different hydrogens are labelled as I-V and are indicated as dashed lines.

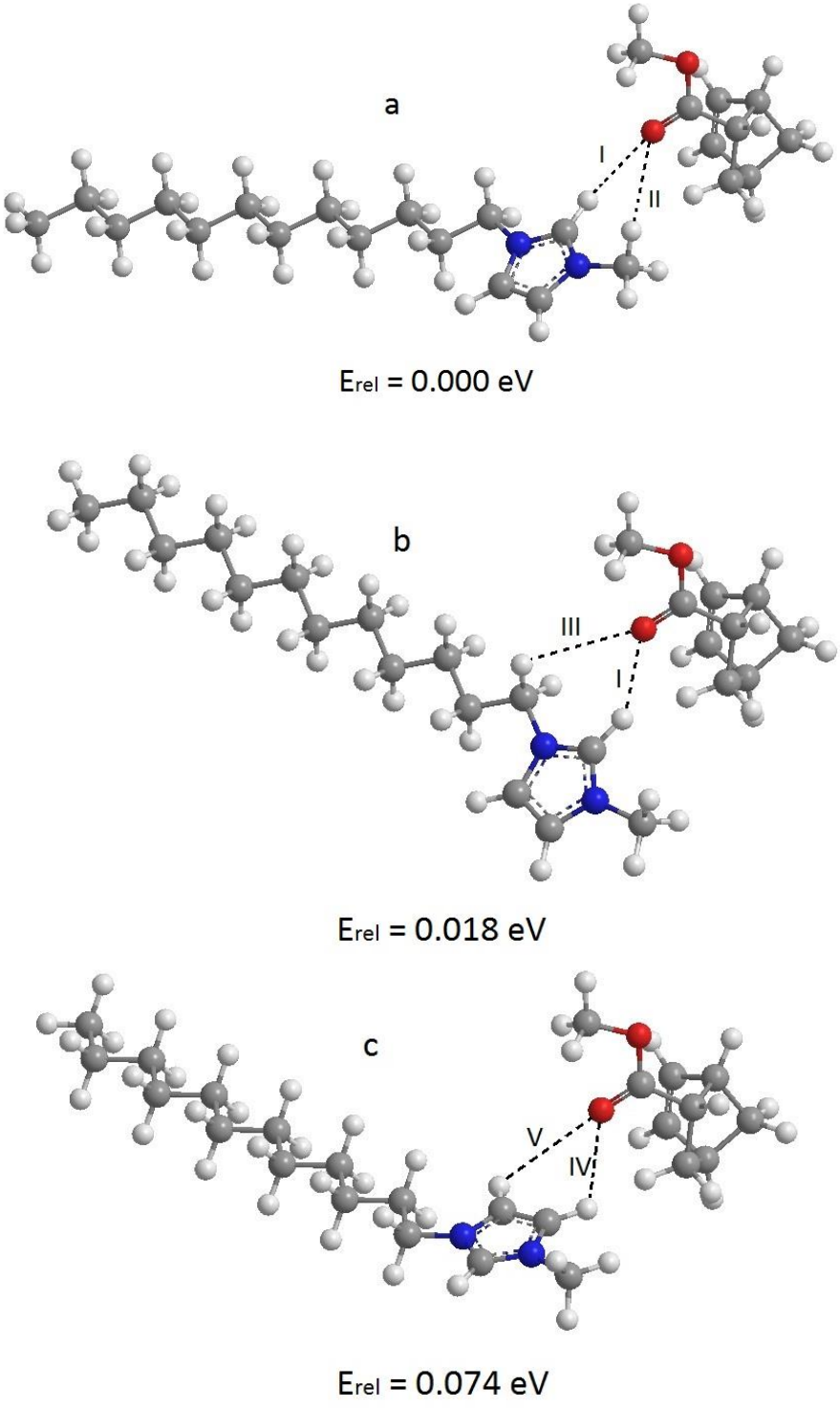

Figure 3.38: Geometric structures (B3LYP/6-311+G(d,p)) of the $[C_{12}MIM]^{+}$▪*endo* cluster with relative energy (MP2/aug-cc-pVTZ) displayed under each cluster isomer. H-bonds between the carbonyl oxygen and different hydrogens are labelled as I-V and are indicated as dashed lines.

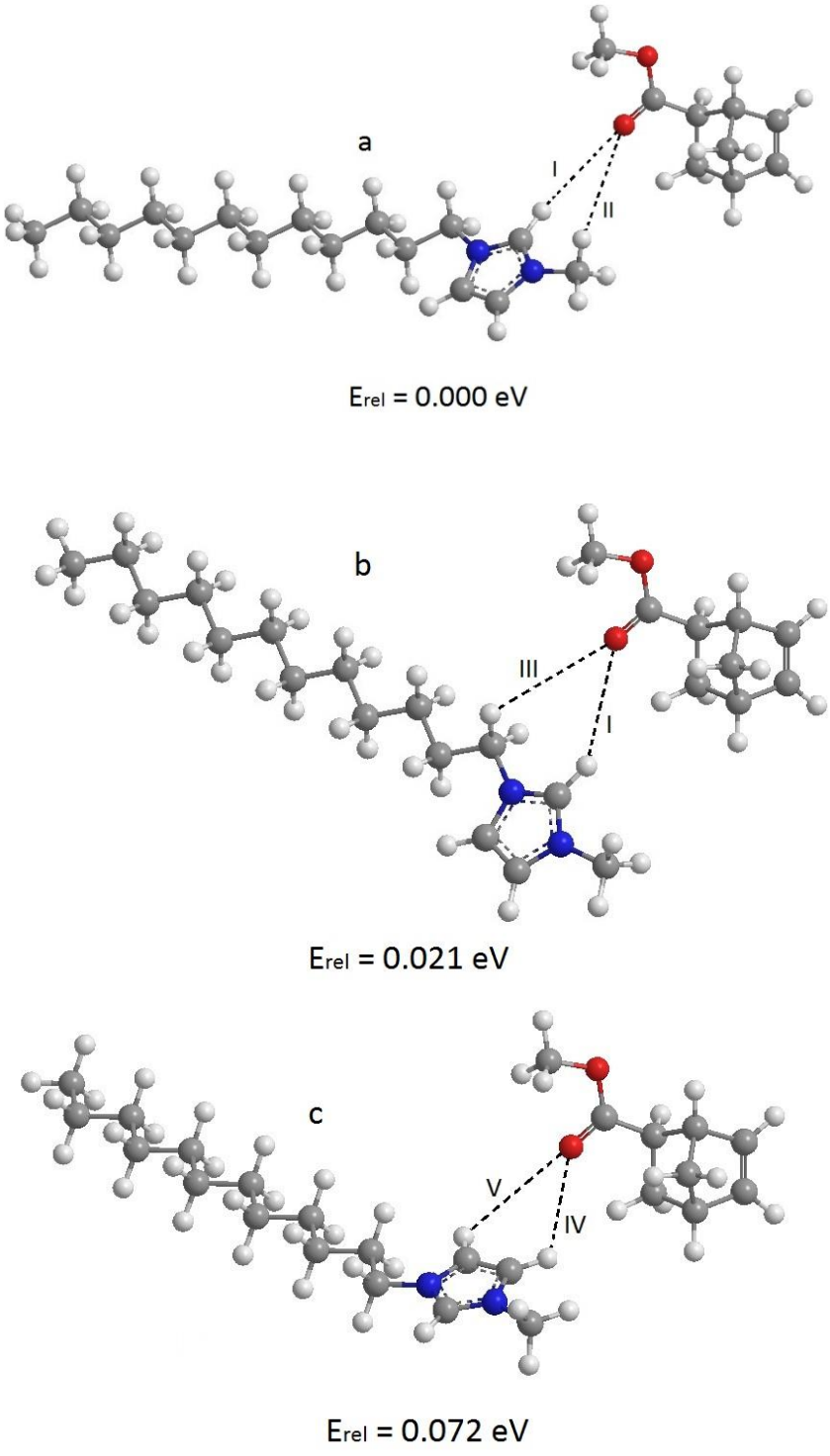

Figure 3.39: Geometric structures (B3LYP/6-311+G(d,p)) of the $[C_{12}MIM]^{+}$▪*exo* with relative energy (MP2/aug-cc-pVTZ) displayed under each cluster isomer. H-bonds between the carbonyl oxygen and different hydrogens are labelled as I-V and are indicated as dashed lines.

Table 3.8: Relative energies and abundances of structures of the clusters $[C_{12}MIM]^+$▪[N].

[N]	Relative Energy, E_{rel} / eV			Relative Abundance [a]		
	a	**b**	**c**	**a**	**b**	**c**
MA	0.000	0.016	0.071	61.9%	32.8%	5.3%
endo	0.000	0.018	0.074	63.7%	31.5%	4.8%
exo	0.000	0.021	0.072	64.1%	30.9%	5.1%

[a)] Calculated from the Boltzmann distribution at T = 373 K.

3.3.4 Comparison of $[EMIM]^+$, $[BMIM]^+$ and $[C_{12}MIM]^+$ Clusters

The O···H hydrogen-bond lengths for the optimised isomers of the $[EMIM]^+$, $[BMIM]^+$ and $[C_{12}MIM]^+$ clusters shown in *Figures 3.31-3.39* are listed in *Tables 3.9-3.11*. It is useful to compare the results with the criteria for hydrogen bonds given by Steiner and Jeffrey.[129-131] These criteria are summarised in *Table 3.12* to aid interpretation of the current results.

Table 3.9: O···H hydrogen bond lengths in Å for the clusters $[EMIM]^+$▪[N]. [a]

[N]	Structure **a**		Structure **b**		Structure **c**	
	I	**II**	**I**	**III**	**IV**	**V**
MA	1.764	1.956	1.765	2.268	2.398	2.401
endo	1.713	1.918	1.710	2.205	2.364	2.365
exo	2.138	2.274	2.147	2.295	2.424	2.426

[a)] See *Figures 3.31-3.33* for structures.

Table 3.10: O···H hydrogen bond lengths in Å for the clusters $[BMIM]^+$▪[N]. [a]

[N]	Structure **a**		Structure **b**		Structure **c**	
	I	**II**	**I**	**III**	**IV**	**V**
MA	1.723	1.928	1.721	2.266	2.358	2.360
endo	1.698	1.915	1.691	2.204	2.337	2.339
exo	2.134	2.278	2.141	2.298	2.411	2.412

[a)] See *Figures 3.34-3.36* for structures.

Table 3.11: O···H hydrogen bond lengths in Å for the clusters $[C_{12}MIM]^+$▪[N].[a]

[N]	Structure **a**		Structure **b**		Structure **c**	
	I	**II**	**I**	**III**	**IV**	**V**
MA	1.843	2.033	1.841	2.216	2.372	2.374
endo	1.895	2.124	1.862	2.279	2.375	2.376
exo	2.517	2.683	2.535	2.709	2.629	2.630

[a)] See *Figures 3.37-3.39* for structures.

Table 3.12: Criteria for hydrogen bonds adapted from Steiner and Jeffrey.[129-131]

	Covalent (Strong)	**Ionic (Moderate)**	**Weak ionic dispersion (Weak)**
H·····Y (Å)	1.2-1.5	1.5-2.2	> 2.2
Bond energy (eV)	0.653-1.731	0.176-0.653	< 0.173

It can be observed that for isomers **a** and **b** of all the clusters, the hydrogen bonds formed with C_2 hydrogens (**I**) are always shorter than those with the methyl or methylene group (**II, III**), and can be classified as moderate hydrogen bonds. For the isomer **c** structures, the hydrogen bonds **IV** and **V** are all > 2.3 Å and can be classified as weak. This indicates that the hydrogen bonding associations with the C_2 hydrogens on the imidazolium ring might be the major controlling interaction between the imidazolium cation and the methyl acrylate, and the *endo* and *exo* products, and the relative cluster energies decrease from isomer **a** to **c**. For all the structures of MA with the *endo* clusters, the bond lengths appear to follow a trend of $[BMIM]^+$▪[N] < $[EMIM]^+$▪[N] < $[C_{12}MIM]^+$▪[N] (N = MA or *endo* isomer), which is consistent with the fragmentation energy results from the CID curves in *Section 3.2.4*.

One significant difference between $[C_{12}MIM]^+$▪*exo* and clusters of *exo* isomer with the other two imidazolium cations is that the lengths of hydrogen bonds are relatively long and the hydrogen bonding interaction energy (*Table 3.13*) is

considerably low, indicating that the coordination between $[C_{12}MIM]^+$ and the *exo* isomer is extremely weak referring to the criteria list (*Table 3.12*). Thus, it can be deduced that the $[C_{12}MIM]^+$▪*exo* cluster could be challenging to form compared to other clusters, a result which is consistent with the fragmentation and CID results in *Section 3.2.3* and *Section 3.2.4*.

For further comparison of the clusters with the different imidazolium cations, a series of interaction energies were calculated and are listed in *Table 3.13*. A straightforward way to do this is to follow *Equation 3.5*, although it can be applied in two different ways for the computational results presented here. If the geometry of the dimer A-B was optimised and calculated first, and the geometries of the two monomers were frozen to only change the position between each other, then for each fixed position of A with respect to B the result from the equation would be an energy of interaction. Otherwise the binding energy would be obtained by calculating the geometries of A, B and A-B, respectively. In this case, in order to investigate the solvent effect of imidazolium ionic liquids to the Diels-Alder reaction of methyl acrylate and cyclopentadiene, calculations were conducted following the second route, which means that the change in energy (optimised energy) of the whole cluster was also included together with the interaction of hydrogen bonding. For this reason, basis set superposition error (BSSE) was also added to the equation (*Equation 3.6*) to get more accurate energies.[115, 116]

$$\mathrm{E} = \mathrm{E_{AB}} - \mathrm{E_A} - \mathrm{E_B} \qquad [\mathbf{3.5}]$$

$$\mathrm{E} = \mathrm{E_{AB}} - \mathrm{E_A} - \mathrm{E_B} - \mathrm{E_{BSSE}} \qquad [\mathbf{3.6}]$$

It can be directly seen that the energies of the interactions within the $[EMIM]^+$ clusters are higher than the $[C_{12}MIM]^+$ clusters, while a little bit lower than the $[BMIM]^+$ clusters, which is further consistent with the CID fragmentation energy results presented in *Section 3.2.4*.

Table 3.13: Interaction energies for the structure **a**[a] of $[C_nMIM]^+$▪[N] clusters, where *n* = 2, 4, 12; N = MA, *endo*, *exo*.

[N]	E_i / eV ($[EMIM]^+$)	E_i / eV ($[BMIM]^+$)	E_i / eV ($[C_{12}MIM]^+$)
MA	0.180	0.183	0.177
endo	0.185	0.189	0.175
exo	0.152	0.155	0.012

[a)] Structures **a** in *Figures 3.31-3.39*.

Chapter 4 Summary

4.1 Conclusions

The results presented in *Chapter 3* describe a series of studies that has been performed to try to better understand the role of ionic liquids in determining the *endo/exo* isomer ratio that is produced in a classic Diels Alder reaction (*Scheme 2.1*). This study initially required that a synthetic procedure was found to produce suitable quantities of pure *endo*- and *exo*- isomer products. Once the usable *endo*- and *exo*- isomers were obtained, they were separately mixed with the reagents and products of the model Diels Alder reaction (*Scheme 2.1*), and an ionic liquid solvent, and the solutions were studied using electrospray mass spectrometry. Complexes of the reagents and products with the ionic liquid cations were then studied using collision induced dissociation (CID) to investigate the relative strengths of the interactions between the different constituents. Computational chemistry was then used to help interpret the mass spectrometry results.

Three main synthetic methods were used for the Diels-Alder reaction between methyl acrylate and cyclopentadiene, in order to get a usable mixture of the *endo* and *exo* isomers that could be separated. *Method 1* contained an *in-situ* procedure to generate cyclopentadiene and methyl acrylate and led to a mixture of the *endo* and *exo* isomers with side product contaminations, which was unable to be successfully separated. *Method 2* used water, methanol and hexane as the solvents

separately to give products with different *endo*-to-*exo* ratios at ambient temperature. While the reaction in water gave a pure *endo* isomer straightforwardly with a rather low yield, the reaction in methanol gave a reasonable amount of 97% *endo* isomer after separation. The reaction in hexane was conducted for the purpose of giving an *exo*-dominant product and obtaining a pure *exo* isomer after separation. However, the product failed to be separated. *Method 3* used a similar synthetic procedure to *Method 2* but under a solvent-free condition, which gave a good yield of the mixture of the *endo* and *exo* isomers, and a usable amount of the pure *exo* isomer was finally obtained after several stages of chromatographic separation. For all Diels-Alder reactions, the impurities of unreacted cyclopentadiene and dicyclopentadiene, which can be easily generated in the Diels-Alder reaction and will strongly influence the separation, were finally removed by high vacuum and freezing respectively. While the *endo* isomer could be separated as a pure substance after 1-2 separation procedures, extensive repeated chromatography experiments were needed to get pure *exo* isomer, which appeared much more challenging. Furthermore, a series of imidazolium ionic liquids with the tetrafluoroborate anion (*i.e.* [EMIM][BF_4], [BMIM][BF_4] and [C_{12}MIM][BF_4]) were also successfully synthesised in good yields.

Results from the mass spectrometry experiments in positive ion mode revealed that $[BMIM]^+$ forms the strongest coordination with the Diels-Alder reactants (*i.e.* methyl acrylate and cyclopentadiene) and the *endo* and *exo* isomers. While the $[EMIM]_2^{2+}$▪isomer fragmented into $[EMIM]_2^{2+}$▪MA with higher collision energies, the $[BMIM]_n^{n+}$▪isomer clusters did not produce any $[BMIM]_n^{n+}$▪MA fragments, indicating that a *retro* Diels-Alder reaction did not happen for that system.

Unfortunately, the $[C_{12}MIM]^+$▪CPD and $[C_{12}MIM]^+$▪*exo* clusters were barely observed. While another study investigating the influence of isotropic ILs and liquid crystalline ILs on the Diels-Alder reaction found that the *exo* isomer would react more efficiently in the [C_{12}MIM][BF_4] liquid crystalline IL,[43] results from this study did not show that. This can be attributed to the possibility that the [C_{12}MIM][BF_4]

ionic liquid does not perform a highly ordered liquid crystalline structure in the gas phase, and the large bulk of the $[C_{12}MIM]^+$ cation contrarily blocks the reactants/isomers from forming stable hydrogen bonds.

When comparing the clusters of different neutral molecules (MA, CPD and isomers) with the same imidazolium cation, it can be seen that the fragmentation energies decrease in order of $[C_nMIM]^+$▪*endo*, $[C_nMIM]^+$▪MA, $[C_nMIM]^+$▪CPD, $[C_nMIM]^+$▪*exo* (*n* = 2, 4, 12), showing that the *exo* isomer is most disfavoured by the imidazolium cations studied here, with cyclopentadiene the second most disfavoured due to not having an electronegative oxygen to form proper hydrogen bonds.

The theoretical results obtained were mostly consistent with the results from the ESI-MS-CID experiments described above, with only one exception that the interaction energy of $[C_{12}MIM]^+$ with the *endo* isomer is slightly lower than with methyl acrylate, while there are opposite results for the $[EMIM]^+$ and $[BMIM]^+$ clusters, which need further improved calculations to check its validity. In addition, these computational results also provide an interesting perspective on the conformation of the clusters where none of the O···H hydrogen bonds are linear, with the carbonyl oxygen sitting slightly displaced to form hydrogen bonds with two hydrogens, which has also been observed between the ionic liquid ion pairs (*e.g.* the non-linear hydrogen bonds between $[BMIM]^+$ cation and $[BF_4]$ anion).[39]

While there are extensive studies on how the Diels-Alder reaction would be modified by ionic liquids to give a higher *endo*-to-*exo* ratios, this thesis is the first such study on the interactions between the imidazolium ionic liquids (*i.e.* $[EMIM][BF_4]$, $[BMIM][BF_4]$ and $[C_{12}MIM][BF_4]$) and the Diels-Alder components (*i.e.* methyl acrylate, cyclopentadiene, the *endo* and *exo* isomers).

Overall, the project was successful as the *endo* and *exo* isomers of methyl bicyclo-[2.2.1]-hept-5-ene-2-carboxylate were synthesised as pure isomers. The project was also successful in demonstrating that the interactions between the reagents

and products in the Diels Alder reaction (*Scheme 2.1*) could be probed via collision induced mass spectrometry, as it was possible to use ESI-MS to produce suitable cluster isomer in the gas phase and investigate their relative stability. These results appear to be reliable as they agreed well with computational results that were conducted alongside the experimental work.

4.2 Future Work

Though there have been substantial published studies demonstrating that GC/HPLC techniques are quite efficient and accurate for separation of the Diels-Alder isomers,[40, 85, 132] they can only be used for characterisation and will not give a certain amount of pure isomers. Considering that the separation for obtaining the pure *exo* isomer required extensive work, it would benefit from further development to reduce the time needed for the repeat chromatographic separations. Additionally, while there is little previous study on how to actually partition the *endo* and *exo* isomers of methyl bicyclo-[2.2.1]-hept-5-ene-2-carboxylate, this should still be achievable by refining the method with references on separation of other analogues.

Also, due to the limited amount of time, a majority of which has been spent on synthesis and separation experiments, it would have been helpful to have access to more imidazolium ionic liquids to obtain more systematic results. For example, it is desirable to conduct further ESI-MS-CID on ionic liquids such as $[C_nMIM][BF_4]$ (n = 6, 8, 10) and $[C_nMIM][PF_6]$ (n = 2, 4, 6, 8, 10, 12) with the same Diels-Alder reaction in both positive and negative modes of the mass spectrometer. In addition, it was not possible to obtain sufficient intensities of the clusters of the Diels-Alder reagents and products with the anion of the ionic liquid (*i.e.* $[BF_4]^-$ with methyl acrylate, cyclopentadiene, the *endo* and *exo* isomers) within the mass spectrometer used for this project. Negative ion clusters are generally harder to produce in the quadrupole ion-trap mass spectrometer as they are susceptible to decay by losing

the excess electron. Therefore, it would be interesting to repeat the experiments conducted here in a different type of mass spectrometer that could allow these negatively charged clusters to be produced in greater quantities.

Moreover, more computational works on clusters of the Diels-Alder reactants and products with more than one imidazolium cation (*i.e.* $[EMIM]_n^{n+}$▪[N] and $[BMIM]_n^{n+}$▪[N], *n* = 1-3, N = methyl acrylate, the *endo* and *exo* isomers) need to be investigated to fully support the results from mass spectrometry experiments. Also it would be worth using molecular mechanics to obtain more trial conformational structures and repeating the DFT calculations (*e.g.* M06-2X) with a functional that performs well for the systems studied here.[118]

Abbreviations

°C	Degree Celsius
K	Kelvin
mol	Moles
ml	Millilitre
cm^3	Cubic Centimetre
min	Minute
V	Volt
m/z	Mass-to-Charge Ratio
$E_{1/2}$	Half Energy
MS	Mass Spectrometry
ESI	Electrospray Ionisation
MALDI	Matrix-Assisted Laser Desorption Ionisation
CID	Collision-Induced Dissociation
NMR	Nuclear Magnetic Resonance
IR	Infrared
DFT	Density Functional Theory
MP2	Second-Order Møller-Plesset Perturbation Theory
IL	Ionic Liquid
LCIL	Liquid Crystalline Ionic Liquid
MA	Methyl Acrylate
CPD	Cyclopentadiene
$[EMIM][BF_4]$	1-Ethyl-3-methylimidazolium tetrafluoroborate
$[BMIM][BF_4]$	1-Butyl-3-methylimidazolium tetrafluoroborate
$[C_{12}MIM][BF_4]$	1-Dodecyl-3-methylimidazolium tetrafluoroborate

Appendix: ^{19}F NMR spectra of [BMIM][BF_4] and [C_{12}MIM][BF_4]

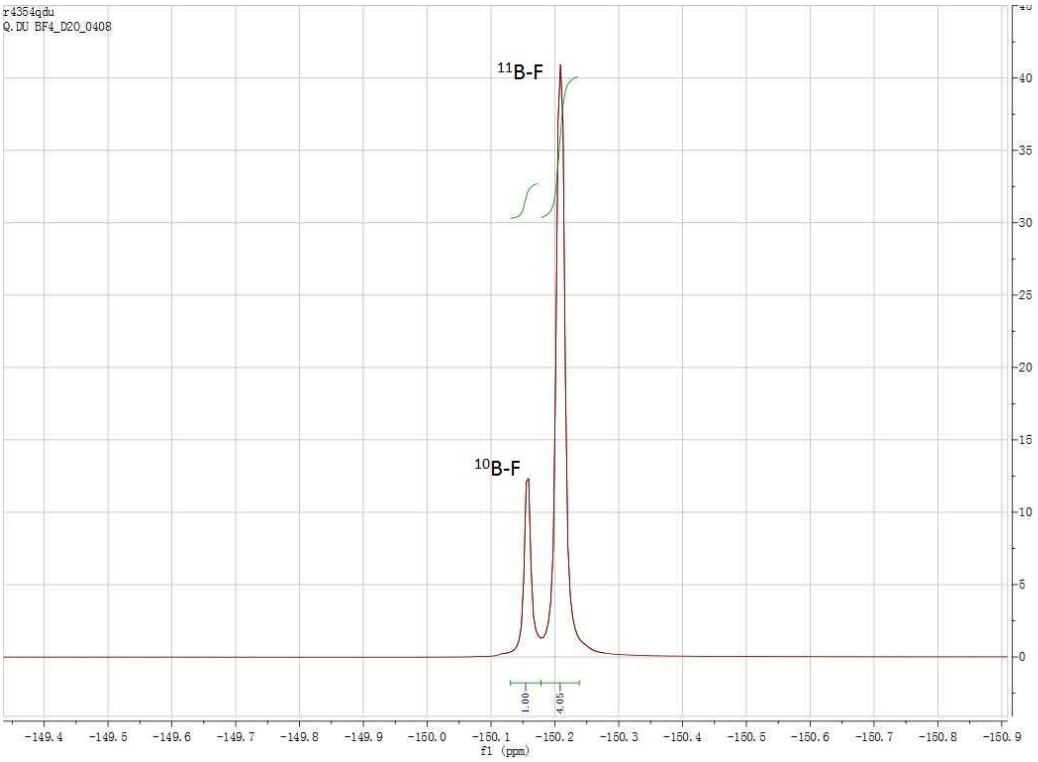

Figure 1: ^{19}F NMR spectrum of the product of [BMIM][BF_4] with each coupling peak assigned and labelled above.

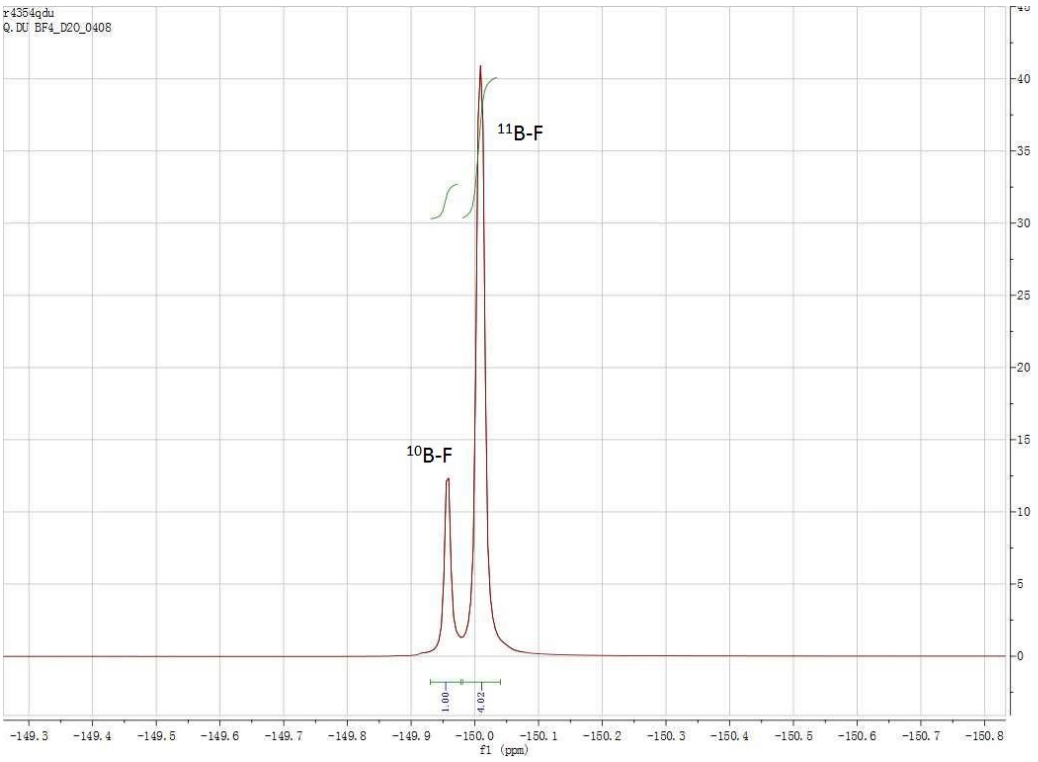

Figure 2: ^{19}F NMR spectrum of the product of [C_{12}MIM][BF_4] with each coupling peak assigned and labelled above.

References

1. J. S. Wilkes, *Green Chem.,* 2002, **4**, 73-80.
2. S. Gabriel, J. Weiner, *Ber. Dtsch. Chem. Ges.,* 1888, **21**, 2669–2679.
3. P. Walden, *Bull. Russian Acad. Sci.,* 1994, **8**, 405-422.
4. H. L. Chum, V. R. Koch, L. L. Miller, R. A. Osteryoung, *J. Am. Chem. Soc.,* 1975, **97**, 3264–3265.
5. J. S. Wilkes, J. A. Levisky, R. A. Wilson, C. L. Hussey, *Inorg. Chem.,* 1982, **21**, 1263–1264.
6. F. Endres, S. Z. E. Abedin, *Phys. Chem. Chem. Phys.,* 2006, **8**, 2101–16.
7. N. V. Plechkova, K. R. Seddon, *Chem. Soc. Rev.,* 2008, **37**, 123.
8. J. Pernak, T. Rzemieniecki, K. Materna, *Chemik,* 2016, **70**, 471-480.
9. T. Welton, *Green Chem.*, 2011, **13**, 225-225.
10. R. Kawano, H. Matsui, C. Matsuyama, A. Sato, M. A. B. H. Susan, N. Tanabe, M. Watanabe, *J. Photochem. Photobiol. A: Chemistry,* 2004, **164**, 87-92
11. M. Freemantle, *Chem. Eng. News,* 1998, **76**, 32–37.
12. P. D. McCrary, R. D. Rogers, *Chem. Commun.,* 2013, **49**, 6011–6014.
13. M. Smiglak, A. Metlen, R. D. Rogers, *Acc. Chem. Res.,* 2007, **40**, 1182–1192.
14. J. Pernak, J. Nawrot, M. Kot, B. Markiewicz, M. Niemczak, *RSC Adv.,* 2013, 25019–25029.
15. J. Pernak, F. Walkiewicz, M. Maciejewska, M. Zaborski, *Ind. Eng. Chem. Res.,* 2010, **49**, 5012–5017.
16. A. Pernak, K. Iwanik, P. Majewski, M. Grzymisławski, J. Pernak, *Acta Histochem.,* 2005, **107**, 149–156.
17. K. R. Seddon, *Chem. Commun.,* 2001, **23**, 2399-2407.
18. P. A. Thomas, B. Marvey, *Molecules,* 2016, **21**, 184-199.
19. M. J. Earle and K. R. Seddon, *Pure Appl. Chem.,* 2000, **72,** 1392-1398.
20. C. W. Lee, *Tetrahedron Lett.,* 1999, **40**, 2461.
21. T. Fischer, A. Sethi, T. Welton, J. Woolf, *Tetrahedron Lett.,* 1999, **40**, 793.
22. L. Xu, W. Chen, J. Xiao, *Organometallics*, 2000, **19**, 1123.
23. L. Xu, W. Chen, J. Ross, J. Xiao, *Org. Lett.,* 2001, **3**, 295.

24. V. P. W. Böhm, W. A. Herrmann, *Chem. Eur. J.,* 2000, **6**, 1017.
25. V. L. Boulaire, R. Grée, *Chem. Commun.*, 2000, 2195.
26. C. P. Mehnert, N. C. Dispenziere, R. A. Cook, *Chem. Commun.,* 2002, 1610.
27. S. T. Handy, X. Zhang, *Org. Lett.,* 2001, **3**, 233.
28. J. Ross, J. Xiao, *Green Chem.,* 2002, **4**, 129.
29. K. S. Yeung, M. E. Farkas, Z. Qiu, Z. Yang, *Tetrahedron Lett.,* 2002, **43**, 5793.
30. T. Itoh, S. H. Han, Y. Matsushita, S. Hayase, *Green Chem.,* 2004, **6**, 437.
31. T. Ito, *Yuki Gosei Kagaku Kyokaishi (J. Synth. Org. Chem. Jpn.),* 2009, **67**, 143.
32. (a) H. Du, K. Ding, *Handb. Cycl. Reac.,* 2010, **1**, 1. (b) S. S. Gujral, A. Popli, *Indo Am. J. Pharm. Res.,* 2013, **3**, 3192-3215.
33. B. Rickborn, *Org. Reac.,* 2004, **52**, 1-393
34. N. Grimblat, A. M. Sarotti, P. L. Pisanoa, S. C. Pellegrinet, *New J. Chem.,* 2016, **40**, 1966-1969.
35. D. C. Rideout, R. Breslow, *J. Am. Chem. Soc.,* 1980, **102**, 7816-7817.
36. D. A. Jaeger, C. E. Tucker, *Tetrahedron Lett.,* 1989, **30**, 1785-1788.
37. C. W. Lee, *Tetrahedron Lett.,* 1999, **40**, 2461-2464.
38. I. Meracz, T. Oh, *Tetrahedron Lett.,* 2003, **44**, 6465-6468.
39. P. A. Hunt, C. R. Ashworth, R. P. Matthews, *Chem. Soc. Rev.,* 2015, **44**, 1257-1288.
40. A. Aggarwal, N. L. Lancaster, A. R. Sethi, T. Welton, *Green Chem.,* 2002, **4**, 517-520.
41. M. J. Earle, P. B. McCormac, K. R. Seddon, *Green Chem.,* 1999, **1**, 23.
42. S. V. Dzyuba, R. A. Bartsch, *Tetrahedron Lett.,* 2002, **43**, 4657.
43. D. W. Bruce, Y. Gao, J. N. C. Lopes, K. Shimizu, J. M. Slattery, *Chem. Eur. J.,* 2016, **22**, 16113-16123.
44. M. Yamashita, J. B. Fenn, *J. Phys. Chem.*, 1984, **88**, 4671-4675.
45. J. B. Fenn, M. Mann, C. K. Meng, S. F. Wong and C. M. Whitehouse, *Science*, 1989, **246**, 64-71.
46. J. B. Fenn, M. Mann, C. K. Meng, S. F. Wong, C. M. Whitehouse, *Mass Spectrom. Rev.*, 1990, **9**, 37-70.
47. M. Karas, D. Bachmann and F. Hillenkamp, *Anal. Chem.*, 1985, **57**, 2935-2939.
48. J. B. Fenn, *Angew. Chem. Int. Ed.*, 2003, **42**, 3871-3894.

49. K. Tanaka, H. Waki, Y. Ido, S. Akita, Y. Yoshida, T. Yoshida, T. Matsuo, *Rapid Commun. Mass Spectrom.*, 1988, **2**, 151-153.
50. T. Wyttenbach, M. T. Bowers, *Annu. Rev. Phys. Chem.*, 2007, **58**, 511-533.
51. J. Zhang, X. Shen, *J. Phys. Chem. B,* 2011, **115**, 11852–11861.
52. D. Ondo, M. Tkadlecová, V. Dohnal, J. Rak, J. Kvícala, J.K. Lehmann, A. Heintz, N. J. Ignatiev, *J. Phys. Chem. B*, 2011, **115**, 10285–10297.
53. L. P. N. Rebelo, J. N. C. Lopes, J. M. S. S. Esperança, E. Filipe, *J. Phys. Chem. B,* 2005, **109**, 6040.
54. C. J. Johnson, J. A. Fournier, C. T. Wolke, M. A. Johnson, *J. Chem. Phys.,* 2013, **139**, 224305.
55. M. J. Earle, J. M. S. S. Esperança, M. A. Gilea, J. N. C. Lopez, L. P. N. Rebelo, J. W. Magee, K. R. Seddon, J. A. Widegren, *Nature,* 2006, **439**, 831–834.
56. P. Wasserscheid, *Nature,* 2006, **439**, 797.
57. R. Ludwig, U. Kragl, *Angew. Chem. Int. Ed.,* 2007, **46**, 6582–6584.
58. M. Z. Moghaddam, R. Krüger, E. Heinzle, A. Tholey, *J. Mass Spectrom.,* 2004, **39**, 1494.
59. M. A. Henderson, J. S. McIndoe, *Chem. Commum.,* 2006, 2872-2874.
60. J. P. Leal, J. M. M. S. Esperança, M. E. M. da Piedade, J. N. C. Lopes, L. P. N. Rebelo, K. R. Seddon, *J. Phys. Chem. A,* 2007, **111**, 6167-6182.
61. M. Yoshizawa, W. Xu, C. A. Angell, *J. Am. Chem. Soc.,* 2003, **125**, 15411.
62. U. P. Kreher, A. E. Rosamila, C. L. Raston, J. L. Scott, C. R. Strauss, *Molecules,* 2004, **9**, 387.
63. R. G. Treble, K. E. Johnson, E. Tosh, *Can. J. Chem.,* 2006, **84**, 915
64. C. S. Ho, C. W. K. Lam, M. H. M. Chan, R. C. K. Cheung, L. K. Law, L. C. W. Lit, K. F. Ng, M. W. M. Suen, H. L. Tai, *Clin. Biochem. Rev.,* 2003, **24**, 3-12.
65. Y. Chen, M. T. Rodgers, *J. Am. Chem. Soc.,* 2012, **134**, 2313.
66. Y. Chen, M. T. Rodgers, *J. Am. Chem. Soc.,* 2012, **134**, 5863.
67. R. Cody, R. Burnier, C. Cassady, B. S. Freiser, *Anal. Chem.,* 1982, **54**, 2225.
68. E. de Hoffmann, V. Stroobant, *Mass Spectrometry Principles and Applications, Third Edition,* J. Wiley and Sons, 2007, 1-3.
69. S. A. McLuckey and D. E. Goeringer, *J. Mass Spectrom.,* 1997, **32**, 461-474.

70. K. L. Busch, G. L. Glish, S. A. McLuckey, *Mass Spectrometry/Mass Spectrometry: Techniques and Applications of Tandem Mass Spectrometry*, VCH, 1988.
71. L. Sleno and D. A. Volmer, *J. Mass Spectrom.,* 2004, **39**, 1091-1112.
72. A. M. Fernandes, B. Schröder, T. Barata, M. G. Freire, J. A. P. Coutinho, *J. Am. Soc. Mass Spectrom.,* 2014, **25**, 852-860.
73. J. S. Brodbelt, *Int. J. Mass Spectrom.,* 2000, **200**, 57–69.
74. C. A. Schalley, *Mass Spectrom. Rev.,* 2001, **20**, 253–309.
75. B. Baytekin, H. T. Bayetkin, C. A. Schalley, *Org. Biomol. Chem.,* 2006, **4**, 2825-2841.
76. J. F. de la Mora, G. J. V. Berkel, C. G. Enke, *J. Mass. Spectrom.*, 2000, **35**, 529-39.
77. N. B. Cech, C. G. Enke, *Mass Spectrom. Rev.,* 2001, **20**, 87-362.
78. T. C. Rohner, N. Lion, H. H. Girault, *Phys. Chem. Chem. Phys.,* 2004, **6**, 68-3056.
79. E. de Hoffmann, V. Stroobant, *Mass Spectrometry Principles and Applications, Third Edition,* J. Wiley and Sons, 2007, 195-196.
80. A. M. Fernandes, M. A. A. Rocha, M. G. Freire, I. M. Marrucho, J. A. P. Coutinho, L. M. N. B. F. Santos, *J. Phys. Chem. B,* 2011, **115**, 4033-4041.
81. Z. B. Alfassi, R. E. Huie, B. L. Milman, P. Neta, *Anal. Bioanal. Chem.* 2003, **377**, 159.
82. A. J. A. Harvey, A. Sen, N. Yoshikawa, C. E.H. Dessent, *Chem. Phys. Lett.,* 2015, **634**, 216-220.
83. J. M. Voss, B. M. Marsh, J. Zhou and E. Garand, *Phys. Chem. Chem. Phys.,* 2016, **18**, 18905-18913.
84. D. Huertas, M. Florscher, V. Dragojlovic, *Green Chem.,* 2009, **11**, 91-95.
85. C. Cativiela, J. I. García, J. A. Mayoral, L. Salvatella, *J. Chem. Soc., Perkin Trans. 2,* 1994, 847.
86. A. Vidiš, C. A. Ohlin, G, Laurenczy, E. Küsters, G. Sedelmeier, P. J. Dyson, *Adv. Synth. Catal.,* 2005, **347**, 266-274.
87. E. Alcalde, I. Dinarès, A. Ibáñez, N. Mesquida, *Molecules,* 2012, **17**, 4007-4027.
88. L. Zhou, R. Jiang (2011, Aug. 10). *"The Synthesis of Ionic Liquids [BMIM]BF_4"* Sciencepaper Online. Available:

http://www.paper.edu.cn/html/releasepaper/2011/08/161/. [Accessed: Jan. 3, 2017].

89. W. Xu, K. Chu, H. Li, Y. Zhang, H. Zheng, R. Chen, L. Chen, *Molecules*, 2012, **17**, 14323-14335.
90. J. D. Holbrey, K. R. Seddon, *J. Chem. Soc., Dalton Trans.,* 1999, 2133-2139.
91. Bruker-Daltronics, *Esquire 6000 manual*
92. D. Collins, M. Lee, *Anal. Bioanal. Chem.*, 2002, **372**, 66-73.
93. B. T. Ruotolo, J. L. P. Benesch, A. M. Sandercock, S. J. Hyung, C. V. Robinson, *Nat. Protocols*, 2008, **3**, 1139-1152.
94. E. de Hoffmann, V. Stroobant, *Mass Spectrometry Principles and Applications, Third Edition,* J. Wiley and Sons, 2007, 43-45.
95. E. de Hoffmann, V. Stroobant, *Mass Spectrometry Principles and Applications, Third Edition,* J. Wiley and Sons, 2007, 44.
96. E. de Hoffmann, V. Stroobant, *Mass Spectrometry Principles and Applications, Third Edition,* J. Wiley and Sons, 2007, 45.
97. G. Taylor, *Proc. R. Soc. London, Ser. A,* 1964, **280**, 383-397.
98. J. V. Iribarne, B. A. Thomson, *J. Chem. Phys.*, 1976, **64**, 2287-2294.
99. M. Dole, L. L. Mack, R. L. Hines, R. C. Mobley, L. D. Ferguson, M. B. Alice, *J. Chem. Phys.*, 1968, **49**, 2240-2249.
100. L. L. Mack, P. Kralik, A. Rheude, M. Dole, *J. Chem. Phys.*, 1970, **52**, 4977-4986.
101. V. Znamenskiy, I. Marginean, A. Vertes, *J. Phys. Chem. A*, 2003, **107**, 7406-7412.
102. S. Banerjee, S. Mazumdar, *Int. J. Anal. Chem.*, 2012, 40.
103. E. de Hoffmann, V. Stroobant, *Mass Spectrometry Principles and Applications, Third Edition,* J. Wiley and Sons, 2007, 106.
104. R. E. March, *J. Mass Spectrom.*, 1997, **32**, 351-369.
105. W. Paul, *Angew. Chem. Int. Ed.*, 1990, **29**, 739-748.
106. É. Mathieu, *Journal de Mathématiques Pures et Appliquées,* 1868, 137-203.
107. J. N. Louris, R. G. Cooks, J. E. P. Syka, P. E. Kelley, G. C. Stafford and J. F. J. Todd, *Anal. Chem.*, 1987, **59**, 1677-1685.
108. K. Hart, S. McLuckey, *J. Am. Soc. Mass Spectrom.*, 1994, **5**, 250-259.
109. W. E. Boxford, C. E. H. Dessent, *Phys. Chem. Chem. Phys.,* 2006, **8**, 5151-5165.

110. M. Satterfield and J. S. Brodbelt, *Inorganic Chemistry*, 2001, **40**, 5393-5400.
111. "*The Gaussian 09 User's Reference".* Available: http://www.gaussian.com/g_tech/g_ur/g09help.htm [Accessed: Jan. 3, 2017].
112. "*The Gaussian 09 User's Reference".* Available: http://www.gaussian.com/g_tech/g_ur/k_mp.htm [Accessed: Jan. 3, 2017].
113. *"The Gaussian 09 User's Reference".* Available: http://www.gaussian.com/g_tech/g_ur/k_b3lyp.htm [Accessed: Jan. 3, 2017].
114. *"The Gaussian 09 User's Reference".* Available: http://www.gaussian.com/g_tech/g_ur/k_dft.htm [Accessed: Jan. 3, 2017].
115. S. F. Boys, R. Bernardi, *Mol. Phys.,* 1970, **19**, 553.
116. F. B. van Duijneveldt, J. G. C. M van D. de Rijdt, J. H. van Lenthe, *Chem. Rev.,* 1994, **94**, 1873.
117. A. D. Becke, *J. Chem. Phys.,* 1993, **98**, 5648-5652.
118. M. Walker, A. J. A. Harvey, A. Sen, C. E. H. Dessent, *J. Phys. Chem. A,* 2013, **117**, 12590-12600.
119. P. J. Hay and W. R. Wadt, *J. Chem. Phys.*, 1985, **82**, 270-283.
120. "*Increasing the Ability of an Experiment to Measure an Effect".* Available: http://www.sciencebuddies.org/science-fair-projects/top_research-project_signal-to-noise-ratio.shtml [Accessed: Jan. 3, 2017].
121. D. L. Vaux, *Nature,* 2012, **492**, 180-181.
122. C. J. Taylor, B. Wu, C. E. H. Dessent, *Int. J. Mass Spectrom.,* 2008, **31**, 276.
123. G. B. McGaughey, M. Gagné, A. K. Rappé, *J. Biol. Chem.,* 1998, **273**, 15458-15463.
124. S. A. Katsyuba, E. E. Zvereva, Ana Vidiš, P. J. Dyson, *J. Phys. Chem. A,* 2007, **111**, 352-370.
125. B. Jursic, Z. Zdravkovski, *J. Chem. Soc., Perkin Trans. 2,* 1995, 1223-1226.
126. L. R. Domingo, *Tetrahedron,* 2002, **58**, 3765-3774.
127. (a) S. T. Keaveney, J. B. Harper, A. K. Croft, *RSC. Adv.,* 2015, **5**, 35709-35729. (b) F. Dommert, K. Wendler, R. Berger, L. D. Site, C. Holm, *Chem. Phys. Chem.,* 2012, **13**, 1625-1637. (c) E. Rezabal, T. Schäfer, *J. Phys. Chem. B,* 2012, **117**, 553-562. (d) E. I. Izgorodina, U. L. Bernard, D. R. MacFarlane, *J. Phys. Chem. A,* 2009, **113**, 7064-7072.

128. R. C. Dunbar, *J. Chem. Edu.,* 1982, **59**, 22.
129. T. Steiner, *Angew. Chem. Int. Ed.,* 2002, **41**, 48–76.
130. S. J. Grabowski, Springer, Dordrecht, *Hydrogen Bonding: New Insights,* ed. 2006.
131. G. A. Jeffrey, *An Introduction to Hydrogen Bonding*, Oxford University Press, 1997.
132. R. Bini, C. Chiappe, V. L. Mestre, C. S. Pomelli, T. Welton, *Org. Biomol. Chem.,* 2008, **6**, 2522-2529.